FREQUENCY AND PHASE LOCKING OF OSCILLATORS AND MAGNETRONS

A THESIS SUBMITTED TO
THE GRADUATE SCHOOL OF NATURAL AND APPLIED SCIENCES
OF
MIDDLE EAST TECHNICAL UNIVERSITY

BY

IŞIL SALUR

IN PARTIAL FULFILLMENT OF THE REQUIREMENTS
FOR
THE DEGREE OF MASTER OF SCIENCE
IN
ELECTRICAL AND ELECTRONICS ENGINEERING

JUNE 2018

Approval of the thesis:

FREQUENCY AND PHASE LOCKING OF OSCILLATORS AND MAGNETRONS

submitted by **IŞIL SALUR** in partial fulfillment of the requirements for the degree of **Master of Science in Electrical and Electronics Engineering Department, Middle East Technical University** by,

Prof. Dr. Halil Kalıpçılar _____
Dean, Graduate School of **Natural and Applied Sciences**

Prof. Dr. Tolga Çiloğlu _____
Head of Department, **Electrical and Electronics Engineering**

Prof. Dr. Şimşek Demir _____
Supervisor, **Electrical and Electronics Eng. Dept., METU**

Examining Committee Members:

Prof. Dr. Sencer Koç
Electrical and Electronics Engineering Dept., METU _____

Prof. Dr. Şimşek Demir
Electrical and Electronics Engineering Dept., METU _____

Prof. Dr. Gönül Turhan Sayan
Electrical and Electronics Engineering Dept., METU _____

Assoc. Prof. Dr. Lale Alatan
Electrical and Electronics Engineering Dept., METU _____

Assist. Prof. Dr. Avni Aksoy
Institute of Accelerator Technologies, Ankara University _____

Date: **28.06.2018**

I hereby declare that all information in this document has been obtained and presented in accordance with academic rules and ethical conduct. I also declare that, as required by these rules and conduct, I have fully cited and referenced all material and results that are not original to this work.

Name, Last Name: IŞIL SALUR

Signature :

ABSTRACT

FREQUENCY AND PHASE LOCKING OF OSCILLATORS AND MAGNETRONS

Salur, Işıl
M.S., Department of Electrical and Electronics Engineering
Supervisor : Prof. Dr. Şimşek Demir

June 2018, 97 pages

Phase control of oscillators is a method used to improve both frequency stability and phase noise. Despite magnetrons are simple and cost effective high power microwave generators, they suffer from frequency and phase instabilities. Therefore, array construction with magnetrons is a difficult task. Using injection locking method, phase control can be established, hence output stabilities of generators can be improved. As a result, output power signals of the locked magnetrons can be added in the radiation field without using a combiner. In this thesis, Adler's injection locking theory is verified using a 300 MHz solid-state oscillator circuit with three locking configurations such as master-slave, peer-peer and self-locking. Phase and frequency locking is achieved for three cases. In the master-slave experiment, it is observed that phase noise of free-running oscillator, being locked to master oscillator, is improved about 11 dBc/Hz at 100 kHz offset. For peer-peer locking, an improvement of 3 dBc/Hz at 100 kHz offset and for self-locking, an improvement of 5 to 10 dBc/Hz at 100 kHz is observed according to the coaxial cable length. Observing the agreement between theory and application, an experimental setup for master-slave locking of two

industrial magnetrons is proposed.

Keywords: Phase Locking, Adler's Equation, Magnetron, Phase Noise, Power Combining

ÖZ

OSİLATÖRLERİN VE MAGNETRONLARIN FREKANS VE FAZ KİLİTLEMELERİ

Salur, Işıl
Yüksek Lisans, Elektrik ve Elektronik Mühendisliği Bölümü
Tez Yöneticisi : Prof. Dr. Şimşek Demir

Haziran 2018 , 97 sayfa

Osilatörlerin faz kontrolü frekans kararlılığı ve faz gürültüsünü iyileştirmek için kullanılan bir yöntemdir. Magnetronlar, basit ve uygun maliyetli yüksek güçlü mikrodalga üreteçleri olmalarına rağmen frekans ve faz kararlılıkları bakımından zayıftırlar. Bu nedenle, magnetronlarla dizi yapısı oluşturmak zordur. Faz kontrolü enjeksiyon kilitleme yöntemi kullanılarak sağlanabilir, böylece üreteçlerin çıkış kararlılıkları iyileştirilebilir. Sonuç olarak, kilitli magnetronların çıkış gücü sinyalleri, bir birleştirici kullanılmadan radyasyon alanında birbirlerine eklenebilir. Bu tezde, Adler'in enjeksiyon kilitleme teorisi, ana-bağımlı, eşler arası ve kendinden kilitleme düzenekleriyle 300 MHz'lik bir katı hal osilatör devresi kullanılarak doğrulanmıştır. Üç durum için de faz ve frekans kilitlenmesi sağlanmıştır. Ana-bağımlı deneyinde, serbest çalışan osilatörün faz gürültüsünün 100 kHz ofsette 11 dBc/Hz iyileşme ile ana osilatöre kilitlendiği gözlenmiştir. Eşler arası kilitlemede 100 kHz ofsette 3 dBc/Hz ve kendinden kilitlemede 100 kHz ofsette koaksiyel kablo uzunluğuna göre 5 ila 10 dBc/Hz arasında iyileşme kaydedilmiştir. Teori ve uygulama arasındaki mutabakat göz önünde bulundurularak, iki endüstriyel magnetronun ana-bağımlı kilitlemesi için

bir deney düzeneği önerilmiştir.

Anahtar Kelimeler: Faz Kilitlemesi, Adler'in Eşitliği, Magnetron, Faz Gürültüsü, Güç Birleştirmesi

To my family

ACKNOWLEDGMENTS

I would like to express my sincere gratitude to my supervisor Prof. Dr. Şimşek Demir for his guidance during the course of this thesis work. The theoretical background from his microwave courses and his practical approach encouraged me to specialize in RF and microwave engineering. I also thank him for joining the experiments with magnetrons to avoid accidents in the laboratory.

I would like to thank Enis Kobal for his hours in the EMT laboratory during the high power component measurements despite his tight schedule.

I want to thank my dear friend Arsen Turhaner for his help with LPKF machine to print oscillator circuit board.

I am grateful to ASELSAN Inc. for providing me time and laboratory environment to conduct my studies. I sincerely thank Çetin Üzel and Mustafa Özme for mentoring me and being great colleagues. I also thank Talat Çetin, Can Önol and all my colleagues in our cubicle for making it a fun workplace.

I specially thank my dear Bahattin for his help me to write grammatically correct sentences and for his endless support.

I would like to thank jury members Prof. Dr. Sencer Koç, Prof. Dr. Gönül Turhan Sayan, Assoc. Prof. Dr. Lale Alatan and Assist. Prof. Dr. Avni Aksoy for allocating their precious time for my thesis defence.

And last but not the least, I would like to heartily thank my family for their endless care, support and love. I would like to honour the memory of my grandfather, who would have been most happy to see me finish this thesis.

TABLE OF CONTENTS

ABSTRACT v

ÖZ vii

ACKNOWLEDGMENTS x

TABLE OF CONTENTS xi

LIST OF TABLES xiv

LIST OF FIGURES xv

LIST OF ABBREVIATIONS xx

CHAPTERS

1 INTRODUCTION 1

1.1 Motivation of The Thesis 1

1.2 Review of Literature 4

1.2.1 Phase Locking of Oscillators 4

1.2.2 Phase Noise of Coupled Oscillators 5

1.2.3 Locking of Magnetrons 6

1.3 Focus of the Thesis and Organization 7

2 THEORY OF OPERATION 9

2.1 Introduction 9

2.2 Injection Locking Theory 9

2.2.1 Master-Slave Locking 15

2.2.2 Peer-Peer Locking 18

2.2.2.1 Zero coupling ($\beta_{ij} \rightarrow 0$) 21

2.2.2.2 Weak Coupling ($0 < \beta_{ij} \ll 1$) 21

2.2.2.3 Strong Coupling ($0 \ll \beta_{ij} < 1$) . . . 22

2.3 Phase Noise In Coupled Oscillators 22

3 DESIGN AND SIMULATION OF A COUPLED OSCILLATOR SYSTEM 27

3.1 Introduction 27

3.2 Design of A Colpitts Oscillator 27

3.2.1 DC Biasing 28

3.2.2 Frequency Determination 29

3.3 Design of A Locking System 30

3.3.1 Master-Slave System 30

3.3.2 Peer-Peer System 30

3.4 Simulation Results 31

3.4.1 A Single Colpitts Oscillator 32

3.4.1.1 DC Simulation 32

3.4.1.2 Transient Simulation 34

3.4.1.3 Harmonic Balance Simulation 36

3.4.2 Master-Slave System 37

3.4.3 Peer-Peer System 49

4 EXPERIMENTS AND MEASUREMENT RESULTS OF FREE-RUNNING AND LOCKED COLPITTS OSCILLATORS 57

4.1 Introduction 57
4.2 Measurement Results of Single Oscillator 57
4.3 Measurement Results of Master-Slave System 59
4.4 Measurement Results of Peer-Peer System 67
4.5 Measurement Results of Self-Locked Oscillator 70
5 MAGNETRONS AND INJECTION LOCKING OF MAGNETRONS 75
5.1 Introduction 75
5.2 Theory of Operation 75
5.2.1 Physical Structure 75
5.2.2 Space Charge and DC Voltage - Magnetic Field Relationship 77
5.3 Proposal of Experimental Setups for Magnetron Measurements 80
5.3.1 Setup for an Industrial Magnetron Measurement . . 81
5.3.2 Setup for Master-Slave Locked Magnetron Measurement 81
6 CONCLUSION AND FUTURE WORK 83
6.1 Conclusion 83
6.2 Future Work 84
REFERENCES 87
APPENDICES
A INTEGRAL CALCULATION OF OSCILLATOR OUTPUT VOLTAGE 91
B DESIGN OF A COLPITTS OSCILLATOR 95

LIST OF TABLES

TABLES

Table 3.1 Locking Range for $R_c = 330\Omega$ 52

Table 3.2 Locking Range for $R_c = 1k\Omega$ 52

Table 4.1 Trimmer Capacitance and Oscillation Frequency with Output Power 59

Table 4.2 Frequency of Signal Generator and Output of the Colpitts Oscillator 60

Table 4.3 Amplitude of the Signal Generator and Output of the Colpitts Oscillator 62

Table 4.4 Self-Locking Measurement Results for Cable RG178 71

Table 4.5 Self-Locking Measurement Results for Cable RG316 71

LIST OF FIGURES

FIGURES

Figure 1.1 (a) Antenna Array with Phase Shifters and (b) Antenna Array with Phase Locking 3

Figure 1.2 A Magnetron [1] 3

Figure 1.3 Adler's Circuit for Locking [2] 4

Figure 2.1 (a) Series-Tuned Oscillator and (b) Parallel-Tuned Oscillator 10

Figure 2.2 Two Series-Tuned Coupled Oscillators 10

Figure 2.3 Injection Locking System 11

Figure 2.4 (a) Unilateral Coupling Between Two Oscillators and (b) Unilateral Coupling Between N Oscillators 16

Figure 2.5 Bilateral Coupling Between Two Oscillators 19

Figure 2.6 (a) Bilateral Coupling, (b) Coupling Through N-Port Network and (c) Global Coupling 19

Figure 2.7 Oscillator Model with Noise Admittance 22

Figure 3.1 A Schematic Diagram of A One-Port Oscillator 27

Figure 3.2 Colpitts Oscillator Configuration 28

Figure 3.3 Master-Slave Locking System 30

Figure 3.4 Master-Slave Locking Simplified Circuit 31

Figure 3.5 Peer-Peer Locking System 31

Figure 3.6 Peer-Peer Locking Simplified Circuit 31

Figure 3.7 Circuit Schematic for DC Simulation 32

Figure 3.8 BFG520W Operating Point 33

Figure 3.9 Results of DC Analysis 33

Figure 3.10 Circuit Schematic for Transient Analysis 34

Figure 3.11 Transient Response of the Oscillator for (a) 0-500 nsec (b) 450-500 nsec 35

Figure 3.12 FFT of the Time Domain Signal for 450-500 nsec 35

Figure 3.13 Circuit Schematic for Harmonic Balance Simulation 36

Figure 3.14 (a) Harmonic Balance Simulation Frequency Response (b) Harmonic Balance Simulation Time-Domain Response 37

Figure 3.15 Phase Noise of Colpitts Oscillator 38

Figure 3.16 Trimmer Capacitance vs. Oscillation Frequency 38

Figure 3.17 Circuit Schematic for Master-Slave Simulations 39

Figure 3.18 Time Domain Results for (a) $R_{coupling} = 330\Omega$, (b) $R_{coupling} = 1k\Omega$, (c) $R_{coupling} = 4.7k\Omega$ and (d) $R_{coupling} = 10k\Omega$ 40

Figure 3.18 Time Domain Results for (a) $R_{coupling} = 330\Omega$, (b) $R_{coupling} = 1k\Omega$, (c) $R_{coupling} = 4.7k\Omega$ and (d) $R_{coupling} = 10k\Omega$ 41

Figure 3.19 FFT Results for (a) $R_{coupling} = 330\Omega$, (b) $R_{coupling} = 1k\Omega$, (c) $R_{coupling} = 4.7k\Omega$ and (d) $R_{coupling} = 10k\Omega$ 42

Figure 3.19 FFT Results for (a) $R_{coupling} = 330\Omega$, (b) $R_{coupling} = 1k\Omega$, (c) $R_{coupling} = 4.7k\Omega$ and (d) $R_{coupling} = 10k\Omega$ 43

Figure 3.20 Time Domain Results for (a) $f_m = 346MHz$, (b) $f_m = 354MHz$, (c) $f_m = 362MHz$ and (d) $f_m = 372MHz$ 44

Figure 3.20 Time Domain Results for (a) $f_m = 346MHz$, (b) $f_m = 354MHz$, (c) $f_m = 362MHz$ and (d) $f_m = 372MHz$ 45

Figure 3.21 FFT Results for (a) $f_m = 346MHz$, (b) $f_m = 354MHz$, (c) $f_m = 362MHz$ and (d) $f_m = 372MHz$ 46

Figure 3.21 FFT Results for (a) $f_m = 346MHz$, (b) $f_m = 354MHz$, (c) $f_m = 362MHz$ and (d) $f_m = 372MHz$ 47

Figure 3.22 (a) Time Domain and (b) FFT Results $V_m = 2.5V$ 48

Figure 3.23 (a) Time Domain and (b) FFT Results $V_m = 2V$ 49

Figure 3.24 Circuit Schematic for Peer-Peer Simulations 50

Figure 3.25 (a) Time Domain and (b) FFT Results for No Coupling Resistor . . 53

Figure 3.26 Time Domain Results for (a) $C_8 = 6pF$, (b) $C_8 = 12pF$ and (c) $C_8 = 17pF$ 54

Figure 3.26 Time Domain Results for (a) $C_8 = 6pF$, (b) $C_8 = 12pF$ and (c) $C_8 = 17pF$ 55

Figure 3.27 FFT Results for (a) $C_8 = 6pF$, (b) $C_8 = 12pF$ and (c) $C_8 = 17pF$. 55

Figure 3.27 FFT Results for (a) $C_8 = 6pF$, (b) $C_8 = 12pF$ and (c) $C_8 = 17pF$. 56

Figure 4.1 Manufactured Oscillator Circuit 58

Figure 4.2 (a) Start and (b) Steady-State of the Oscillation in Time-Domain . . 58

Figure 4.3 (a) Output Signal of Single Colpitts Oscillator and (b) Phase Noise Measurement of Output Signal 59

Figure 4.4 Experimental Setup for Spectrum Analyzer Measurements 60

Figure 4.5 Output of the Slave Oscillator for $f_m = 301.4$ MHz 61

Figure 4.6 Output of the Slave Oscillator for (a) $f_m = 301.5$ MHz and (b) $f_m = 298.5$ MHz 61

Figure 4.7 Output of the Slave Oscillator for (a) $A_m = 2$ dBm and (b) $A_m = -10$ dBm 62

Figure 4.8 Experimental Setup for Oscilloscope Measurements 63

Figure 4.9 Time-Domain Output Signals of Master and Slave Oscillators for Unlocked Case 63

Figure 4.10 (a) Output Signals of SMA100A and Free-Running Oscillator and (b) Narrower Spectrum of Same Signals 64

Figure 4.11 Time-Domain Output Signals of Master and Slave Oscillators for Locked Case 64

Figure 4.12 (a) Output Signals of SMA100A and Free-Running Oscillator Under Locking and (b) Narrower Spectrum of Same Signals 65

Figure 4.13 Phase Difference Between SMA100A and Free-Running Oscillator Over Time 66

Figure 4.14 Phase Noise Measurements of (a) SMA100A Signal Generator and (b) Locked Output Signal 66

Figure 4.15 Phase Noise Measurements of SMA100A, Colpitts Oscillator and Locked Signal 67

Figure 4.16 Experimental Setup for Oscilloscope Measurements 67

Figure 4.17 Time-Domain Output of Two Unlocked Colpitts Oscillators 68

Figure 4.18 (a) Output Signals of Two Unlocked Colpitts Oscillators and (b) Narrower Spectrum of Same Signals 68

Figure 4.19 Time Domain Output of Two Locked Colpitts Oscillators 69

Figure 4.20 (a) Output Signals of Two Locked Colpitts Oscillators and (b) Narrower Spectrum of Same Signals 69

Figure 4.21 Phase Difference Between Two Locked Colpitts Oscillators 70

Figure 4.22 Experimental Setup for Self-Locking Experiments 70

Figure 4.23 Phase Noise Measurements of Self-Locked Oscillator for $l = \lambda$ with Cables (a) RG178 and (b) RG316 72

Figure 4.24 Phase Noise Measurements of Self-Locked Oscillator for $l = 2\lambda$ with Cables (a) RG178 and (b) RG316 72

Figure 4.25 Phase Noise Measurements of Self-Locked Oscillator for $l = \frac{\lambda}{2}$ with Cables (a) RG178 and (b) RG316 73

Figure 5.1 A Simple Magnetron Structure 76

Figure 5.2 Resonant Cavitiy and Resembled Tank Circuit 77

Figure 5.3 Path Followed by A Single Electron in A Non-Oscillating Magnetron 78

Figure 5.4 Possible Paths of An Electron Under E and B Fields 78

Figure 5.5 Space Charge in Oscillating Magnetron 79

Figure 5.6 Magnetron Operation Regions According to $B_o - V_o$ Parameters . . 80

Figure 5.7 Experimental Setup for Measurements of Independent Magnetrons 81

Figure 5.8 Experimental Setup for Master-Slave Locked Magnetrons 82

Figure B.1 Conventional Colpitts Oscillator Configuration 95

LIST OF ABBREVIATIONS

BJT	Bipolar Junction Transistor
CSV	Comma-Separated Values
CW	Continuous Wave
DR	Dielectric Resonator
FET	Field Effect Transistor
FFT	Fast Fourier Transform
HPM	High Power Microwaves
LO	Local Oscillator
LTIV	Linear Time Invariant
OCXO	Oven Controlled Crystal Oscillator
PLL	Phase Locked Loop
RF	Radio Frequency
TCXO	Temperature Controlled Crystal Oscillator
VCO	Voltage Controlled Oscillator

CHAPTER 1

INTRODUCTION

1.1 Motivation of The Thesis

The first known electrical oscillator was built by Heinrich Hertz to prove Maxwell's equations experimentally around 1880s. He needed to observe and measure electromagnetic waves in his laboratory; hence, a few meters wavelength was required. However, electromechanical oscillating systems could generate only a few kilocycles per second. Hertz built a spark gap oscillator that acts as a resonator and a dipole that takes the energy and radiates it. Another dipole was used as a receiver and with this, Hertz also established the primitive radio receiver and transmitter. Through 20th century, inspired by Hertz's work, radio engineers Marconi, Armstrong, Tesla and Braun built wireless communication systems around the same time in different countries [3].

In 1915, Edwin H. Armstrong built the lumped element oscillator consisted of a capacitor and an inductor as a tank circuit and a triode vacuum tube for amplification [4]. In 1918, Edwin H. Colpitts invented an oscillator with capacitive voltage divider which now carries his name [5]. He added positive feedback between tank circuit and amplification circuit. Without amplification, oscillations would die out quickly due to losses. Hence, active devices are key elements for oscillator circuits to keep oscillations going indefinitely. There were several engineers worked independently on the tank circuit architectures around the same time. Ralph Hartley's tank circuit uses inductors as voltage divider while Colpitts' uses capacitors for the same purpose [6]. Clapp and Gouriet put an additional capacitor to the tank circuit which is used to vary the frequency of oscillation without changing the feedback voltage [7].

Today, oscillators are key elements for wireless and radio communications as well as

RF test and measurement equipment. They are mostly used for frequency conversion and carrier generation. LOs and VCOs are the most widely used oscillators in RF and microwave frequency circuits. These oscillators are mostly solid-state oscillators with BJT or FET. Digital circuits require stable clock generators, like TCXO or OCXO, which are constructed using crystal and SAW oscillators. Vacuum tube oscillators such as magnetrons, klystrons and vircators are used as HPM sources for industrial purposes. The two important features of a good oscillator are minimum spurious and noise signals, and low phase noise. A simple oscillator with BJT or FET as active device suffers from frequency stability and phase noise. Therefore, crystal oscillators with PLL structure are used as high accuracy frequency references in most communication systems [8].

In 17th century Huygens realized that the pendulums of two clocks ticked together when they were hung close to each other. He concluded that there is an interaction between the clocks through the wall [9]. Also, it is observed that when humans are isolated from nature, they have a daily period of 25 hours. However, after they are brought back, they are locked to Earth's 24-hour cycle [10].

Injection locking of electrical oscillators has been studied for many years. It is useful for many applications such as frequency division, quadrature generation, and fine phase separation [11]. In antenna arrays, each antenna is fed from a single source through a phase shifter to guide the beam. However, phase shifters are expensive and hard to build. This array structure is shown in Figure 1.1a. Another approach is to feed each antenna with separate oscillators and lock these oscillators to a single source as shown in Figure 1.1b. Each oscillator can be locked to an injected signal. By changing the locked phase, beam can be directed. This phenomena is called as spatial power combining. This way, combiner loss can be avoided.

Magnetrons are the simplest HPM sources. They are widely used in industrial processing, microwave ovens and radar applications. A magnetron with its typical elements is shown in Figure 1.2. They are low-cost, robust and efficient in energy conversion. Magnetrons can generate high output power. While average power levels are around several kWs, a single magnetron can generate an output power over 1 MW, in pulse mode [12]. However, they suffer from frequency, phase and amplitude

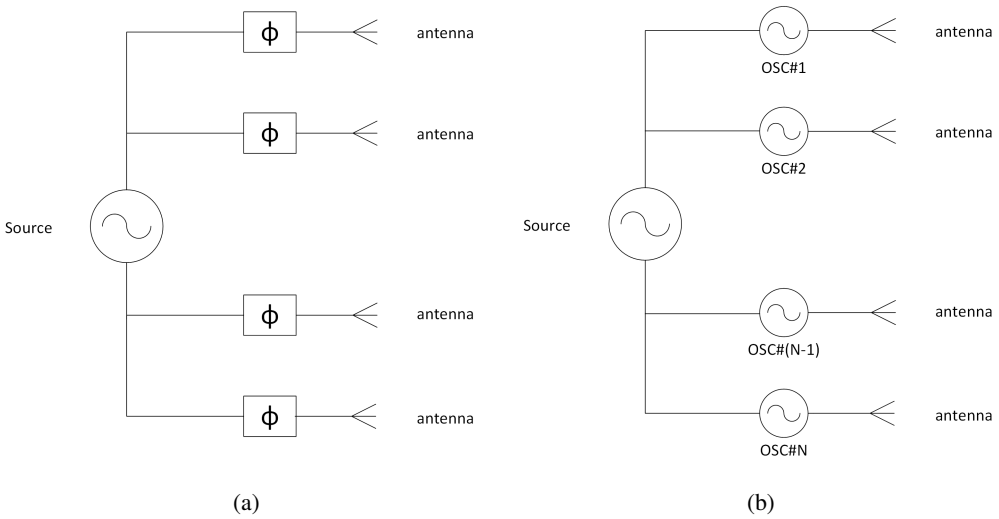

(a) (b)

Figure 1.1: (a) Antenna Array with Phase Shifters and (b) Antenna Array with Phase Locking

instability. To overcome this problem phase locking of magnetrons is an option.

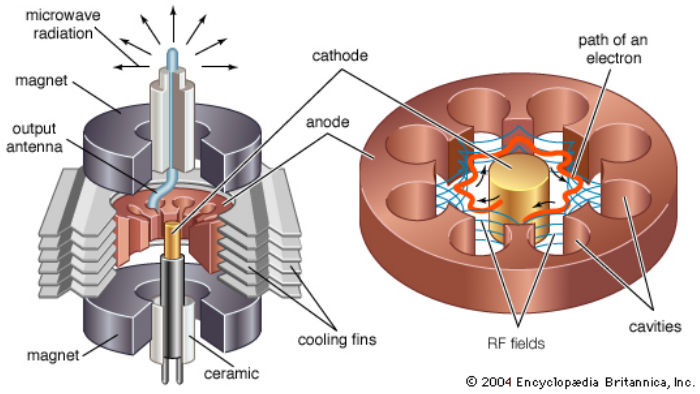

Figure 1.2: A Magnetron [1]

Phase locking of magnetrons can be used for spatial combining of output power. By combining outputs of N magnetrons, power produced in the radiation field can be N^2 times power of a single magnetron. By locking, improvements in frequency stability and phase noise are also expected.

1.2 Review of Literature

Phase and frequency locking of oscillators has been researched for many years. Engineers and scientists have been studying the subject for solid-state oscillators as well as high power oscillators. Phase noise performance of locked oscillators has also been considered.

1.2.1 Phase Locking of Oscillators

The interaction between two oscillators was considered as an electromotive force to a triode oscillator by Van der Pol [13] in 1934. It was shown that free oscillations of the triode oscillator are absent but only forced oscillations were present at the output. However, Van der Pol's differential equation did not give a clear insight for locking phenomena. Therefore, several authors also discussed injection locking of nonlinear oscillators.

Adler [2] explained locking phenomena of a triode oscillator with an injected signal using a vector diagram and derived a differential equation for the oscillator phase as a function of time. Solving the equation for locked case, he defined a locking bandwidth in which locking could occur. He also suggested a mechanical analogy, a pendulum in a rotating container, to the electrical oscillator. His work has been a reference for all injection locking research in the literature. Adler's circuit for locking is given in Figure 1.3 where E_1 is injected signal, E_F is resonator's voltage and E is the output signal of the free-running oscillator.

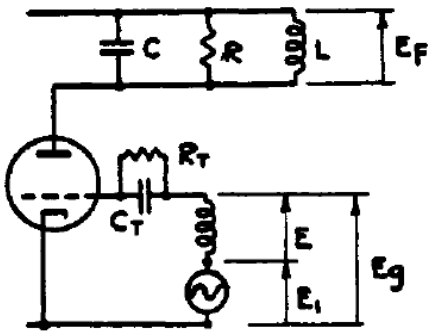

Figure 1.3: Adler's Circuit for Locking [2]

Paciorek [14] examined the case when an oscillator is locked by a pulsed signal. For this case, the time required for locking is important. He developed an equation to solve the problem; however, it is too complicated to understand intuitively. So, he provided curves describing the mechanism to help the designer. Razavi [11] used phase and amplitude equations derived before to express the required nonlinearity of the oscillator circuit. He examined injection locking characteristics and presented a graphical analysis for pulling in oscillators and PLLs. Razavi also mentioned the phase noise reduction of locked oscillators.

In 2004, Şener [15] published a thesis on phase control using injection locking. He conducts experiments on a 1 GHz VCO to observe the phase difference of two locked output signals with respect to frequency of oscillation.

1.2.2 Phase Noise of Coupled Oscillators

Kurokawa [16] presented in his paper that while FM noise is improved considerably, AM noise is degraded slightly for locked oscillators. Schünemann [17] extended Kurokawa's work to the case of arbitrary injection levels. He stated that Kurokawa's theory fails for small injection levels. Chang, Cao and Mishra [18] examined phase noise of N coupled oscillators in their paper. They stated that when coupling phase is chosen properly, near-carrier phase noise is reduced to $\frac{1}{N}$ that of a single oscillator provided that coupling network is reciprocal. Otherwise, noise degradation is observed. Chang, Cao and Vaughan [19] said that this $\frac{1}{N}$ reduction of phase noise is not sufficient for most of the system requirements. They suggested external locking to a low-noise source. Paper extends the previous work to examine the dependence of array size and external locking configuration.

Chang [20] studied phase noise of a self-injection locked oscillator in his last paper. It shows that the behaviour of phase noise is similar to an oscillator locked onto an external low phase noise source.

1.2.3 Locking of Magnetrons

There is an increasing demand in producing an amount of gigawatt-level power using steerable antenna arrays in GHz frequency range. This could be achieved in two ways. One is to build very high power sources and the other is to combine available high power sources in an efficient way. The first approach is limited by the electric field breakdown. So, the second approach is being followed. In order to combine the outputs of multiple high power oscillators, the microwave sources should operate at the same frequency as well as with a constant phase difference with respect to time between them. Accomplishing this, a controllable beam at the far field of an antenna could be obtained using constructive interference.

Phase locking of gigawatt-level sources in an array is a popular topic in the HPM history. There has been experiments using vircators and magnetrons as high power sources in different locking and array configurations. Phase locking of magnetrons by an external signal has a history since 1947 [21].

Since 1990s, there has been a higher interest in locking of HPM generators. Research on master-slave or peer-peer configurations of these sources was conducted in 1989 [22]. In the same year, a study for frequency and phase locking of a high power, S-band, cavity vircator by a relativistic magnetron was conducted [23]. 3-5 ns locking time and peak power between 100-500 MW was reported. Output power of locked vircator was measured 2 or 3 times higher than a free-running vircator [24]. An array of two vircators, peer-peer connected, and an array of two or higher vircators driven by a magnetron as a master oscillator studies were also reported [25].

Phase locking of up to 7 relativistic magnetrons in peer-peer configuration was reported in 1991 [26]. They stated 2 GW output power for 4-magnetron array and 2.9 GW output power for 7-magnetron array at 2.8 GHz. Also, they decided to the geometry that gives the best locking performance. Same group renewed the experiments for 2 pulse driven S-band magnetrons connected by a short waveguide and observed a locking time of $\sim$ 7 ns [27].

Power combining of 15 kW CW magnetrons based on injection locking with 5 MHz locking bandwidth has been analysed lately [28]. A power combining efficiency of

higher than 95% has been obtained using waveguide power combiner.

Self-injection locking of a magnetron is also an interesting topic. A noise reduction of 13 dB at 1 MHz offset for a conventional CW magnetron operates at 2455 MHz was reported [29]. A DR filter placed in the feedback loop provides a tunable operating frequency of magnetron.

1.3 Focus of the Thesis and Organization

This thesis focuses on frequency and phase locking phenomena for electrical oscillators which is aimed to use for spatial power combining of output signals of HPM generators. To serve this goal, theoretical background is provided to comprehend the nature of locking. An oscillator circuit with BJT is designed, simulated and experiments are conducted which verifies the theory. Following the agreement between theory and application, an experimental setup with industrial magnetrons is proposed and experiments are conducted to observe the case for magnetrons. This thesis contributes to the literature by extending experimental knowledge in phase locking of magnetrons and leads to further studies on combining high power generators.

In this introductory chapter, motivation of the thesis, literature review and thesis overview is presented.

In chapter 2, theory of locking is examined. Phase and amplitude equations for locked oscillators and Adler's locking bandwidth equation are derived. Phase noise of locked oscillators is analysed briefly.

In chapter 3, design procedure of the solid state oscillator circuit is given. Simulation results for the designed oscillator and locked oscillators are also presented.

In chapter 4, measurement results of the experiments conducted with the free-running oscillator and master-slave, peer-peer, self-locking systems are given. Phase noise performance for different locking conditions are examined.

In chapter 5, theory of operation of magnetron is given briefly and an experimental setup for master-slave locking of magnetrons is proposed.

Finally, chapter 6 summarizes the work done in this thesis and suggests a future work.

CHAPTER 2

THEORY OF OPERATION

2.1 Introduction

In this chapter, theoretical background for injection locking phenomena is given. In order to understand the behaviour of a coupled oscillator system, a parallel-tuned oscillator model is used. Two differential equations, one for amplitude and one for phase, are derived describing the coupling between oscillators. When phase equation is solved for locked case, Adler's locking bandwidth equation is obtained. Phase and amplitude equations are rewritten for master-slave and peer-peer locking systems considering the strength of the coupling between oscillators [8]. Phase noise of locked oscillators is examined at the end of the chapter.

2.2 Injection Locking Theory

The equivalent model of an electrical oscillator can be given by either series-tuned or parallel-tuned configurations. For each case the coupling or locking analysis is the same. If the active device is modelled as a negative resistance, a series-tuned resonator circuit is employed. On the other hand, if the device is modelled as a negative conductance, a parallel-tuned resonator circuit is used. A series-tuned free-running oscillator can be modelled as in Figure 2.1a. and a parallel-tuned free-running oscillator is shown in Figure 2.1b.

Free-running frequency, quality factor and negative resistance, which is a strong function of oscillator output voltage, can be expressed as follows for a series-tunes oscillator.

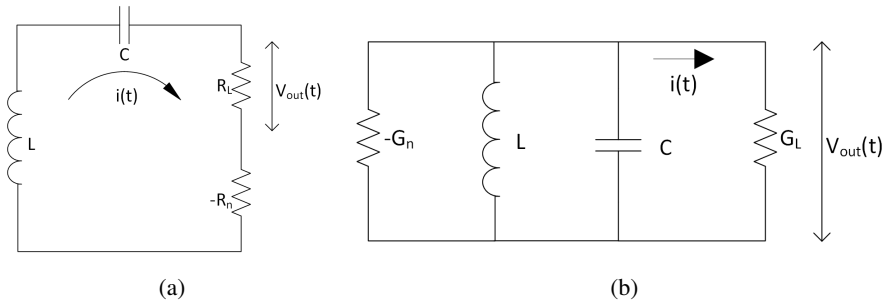

(a) (b)

Figure 2.1: (a) Series-Tuned Oscillator and (b) Parallel-Tuned Oscillator

$$\omega_0 = \frac{1}{\sqrt{LC}} \, , Q = \frac{\omega_0 L}{R_L} \, , Q = \frac{1}{\omega_0 C R_L} \, , R_n \approx R_n \left[\left| V_{out} \left(t \right) \right| \right]$$

From Figure 2.1, output voltage expression can be written as

$$V_{out} \left(t \right) = A \left(t \right) e^{j\theta(t)} = A \left(t \right) e^{j(\omega_0 t + \phi(t))} \tag{2.1}$$

where $\theta \left(t \right)$ is the instantaneous phase, $A \left(t \right)$ is the amplitude term of the output signal and $\phi \left(t \right)$ is the phase term of the output signal. $A \left(t \right)$ and $\phi \left(t \right)$ vary slowly with respect to time in comparison to the output periodic oscillation.

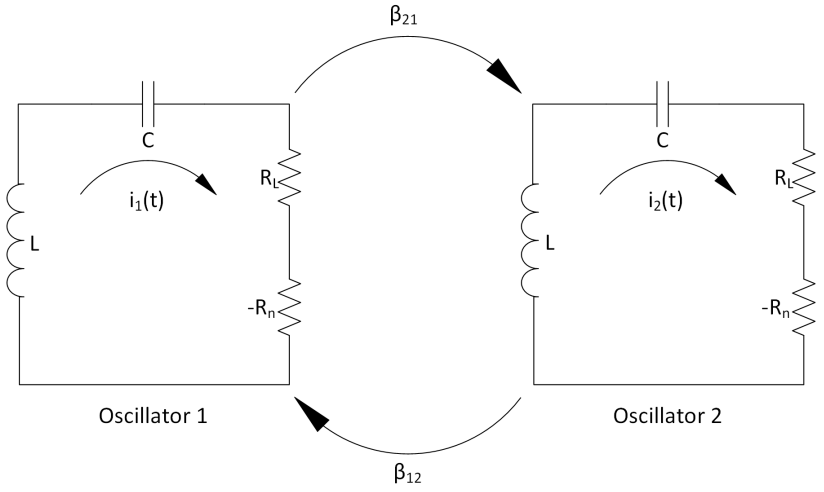

Figure 2.2: Two Series-Tuned Coupled Oscillators

Figure 2.2 shows two identical series-tuned coupled oscillators. There is coupling, through a coupling network, between each oscillator represented by the coupling coefficient β_{12}, from Oscillator 2 to Oscillator 1, and β_{21}, from Oscillator 1 to Oscillator 2.

The coupled system shown in Figure 2.2 can be reduced to an injection system as in

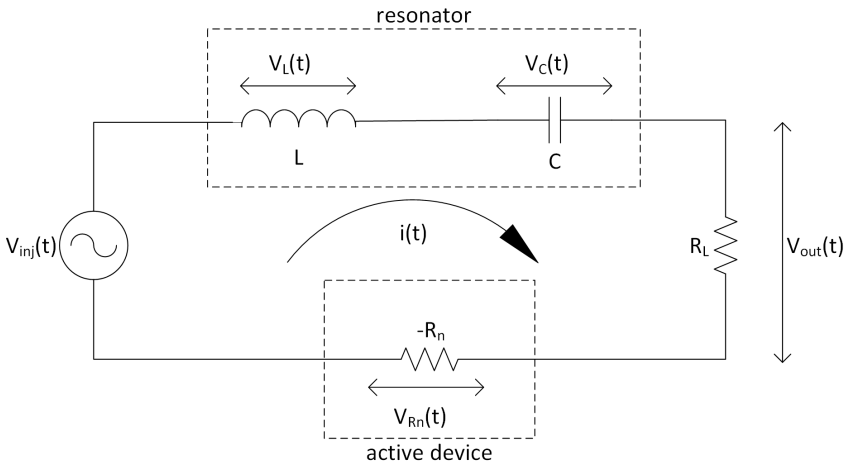

Figure 2.3: Injection Locking System

Figure 2.3. The mesh equation for the circuit in Figure 2.3 is written using Kirchoff's Voltage Law as

$$V_{inj}\left(t\right) = V_L\left(t\right) + V_C\left(t\right) + V_{Rn}\left(t\right) + V_{out}\left(t\right) \tag{2.2}$$

$V_{inj}\left(t\right)$ includes the injected oscillator and coupling network. Similar to $V_{out}\left(t\right)$, $V_{inj}\left(t\right)$ can be written as an oscillator output voltage as follows

$$V_{inj}\left(t\right) = A_{inj}\left(t\right)e^{j\theta_{inj}(t)} = A_{inj}\left(t\right)e^{j(\omega_{inj}t+\psi(t))} \tag{2.3}$$

where $\theta_{inj}\left(t\right)$ is the instantaneous phase of the injected signal, $A_{inj}\left(t\right)$ is the amplitude term of the injected signal and $\psi\left(t\right)$ is the phase term of the injected signal.
The mesh equation, (2.2), is arranged to obtain the equations for amplitude and phase dynamics of the coupled oscillators.

$$V_{inj}\left(t\right) = L\frac{\partial i\left(t\right)}{\partial t} + \frac{1}{C}\int i\left(t\right)dt - R_n i\left(t\right) + R_L i\left(t\right) \tag{2.4}$$

The loop current, $i\left(t\right)$, can be expressed in terms of the oscillator output voltage, $V_{out}\left(t\right)$ as

$$i\left(t\right) = \frac{V_{out}\left(t\right)}{R_L} \tag{2.5}$$

Therefore, right-hand side of (2.4) can be written as a function of $V_{out}\left(t\right)$.

$$V_{inj}(t) = \frac{L}{R_L}\frac{\partial V_{out}(t)}{\partial t} + \frac{1}{CR_L}\int V_{out}(t)\,dt - \frac{R_n}{R_L}V_{out}(t) + V_{out}(t) \tag{2.6}$$

Multiply (2.6) with $\frac{\omega_0}{Q}$

$$\frac{\omega_0}{Q}V_{inj}(t) = \frac{\omega_0 L}{QR_L}\frac{\partial V_{out}(t)}{\partial t} + \frac{\omega_0}{QCR_L}\int V_{out}(t)\,dt + \frac{\omega_0}{Q}\left(1 - \frac{R_n}{R_L}\right)V_{out}(t) \tag{2.7}$$

Now, substitute the quality factor expressions given above for a series-tuned free-running oscillator.

$$\frac{\omega_0}{Q}V_{inj}(t) = \frac{\partial V_{out}(t)}{\partial t} + \omega_0^2\int V_{out}(t)\,dt + \frac{\omega_0}{Q}\left(1 - \frac{R_n}{R_L}\right)V_{out}(t) \tag{2.8}$$

Equation (2.8) is the mesh equation that describes the rate of change in the amplitude and the phase of the oscillator voltage $V_{out}(t)$.

In order to obtain the separate equations for amplitude and phase dynamics, $\int V_{out}(t)$ should be calculated and substituted in (2.8). Following is the expression for $\int V_{out}(t)$. Detailed calculation of the integral is given in Appendix A.

$$\int V_{out}(t)\,dt = -\frac{j2V_{out}(t)}{\omega_0} + \frac{1}{\omega_0^2}\frac{\partial V_{out}(t)}{\partial t} + H.O.T \tag{2.9}$$

Also, the expression for the negative resistance term in (2.8) should be calculated. Following Van der Pol [13], the device saturation and amplitude dependence of the negative resistance is modelled by a quadratic function as

$$\left(1 - \frac{Rn}{R_L}\right) \approx -\mu\left(\alpha_0^2 - |V_{out}|^2\right) \tag{2.10}$$

where α_0 is the free-running amplitude of the oscillation and μ is the empirical non-linearity parameter defined in [13].

Substituting (2.9) and (2.10) into (2.8) and neglecting the higher order terms in (2.9), the following equation is obtained.

$$\frac{\omega_0}{Q}V_{inj}(t) = \frac{\partial V_{out}(t)}{\partial t} + \omega_0^2\left(\frac{-j2V_{out}(t)}{\omega_0} + \frac{1}{\omega_0^2}\frac{\partial V_{out}(t)}{\partial t}\right) - \frac{\omega_0}{Q}V_{out}(t)\,\mu\left(\alpha_0^2 - |V_{out}(t)|\right) \tag{2.11}$$

Arrange (2.11) to obtain $\frac{\partial V_{out}(t)}{\partial t}$

$$\frac{\omega_0}{Q}V_{inj}\left(t\right)=\frac{\partial V_{out}\left(t\right)}{\partial t}-j2\omega_0 V_{out}\left(t\right)+\frac{\partial V_{out}\left(t\right)}{\partial t}-\frac{\omega_0}{Q}V_{out}\left(t\right)\mu\left(\alpha_0^2-\left|V_{out}\left(t\right)\right|\right) \tag{2.12}$$

Rearranging (2.12), $\frac{\partial V_{out}(t)}{\partial t}$ is obtained as a non-homogeneous differential equation.

$$\frac{\partial V_{out}\left(t\right)}{\partial t}=V_{out}\left(t\right)\left[\frac{\omega_0}{2Q}\mu\left(\alpha_0^2-\left|V_{out}\left(t\right)\right|^2\right)+j\omega_0\right]+\frac{\omega_0}{2Q}V_{inj}\left(t\right) \tag{2.13}$$

Equation (2.13) can be seperated into two parts:

1. Rate of change of amplitude term: $\frac{\partial A(t)}{\partial t}$
2. Rate of change of phase term: $\frac{\partial \theta(t)}{\partial t}$

By taking the derivative of (2.1) using the chain rule

$$\frac{\partial V_{out}\left(t\right)}{\partial t}=e^{j\theta(t)}\frac{\partial A\left(t\right)}{\partial t}+A\left(t\right)\frac{\partial e^{j\theta(t)}}{\partial t} \tag{2.14}$$

Insert (2.1) into (2.13)

$$\frac{\partial V_{out}\left(t\right)}{\partial t}=A\left(t\right)e^{j\theta(t)}\left[\frac{\omega_0\mu}{2Q}\left(\alpha_0^2-\left|A\left(t\right)e^{j\theta(t)}\right|^2\right)+j\omega_0\right]+\frac{\omega_0}{2Q}V_{inj}\left(t\right) \tag{2.15}$$

$\left|e^{j2\theta(t)}\right|=1$ and $A\left(t\right)$ is real.

$$\frac{\partial V_{out}\left(t\right)}{\partial t}=A\left(t\right)e^{j\theta(t)}\left[\frac{\omega_0\mu}{2Q}\left(\alpha_0^2-A^2\left(t\right)\right)+j\omega_0\right]+\frac{\omega_0}{2Q}V_{inj}\left(t\right) \tag{2.16}$$

Expand the terms in the brackets.

$$\frac{\partial V_{out}\left(t\right)}{\partial t}=A\left(t\right)e^{j\theta(t)}\frac{\omega_0\mu}{2Q}\left(\alpha_0^2-A^2\left(t\right)\right)+j\omega_0 A\left(t\right)e^{j\theta(t)}+\frac{\omega_0}{2Q}V_{inj}\left(t\right) \tag{2.17}$$

Equation (2.17) can be separated into two parts as

1. $A(t)\, e^{j\theta(t)} \frac{\omega_0 \mu}{2Q} \left(\alpha_0^2 - A^2(t)\right)$
2. $j\omega_0 A(t)\, e^{j\theta(t)} + \frac{\omega_0}{2Q} V_{inj}(t)$

Arrange part 2 as $A(t)\, e^{j\theta(t)}$ is the common term.

$$j\omega_0 A(t)\, e^{j\theta(t)} + \frac{\omega_0}{2Q} V_{inj}(t) = A(t)\, e^{j\theta(t)} \left(j\omega_0 + \frac{\omega_0}{2QA(t)\, e^{j\theta(t)}} V_{inj}(t) \right) \quad (2.18)$$

Insert (2.1) to the denominator of the second term in the parenthesis.

$$j\omega_0 A(t)\, e^{j\theta(t)} + \frac{\omega_0}{2Q} V_{inj}(t) = A(t)\, e^{j\theta(t)} j \left(\omega_0 + \frac{\omega_0}{j2QV_{out}(t)} V_{inj}(t) \right) \quad (2.19)$$

Take the second term in (2.14) and apply the chain rule to $\frac{\partial e^{j\theta(t)}}{\partial t}$.

$$A(t) \frac{\partial e^{j\theta(t)}}{\partial t} = A(t)\, e^{j\theta(t)} j \frac{\partial \theta(t)}{\partial t} \quad (2.20)$$

Equations (2.19) and (2.20) resembles each other. So, the phase equation can be written as

$$\frac{\partial \theta(t)}{\partial t} = \omega_0 + \frac{\omega_0}{2Q} Im \left(\frac{V_{inj}(t)}{V_{out}(t)} \right) \quad (2.21)$$

Imaginary part is taken to cancel the j term in the resulting expression so that $\phi(t)$ should be a real phase function.

Now, take part 1 of equation (2.17)

$$A(t)\, e^{j\theta(t)} \frac{\omega_0 \mu}{2Q} \left(\alpha_0^2 - A^2(t)\right) \quad (2.22)$$

Equation (2.22) resembles $e^{j\theta(t)} \frac{\partial A(t)}{\partial t}$, the amplitude equation can be written as

$$\frac{\partial A(t)}{\partial t} = \mu \frac{\omega_0}{2Q} A(t) \left(\alpha_0^2 - A^2(t)\right) \quad (2.23)$$

To complete equation (2.14) $\frac{\omega_0}{2Q}A\left(t\right)Re\left(\frac{V_{inj}(t)}{V_{out}(t)}\right)$ term is added, since only imaginary part is considered for phase variation term.

$$\frac{\partial A\left(t\right)}{\partial t}=\mu\frac{\omega_0}{2Q}A\left(t\right)\left(\alpha_0^2-A^2\left(t\right)\right)+\frac{\omega_0}{2Q}A\left(t\right)Re\left(\frac{V_{inj}\left(t\right)}{V_{out}\left(t\right)}\right) \tag{2.24}$$

Two transient equations are

$$\frac{\partial A\left(t\right)}{\partial t}=\mu\frac{\omega_0}{2Q}A\left(t\right)\left(\alpha_0^2-A^2\left(t\right)\right)+\frac{\omega_0}{2Q}A\left(t\right)Re\left(\frac{V_{inj}\left(t\right)}{V_{out}\left(t\right)}\right)\rightarrow\text{amplitude dynamics} \tag{2.25}$$

$$\frac{\partial\theta\left(t\right)}{\partial t}=\omega_0+\frac{\omega_0}{2Q}Im\left(\frac{V_{inj}\left(t\right)}{V_{out}\left(t\right)}\right)\rightarrow\text{phase dynamics} \tag{2.26}$$

Insert (2.1) into (2.26)

$$\frac{\partial\theta\left(t\right)}{\partial t}=\omega_0+\frac{\omega_0}{2Q}Im\left(\frac{A_{inj}\left(t\right)e^{j\theta_{inj}(t)}}{A\left(t\right)e^{j\theta(t)}}\right) \tag{2.27}$$

Phase equation is arranged as

$$\frac{\partial\theta\left(t\right)}{\partial t}=\omega_0+\frac{\omega_0}{2Q}\frac{A_{inj}\left(t\right)}{A\left(t\right)}\sin\left[\theta_{inj}\left(t\right)-\theta\left(t\right)\right] \tag{2.28}$$

According to phase equation, phase change of free-running oscillator with respect to time depends on angular free-running frequency, amplitude of injected signal, amplitude of free-running signal and sin of difference between phases of injected and free-running signals.

2.2.1 Master-Slave Locking

The coupling between two oscillators does not have to be bilateral all the time. A stable oscillator, such as a signal generator, can not be affected by a free-running oscillator under coupling configuration. In this situation, stable oscillator becomes

the master and free-running oscillator becomes the slave, as shown in Figure 2.4. Frequency of the slave oscillator follows frequency of the master oscillator. A phase dynamics is also provided at steady-state.

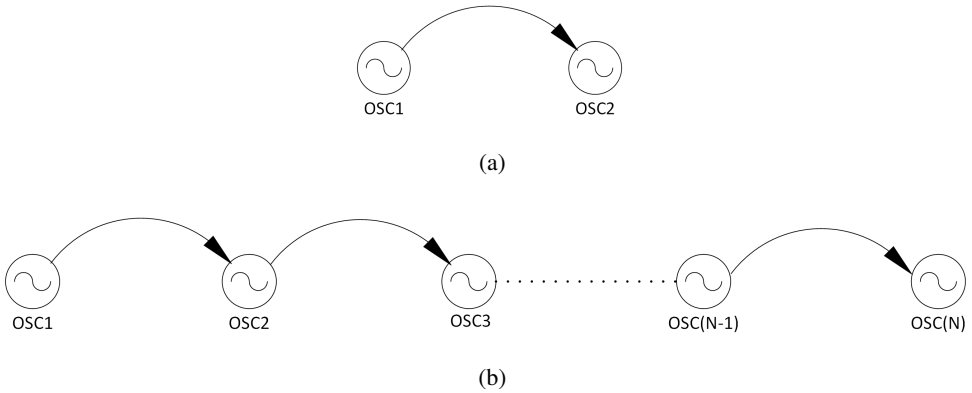

Figure 2.4: (a) Unilateral Coupling Between Two Oscillators and (b) Unilateral Coupling Between N Oscillators

At $t = t_0$, when there is no coupling between the oscillators, phase terms of free-running and injected oscillators are written as follows.

$$\theta(t_0) = \omega_0 t_0 + \phi(t_0) \tag{2.29}$$

$$\theta_{inj}(t_0) = \omega_{inj} t_0 + \psi(t_0) \tag{2.30}$$

At $t = t_0 + \tau$ OSC2 locks onto OSC1. OSC2 begins to oscillate at the injected frequency ω_{inj} at that moment. Phase term equations for the two oscillators become

$$\theta(t_0 + \tau) = \omega_{inj} t_0 + \omega_{inj}\tau + \phi(t_0 + \tau) \tag{2.31}$$

$$\theta_{inj}(t_0 + \tau) = \omega_{inj} t_0 + \omega_{inj}\tau + \psi(t_0 + \tau) \tag{2.32}$$

Inserting (2.31) and (2.32) into (2.28), phase dynamics equation becomes

$$\frac{\partial\theta(t)}{\partial t} = \omega_0 + \frac{\omega_0}{2Q}\frac{A_{inj}(t)}{A(t)}\sin\left[\psi(t_0 + \tau) - \phi(t_0 + \tau)\right] \tag{2.33}$$

Taking the derivative of equation (2.31)

$$\frac{\partial\theta\left(t\right)}{\partial t}=\omega_{inj}+\frac{\partial\phi\left(t\right)}{\partial t} \tag{2.34}$$

Inserting (2.34) into (2.33)

$$\frac{\partial\phi\left(t\right)}{\partial t}=\omega_{0}-\omega_{inj}+\frac{\omega_{0}}{2Q}\frac{A_{inj}\left(t\right)}{A\left(t\right)}\sin\left[\psi\left(t_{0}+\tau\right)-\phi\left(t_{0}+\tau\right)\right] \tag{2.35}$$

At steady-state $\frac{\partial\phi(t)}{\partial t}\rightarrow 0$ means there is no phase variation of slave oscillator under locking.

$$0=\omega_{0}-\omega_{inj}+\frac{\omega_{0}}{2Q}\frac{A_{inj}\left(t\right)}{A\left(t\right)}\sin\left[\psi\left(t_{0}+\tau\right)-\phi\left(t_{0}+\tau\right)\right] \tag{2.36}$$

Define

$$\Delta\phi\left(t\right)=\psi\left(t\right)-\phi\left(t\right) \tag{2.37}$$

Then equation (2.36) becomes

$$\omega_{inj}-\omega_{0}=\frac{\omega_{0}}{2Q}\frac{A_{inj}\left(t\right)}{A\left(t\right)}\sin\left[\Delta\phi\left(t_{0}+\tau\right)\right] \tag{2.38}$$

Rearranging (2.38)

$$\omega_{inj}-\omega_{0}=\Delta\omega_{lock}\sin\left[\Delta\phi\left(t_{0}+\tau\right)\right] \tag{2.39}$$

where $\Delta\omega_{lock}$ is the locking bandwidth, half of the locking range, defined as follows

$$\Delta\omega_{lock}=\frac{\omega_{0}}{2Q}\frac{A_{inj}\left(t\right)}{A\left(t\right)} \tag{2.40}$$

As seen by the equation (2.40) the locking bandwidth is inversely proportional with the quality factor, Q, of the free-running oscillator. This means that there is a trade-off between locking range and phase noise of the oscillator.

The phase difference between master and slave oscillators are expressed using following equations.

$$\sin\left[\Delta\phi\left(t\right)\right] = \frac{\omega_{inj} - \omega_0}{\Delta\omega_{lock}} \tag{2.41}$$

$$\Delta\phi\left(t\right) = \arcsin\left[\frac{\omega_{inj} - \omega_0}{\Delta\omega_{lock}}\right], -\frac{\pi}{2} \leq \Delta\phi\left(t\right) \leq \frac{\pi}{2} \tag{2.42}$$

$$\omega_{inj} = \omega_0 \mp \Delta\omega_{lock}, \Delta\phi\left(t\right) = \mp\frac{\pi}{2} \tag{2.43}$$

From equation (2.43) it can be seen that ω_{inj} is tuned over the locking range of the oscillator $(\omega_0 \mp \Delta\omega_{lock})$ and the associated phase difference $\Delta\phi\left(t\right)$ varies from $-\frac{\pi}{2}$ to $\frac{\pi}{2}$.

$$\Delta\omega_{lock} > \left|\omega_{inj} - \omega_0\right| for -\frac{\pi}{2} < \Delta\phi\left(t\right) < \frac{\pi}{2} \tag{2.44}$$

The oscillator can be synchronized with an injected signal as long as $\Delta\omega_{lock} > |\omega_{inj} - \omega_0|$, where $\Delta\omega_{lock}$ represents half of the entire locking range. If $\Delta\omega_{lock} \leq |\omega_{inj} - \omega_0|$, the oscillator cannot lock onto the injected signal and the nonlinearity of the oscillator will generate mixing products in the coupled oscillator system [8].

2.2.2 Peer-Peer Locking

Peer-peer locking occurs when there is an interaction between each oscillator in the coupled system. For a system of two oscillators, there is coupling from OSC1 to OSC2, as in master-slave locking case, and also there is coupling from OSC2 to OSC1 as shown in Figure 2.5.

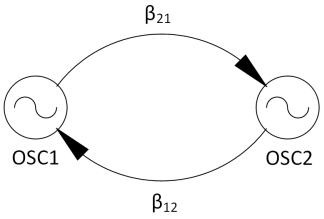

Figure 2.5: Bilateral Coupling Between Two Oscillators

N number of oscillators can be locked as peer-peer in different configurations such as bilateral coupling between nearest neighbours, coupling through an N-Port network and global coupling. These configurations are shown in Figure 2.6.

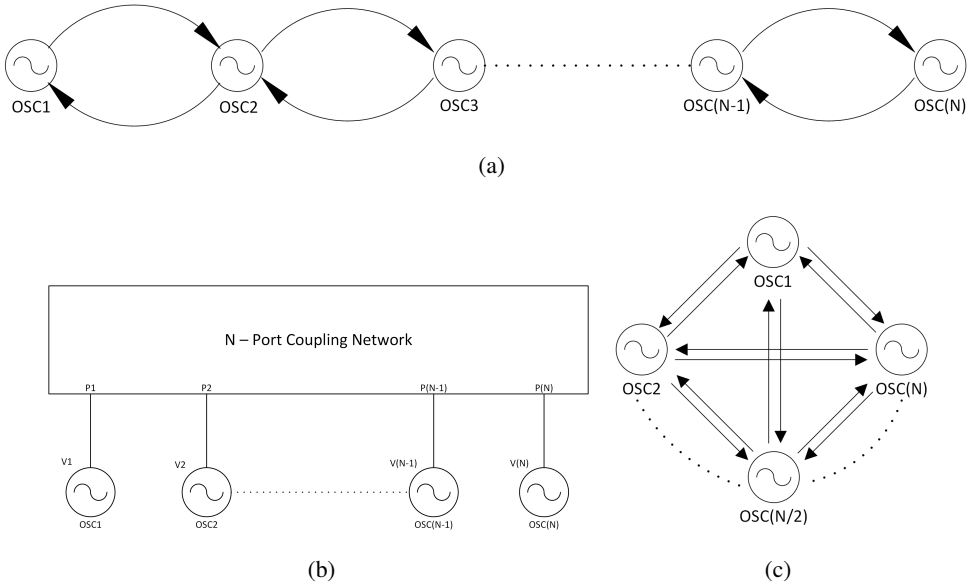

Figure 2.6: (a) Bilateral Coupling, (b) Coupling Through N-Port Network and (c) Global Coupling

For an N-coupled oscillator system coupling between each oscillator is defined using a coupling coefficient as follows

$$\beta_{ij} = \alpha_{ij} e^{-j\varphi_{ij}} \tag{2.45}$$

where β_{ij} is the coupling coefficient between oscillators, α_{ij} is the magnitude of coupling coefficient and φ_{ij} is the phase of coupling coefficient. For a reciprocal system $\beta_{ij} = \beta_{ji}$. The coupling coefficient is unitless.

The injected signal seen by the ith oscillator, $V_{inj}\,(t)$, is defined as

$$V_{inj}(t) = \sum_{\substack{j=1 \\ j \neq i}}^{N} \beta_{ij} V_j(t) \tag{2.46}$$

where $V_j(t)$ is the output voltage of the jth oscillator.

N oscillators have approximately the same Q and μ factors. So, phase dynamics equation (2.26) can be written for this system as

$$\frac{\partial V_i(t)}{\partial t} = V_i(t)\left[\frac{\mu\omega_i}{2Q}\left(\alpha_i^2 - |V_i(t)|^2\right) + j\omega_i\right] + \frac{\omega_i}{2Q} V_{inj}(t) \tag{2.47}$$

Substituting (2.46) into (2.47)

$$\frac{\partial V_i(t)}{\partial t} = V_i(t)\left[\frac{\mu\omega_i}{2Q}\left(\alpha_i^2 - |V_i(t)|^2\right) + j\omega_i\right] + \frac{\omega_i}{2Q}\sum_{\substack{j=1 \\ j \neq i}}^{N} \beta_{ij} V_j(t) \tag{2.48}$$

The output voltage of the ith oscillator is

$$V_i(t) = A_i(t)\, e^{j[\omega_i t + \phi_i(t)]} = A_i(t)\, e^{j\theta_i(t)} \tag{2.49}$$

Taking the derivative of (2.49) and applying chain rule

$$\frac{\partial V_i(t)}{\partial t} = j\left[\omega_i + \frac{\phi_i(t)}{\partial t} - j\frac{1}{A_i(t)}\frac{\partial A_i(t)}{\partial t}\right] V_i(t) \tag{2.50}$$

The same procedure as applied to equation (2.13) is applied here also. Equation (2.48) is divided into two parts to obtain amplitude and phase dynamics equations.

$$\frac{\partial A_i(t)}{\partial t} = A_i(t)\left[\frac{\mu\omega_i}{2Q}\left(\alpha_i^2 - |A_i(t)|^2\right)\right] + \frac{\omega_i}{2Q}\sum_{\substack{j=1 \\ j \neq i}}^{N} \alpha_{ij} A_j(t)\cos\left[\theta_i(t) - \theta_j(t) + \varphi_{ij}\right] \tag{2.51}$$

$$\frac{\partial\theta_i(t)}{\partial t} = \omega_i - \frac{\omega_i}{2Q}\left\{\sum_{\substack{j=1\\ j\neq i}}^{N} \alpha_{ij}\frac{A_j(t)}{A_i(t)}\sin\left[\theta_i(t) - \theta_j(t) + \varphi_{ij}\right]\right\}, i = 1, 2, 3, ..., N \tag{2.52}$$

Amplitude and phase dynamics equations can be rewritten according to the strength of the coupling between the oscillators. Three cases that can be occurred in peer-peer locking configuration are zero coupling, weak coupling and strong coupling. They are examined in detail as follows.

2.2.2.1 Zero coupling ($\beta_{ij} \to 0$)

This case is identical to the case where oscillators operate independently, meaning there is no coupling between oscillators. No locking occurs. Amplitude and phase dynamics equations become

$$\left[\frac{\partial A_i(t)}{\partial t}\right]_{\beta_{ij}=0} = A_i(t)\left[\frac{\mu\omega_i}{2Q}\left(\alpha_i^2 - |A_i(t)|^2\right)\right]; i = 1, 2, 3, ..., N \tag{2.53}$$

$$\left[\frac{\partial\theta_i(t)}{\partial t}\right]_{\beta ij=0} = \omega_i; i = 1, 2, 3, ..., N \tag{2.54}$$

2.2.2.2 Weak Coupling ($0 < \beta_{ij} \ll 1$)

Amplitudes of the oscillators in the N-coupled oscillator system remains close to its free-running values. Therefore, the system dynamics of N-coupled oscillators essentially are governed and influenced by the phase dynamics.

The oscillators in the N-coupled oscillator system lock to a single frequency ω_s for weak coupling system.

$$\left[\frac{\partial\theta_i(t)}{\partial t}\right]_{i=1,2,3,...,N} \to \omega_s \tag{2.55}$$

Phase dynamics equation is arranged to obtain this common frequency as

$$\omega_s = \omega_i - \frac{\omega_i}{2Q}\left\{\sum_{\substack{j=1\\ j\neq i}}^{N} \alpha_{ij}\frac{A_j(t)}{A_i(t)}\sin\left[\theta_i(t) - \theta_j(t) + \varphi_{ij}\right]\right\}; i = 1, 2, 3, ..., N \quad (2.56)$$

2.2.2.3 Strong Coupling ($0 \ll \beta_{ij} < 1$)

As the coupling strength increases, the coupling network will perturb the oscillator and therefore steady-state phase relationships could not be maintained any more. So, strong coupling case will not be analysed.

2.3 Phase Noise In Coupled Oscillators

Phase noise is another concern for coupled oscillators. For each locking scheme, phase noise is expected to improve. In order to observe the improvement analytically, noise term should be added to phase dynamics equation (2.24) and solved for N-oscillator array system. This analysis is presented in references [8] and [18] in detail. Figure 2.7 shows a free-running oscillator with noise impedance added.

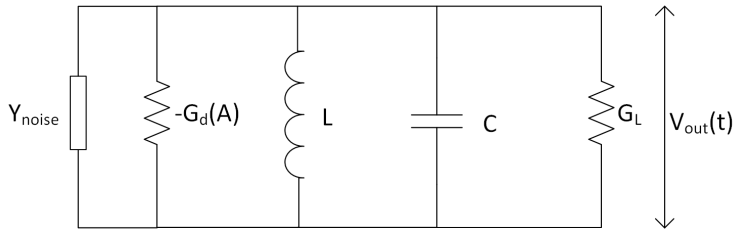

Figure 2.7: Oscillator Model with Noise Admittance

$$Y_{noise} = G_{noise} + jB_{noise} \quad (2.57)$$

$$Y_n = \frac{Y_{noise}}{G_L} = G_n + jB_n \quad (2.58)$$

where G_L is the oscillator load admittance in free-running state, Y_n is the normalized noise admittance with respect to load G_L, G_n is the in-phase component and B_n is the quadrature component of the noise source.

Phase dynamics equation with the noise source component added for N-OSC system:

$$\frac{\partial\theta_i(t)}{\partial t} = \omega_i - \frac{\omega_i}{2Q}\left\{\sum_{\substack{j=1\\ j\neq i}}^{N} \alpha_{ij}\frac{A_j(t)}{A_i(t)}\sin\left[\theta_i(t) - \theta_j(t) + \varphi_{ij}\right]\right\} - \left[\frac{\omega_i}{2Q}B_{ni}\right], i = 1, 2, 3, ..., N \tag{2.59}$$

For noise analysis, phase dynamics equation is perturbed by substituting the following into equation (2.3)

$$A_i \Rightarrow \hat{A}_i + \delta A_i \tag{2.60a}$$

$$\theta_i \Rightarrow \hat{\theta}_i + \delta\theta_i \tag{2.60b}$$

where $\left(\hat{A}_i, \hat{\theta}_i\right)$ are the steady-state solutions for amplitude and phase dynamics equations and $(\delta A_i, \delta\theta_i)$ are the amplitude and phase fluctuations of the ith oscillator. For phase noise analysis there is no need to analyse the amplitude dynamics equation.

Phase dynamics equation becomes as follows

$$\begin{aligned}\frac{\partial\delta\theta_i}{\partial t} = & -\omega_{3dB}\sum_{\substack{j=1\\ j\neq i}}^{N}\frac{\alpha_{ij}\hat{A}_j}{\hat{A}_i}\frac{\delta A_j - \delta A_i}{\hat{A}_i}\sin\left(\hat{\theta}_i - \hat{\theta}_j\right) \\ & -\omega_{3dB}\sum_{\substack{j=1\\ j\neq i}}^{N}\alpha_{ij}\left(\delta\theta_i - \delta\theta_j\right)\frac{\hat{A}_j}{\hat{A}_i}\cos\left(\hat{\theta}_i - \hat{\theta}_j\right) - \omega_{3dB}B_{ni}(t)\end{aligned} \tag{2.61}$$

where $\omega_{3dB} = \frac{\omega_i}{2Q}$ is half the 3 dB bandwidth of the oscillator tank circuit.

Taking Fourier transform of equation (2.61):

$$\left(\frac{j\omega}{\omega_{3dB}}\right)\delta\tilde{\theta}_i = -\sum_{\substack{j=1\\j\neq i}}^{N}\alpha_{ij}\frac{\hat{A}_j}{\hat{A}_i}\left(\frac{\delta\hat{A}_j-\hat{A}_i}{\hat{A}_i}\right)\sin\left(\hat{\theta}_i-\hat{\theta}_j\right) - \sum_{\substack{j=1\\j\neq i}}^{N}\alpha_{ij}\left(\delta\tilde{\theta}_i-\delta\tilde{\theta}_j\right)\frac{\hat{A}_j}{\hat{A}_i}\cos\left(\hat{\theta}_i-\hat{\theta}_j\right)-\tilde{B}_{ni} \tag{2.62}$$

In equation (2.62), the first term of RHS represents AM-to-PM noise and the second term is the PM-to-PM noise. There is no transformation between the AM noise and the PM noise when the oscillators in the array are in-phase, i.e. $\theta_i = \theta_j$ for all $i \neq j$. Therefore, equation (2.62) reduces to the following under this assumption.

$$\left(\frac{j\omega}{\omega_{3dB}}\right)\delta\tilde{\theta}_i = -\sum_{\substack{j=1\\j\neq i}}^{N}\alpha_{ij}\left(\delta\tilde{\theta}_i-\delta\tilde{\theta}_j\right)\frac{\hat{A}_j}{\hat{A}_i}\cos\left(\hat{\theta}_i-\hat{\theta}_j\right)-\tilde{B}_{ni} \tag{2.63}$$

Focusing on PM-to-PM noise conversion for simplicity and assuming all steady-state amplitudes are identical, phase noise of the ith uncoupled oscillator can be written as

$$\left|\delta\tilde{\theta}_i\right|^2_{uncoupled} = \frac{\left|\tilde{B_{ni}}\right|^2}{\left(\frac{\omega}{\omega_{3dB}}\right)^2} \tag{2.64}$$

1. Globally Coupled Oscillator Arrays

   By connecting the oscillators through coupling circuits as in Figure 2.6.c, phase noise of each oscillator and the total phase noise of the array reduces in direct proportion to the number of oscillators in the array near the carrier frequency as in equations (2.65) and (2.66). Phase noise far from the carrier is the same as phase noise of a free-running oscillator as in equation (2.67)

   Total phase noise of the array:

   $$\left|\delta\tilde{\theta}_{total}\right|^2 = \frac{1}{N}\left|\delta\tilde{\theta}_i\right|^2_{uncoupled} \tag{2.65}$$

   Phase noise near the carrier ($\omega \ll \Delta\omega_{lock}$):

   $$\left|\delta\tilde{\theta}_i\right|^2 \longrightarrow \frac{1}{N}\left|\delta\tilde{\theta}\right|^2_{uncoupled} \tag{2.66}$$

Phase noise far from the carrier:

$$\left|\delta\tilde{\theta}_i\right|^2 \longrightarrow \left|\delta\tilde{\theta}\right|^2_{uncoupled} \tag{2.67}$$

2. Nearest-Neighbour Bilateral Arrays

   Phase noise of each oscillator reduces to $\frac{1}{N}$ of the phase noise of a free-running oscillator as in the case for globally coupled arrays as long as $\cos\delta\theta \neq 0$ as shown in equation (2.68). Phase noise immediately returns to its free-running value at the locking range edge. Therefore, locking has no effect on PM noise outside the locking range.

$$\frac{\left|\delta\tilde{\theta}_i\right|^2_{\delta\hat{\theta}\neq 0}}{\left|\delta\tilde{\theta}_i\right|^2_{uncoupled}} \approx \frac{1}{N} \tag{2.68}$$

3. Unilaterally Injection Locked Arrays

   This locking scheme is the master-slave configuration as in Figure 2.4.b. At the carrier frequency, phase noise of the output signal is equal to the 1st stage oscillator, i.e. the master oscillator. The total noise of the array could be significantly reduced using a low noise source at the 1st stage.

   Phase noise of the total array and slave oscillators do not improve by this configuration. A low phase noise can only be obtained by using a low noise master oscillator.

4. Coupling Through N-Port Network

   The result for this configuration, shown in Figure 2.6b, is the same as the globally coupled oscillator arrays. One can conclude that the total PM noise of N oscillators coupled through an arbitrary reciprocal network always leads to a $\frac{1}{N}$ reduction in the total phase noise.

$$\left|\delta\tilde{\theta}_{total}\right|^2 = \frac{1}{N}\left|\delta\tilde{\theta}_i\right|^2_{uncoupled} \tag{2.69}$$

CHAPTER 3

DESIGN AND SIMULATION OF A COUPLED OSCILLATOR SYSTEM

3.1 Introduction

In this chapter, a Colpitts oscillator is designed in order to verify the locking theory given in Chapter 2. Time-domain and frequency-domain simulations are run through the design using ADS simulation environment for both free-running oscillator circuit and coupled systems. The reason of choosing Colpitts oscillator is that it is the most frequently used design for high performance circuits.

3.2 Design of A Colpitts Oscillator

An oscillator circuit must be consisted of three parts, namely active device, resonator circuit and a load circuit as shown in Figure 3.1. Resonator circuit determines the frequency of oscillation and the active device is responsible for the gain of the oscillator.

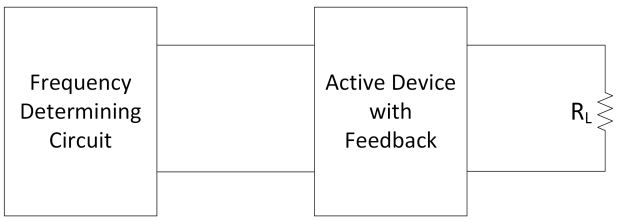

Figure 3.1: A Schematic Diagram of A One-Port Oscillator

A conventional Colpitts oscillator is chosen as shown in Figure 3.2. There are variations of this circuit as Hartley and Clapp-Gouriet circuits. Interested readers may find the design and derivation of the three oscillator circuits in references [5], [6] and [7].

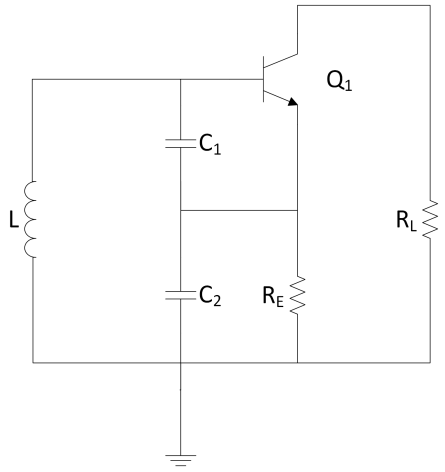

Figure 3.2: Colpitts Oscillator Configuration

The basic design procedure of a Colpitts oscillator is the same whether using FET or BJT as the active device. BJTs are used up to 20 GHz and easily available both in simulation world and real world. So, NXP BFG520W transistor is chosen for the experiments because it is a highly linear transistor and there are verified oscillator circuits using this transistor [30].

3.2.1 DC Biasing

While designing the circuit, phase noise is not a concern. In fact, phase noise should be degraded to obtain a wider locking bandwidth. Equation (2.40), derived in Chapter 2, gives the relation between the locking range and the quality factor. The higher the quality factor, the narrower the locking range.

From equation (2.40) the relation between phase noise and locking bandwidth can easily be seen.

$$\Delta\omega_{lock} \propto \frac{1}{Q} \tag{3.1}$$

Since phase noise is not a concern, the biasing circuit aims not to reduce the flicker noise and distortion but to maximize the output power of the oscillator. Bias resistors and emitter resistor are optimized to maximize the output power and the current driven from the supply.

The emitter current, I_E , is set to 16.75 mA and collector-emitter voltage, V_{CE} , is set to 4 V. Supply voltage is chosen as 12 V. So,

$$V_C = 12V \tag{3.2a}$$

$$V_E = V_C - V_{CE} \tag{3.2b}$$

$$R_E = \frac{V_E}{I_E} = 477\Omega \tag{3.2c}$$

R_E is set to 475Ω .

$$V_B = V_C \frac{R_2}{R_1 + R_2} \tag{3.3a}$$

$$V_B = V_{BE} + V_E \tag{3.3b}$$

where $V_{BE} = 0.8V$ from the datasheet of the transistor. Therefore

$$\frac{R_1}{R_2} = 0.36 \tag{3.4}$$

3.2.2 Frequency Determination

The resonator circuit is designed to obtain an oscillation frequency above 300 MHz. The output frequency can be calculated using the following equation

$$\omega_0 = \sqrt{\frac{1}{L}\left(\frac{1}{C_1} + \frac{1}{C_2}\right)} \tag{3.5}$$

Choosing $L = 22nH$ and $C_1, C_2 = 15pF$ in Figure 3.2, the oscillation frequency of the resonator circuit is determined as $f_0 = 391$ MHz by calculation. However, due to the parasitic effects, frequency of the real circuit will be different from this theoretical value. Also, even the model of the transistor is given, the simulation results may give a different frequency of oscillation.

Frequency control of the resonator circuit is needed to be able to stay in the Adler's locking bandwidth throughout the experiments. In order to control the frequency of oscillation a trimmer capacitor is connected parallel to C_2 . Trimmer capacitors are mechanically controlled capacitors. They are used in applications where there are no need to re-adjust the capacitance after the initial adjustment. It is chosen here, instead of a varactor, to minimize the complexity of the circuit.

Detailed design of a Colpitts oscillator is given in Appendix B.

3.3 Design of A Locking System

Two system designs will be applied to observe phase and frequency locking. These systems are master-slave and peer-peer systems as mentioned in Chapter 2.

3.3.1 Master-Slave System

This system will be consisted of a signal generator as master and Colpitts oscillator as slave. The two will be connected through a coupling resistor. The frequency control belongs to the master oscillator in this system. The system is shown in the Figure 3.3.

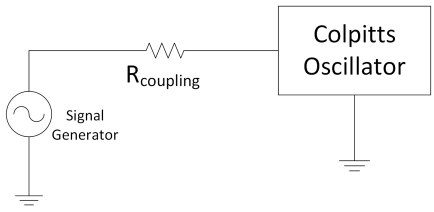

Figure 3.3: Master-Slave Locking System

The injection will be given through the base of the Colpitts oscillator. The simple circuit schematic is shown in Figure 3.4.

3.3.2 Peer-Peer System

Peer-peer system is consisted of two Colpitts oscillators. They are connected through the base of each oscillator. Oscillation frequency is determined by both of them. The

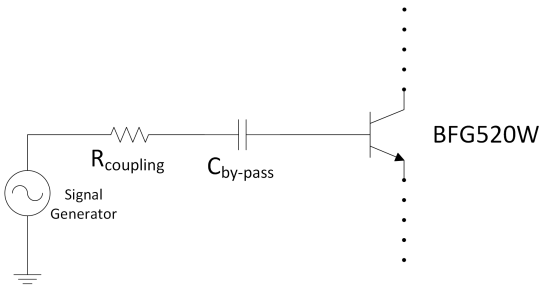

Figure 3.4: Master-Slave Locking Simplified Circuit

system is shown in Figure 3.5

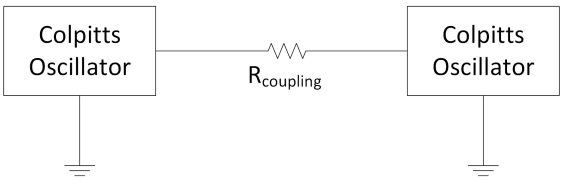

Figure 3.5: Peer-Peer Locking System

The two peer oscillators are connected through bases of their transistors. The simplified circuit schematic is shown in Figure 3.6.

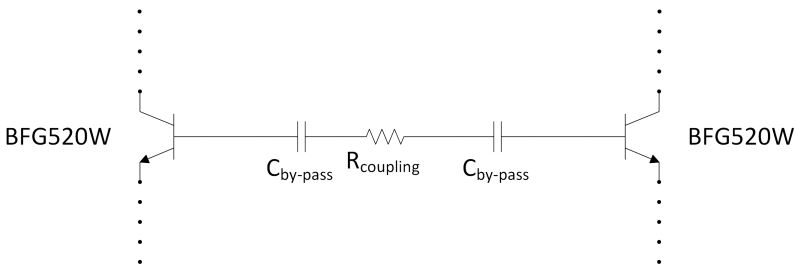

Figure 3.6: Peer-Peer Locking Simplified Circuit

3.4 Simulation Results

In order to observe locking phenomena through designs given in sections above simulations are conducted using Advanced Design System environment.

3.4.1 A Single Colpitts Oscillator

DC, transient and harmonic balance simulations of the oscillator circuit are conducted for $C_2 = 15pF$ given in Figure 3.2. A harmonic balance simulation is done by sweeping C_2 to simulate trimmer capacitor and observe capacitance versus oscillation frequency.

3.4.1.1 DC Simulation

First, DC simulation is done and bias resistors satisfying the given voltage conditions are determined. Figure 3.7 shows the circuit schematic for DC analysis.

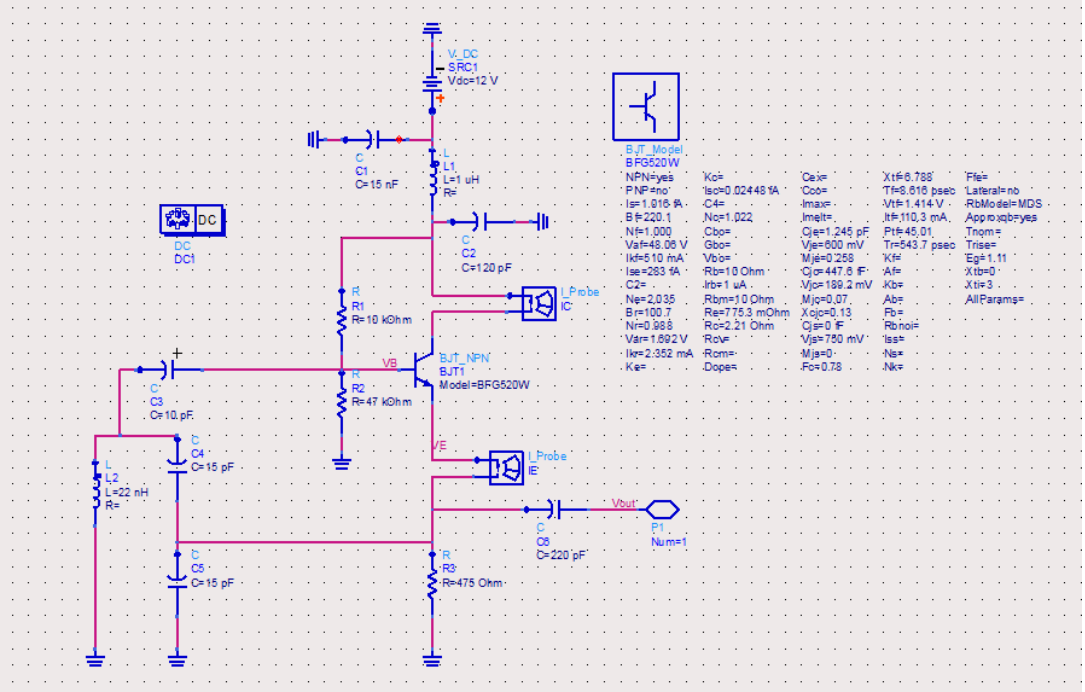

Figure 3.7: Circuit Schematic for DC Simulation

$R_1 = 10k\Omega$ is chosen and R_2 is determined as $47k\Omega$ by trial and error in order to obtain the required emitter voltage, V_E, and collector current, I_C. Figure 3.8 shows the transistor operating point for $R_1 = 10k\Omega$ and $R_2 = 47k\Omega$.

V_B, V_E voltages and I_C, I_E currents are shown in Figure 3.9 as a result of DC simulation. $V_{CE} = 4V$ and $I_E = 16.75mA$ is satisfied according to these results.

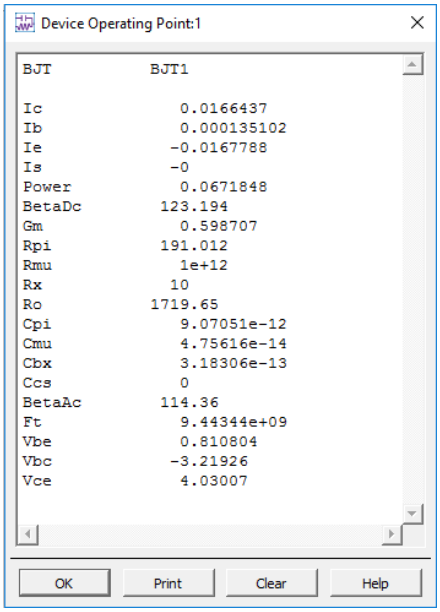

Figure 3.8: BFG520W Operating Point

freq	VB	VE	IC.i	IE.i
0.0000 Hz	8.781 V	7.970 V	16.64 mA	16.78 mA

Figure 3.9: Results of DC Analysis

3.4.1.2 Transient Simulation

Transient simulation of the oscillator circuit is conducted in order to observe the response in time-domain. The circuit schematic for this analysis is shown in Figure 3.10. As seen in Figure 3.11a oscillation starts before 50 nsec. Figure 3.11b shows the steady-state oscillations.

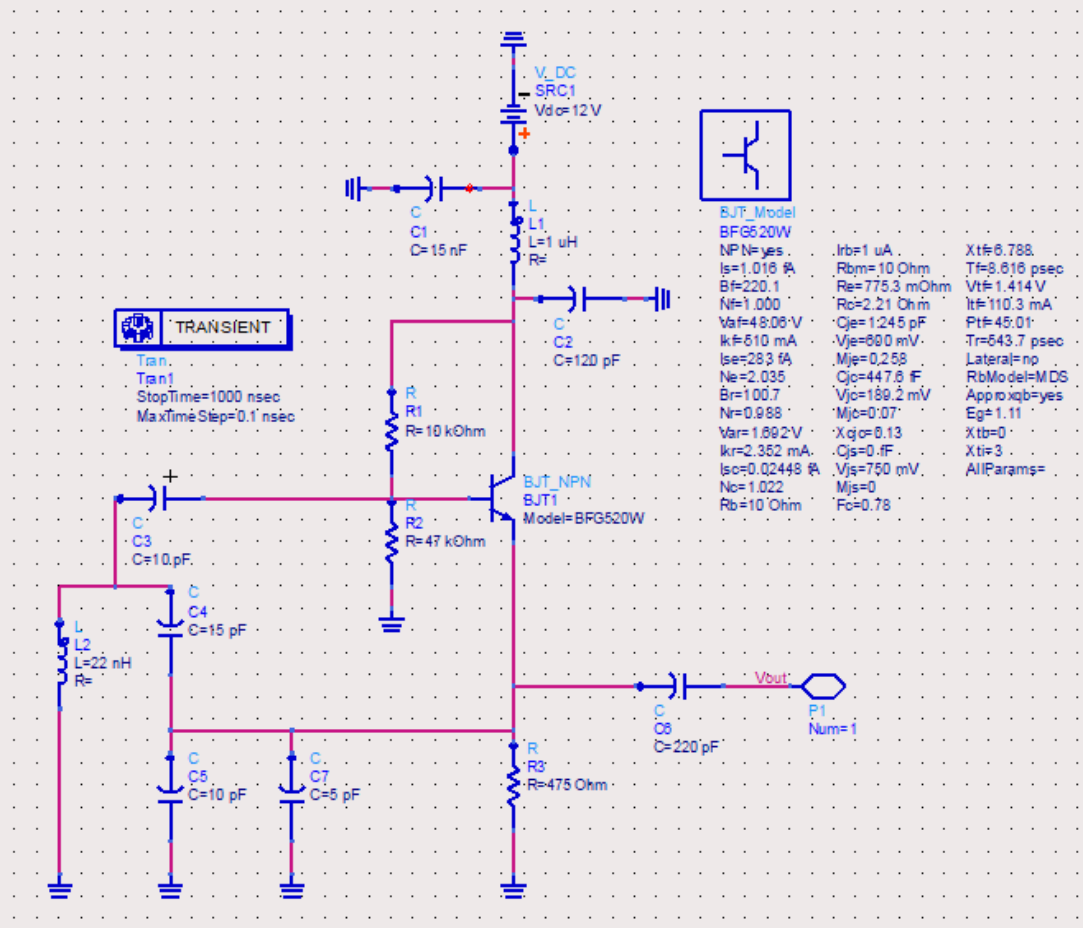

Figure 3.10: Circuit Schematic for Transient Analysis

Figure 3.12 shows the FFT of Figure 3.11b. FFT is applied to time domain output signal between 450-500 ns. So, a rectangular window is applied in time domain which results in a sinc function with side lobes in frequency domain. The products with $\Delta f = 20$ MHz around the fundamental signal are results of the rectangular window. Side lobes in frequency domain can be controlled by selecting different windows in time domain. Second harmonic of the fundamental signal with sinc side lobes is also seen at 720 MHz.

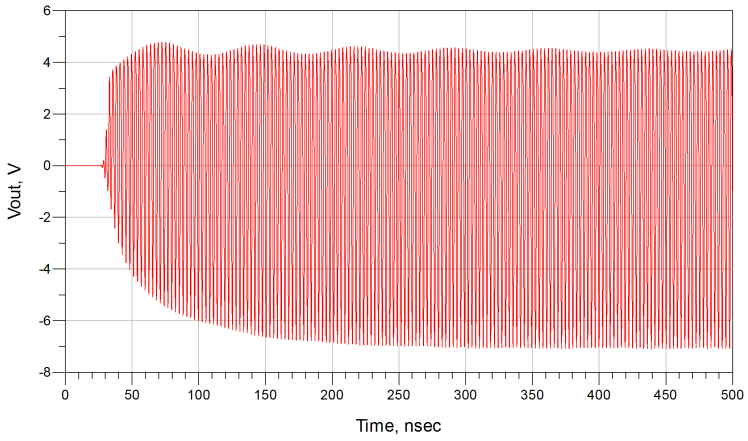

(a)

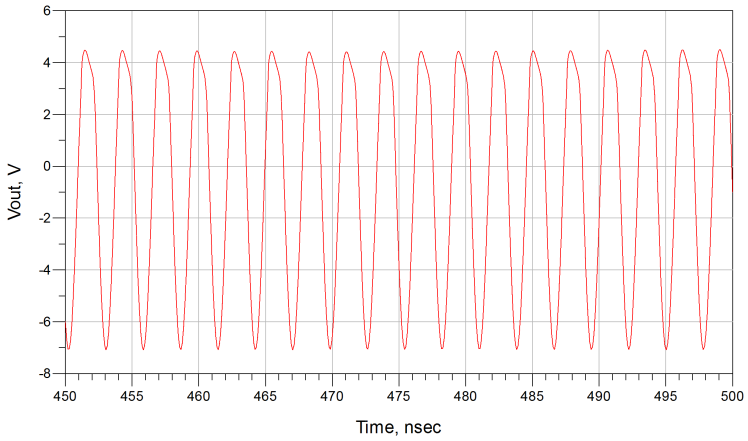

(b)

Figure 3.11: Transient Response of the Oscillator for (a) 0-500 nsec (b) 450-500 nsec

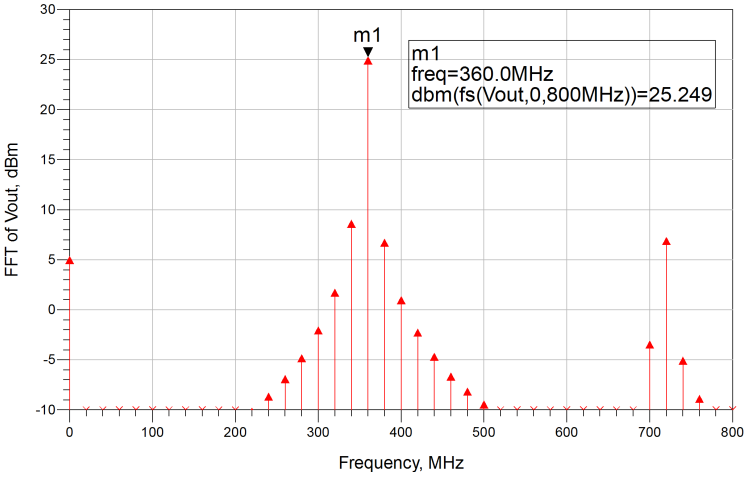

Figure 3.12: FFT of the Time Domain Signal for 450-500 nsec

3.4.1.3 Harmonic Balance Simulation

Harmonic balance analysis is performed to obtain a frequency-domain simulation result. Circuit schematic for this simulation is shown in Figure 3.13. An element called "OscPort" has to be placed between resonator and active device. The frequency-domain result and inverse fast Fourier transform of this result is shown in Figure 3.14.

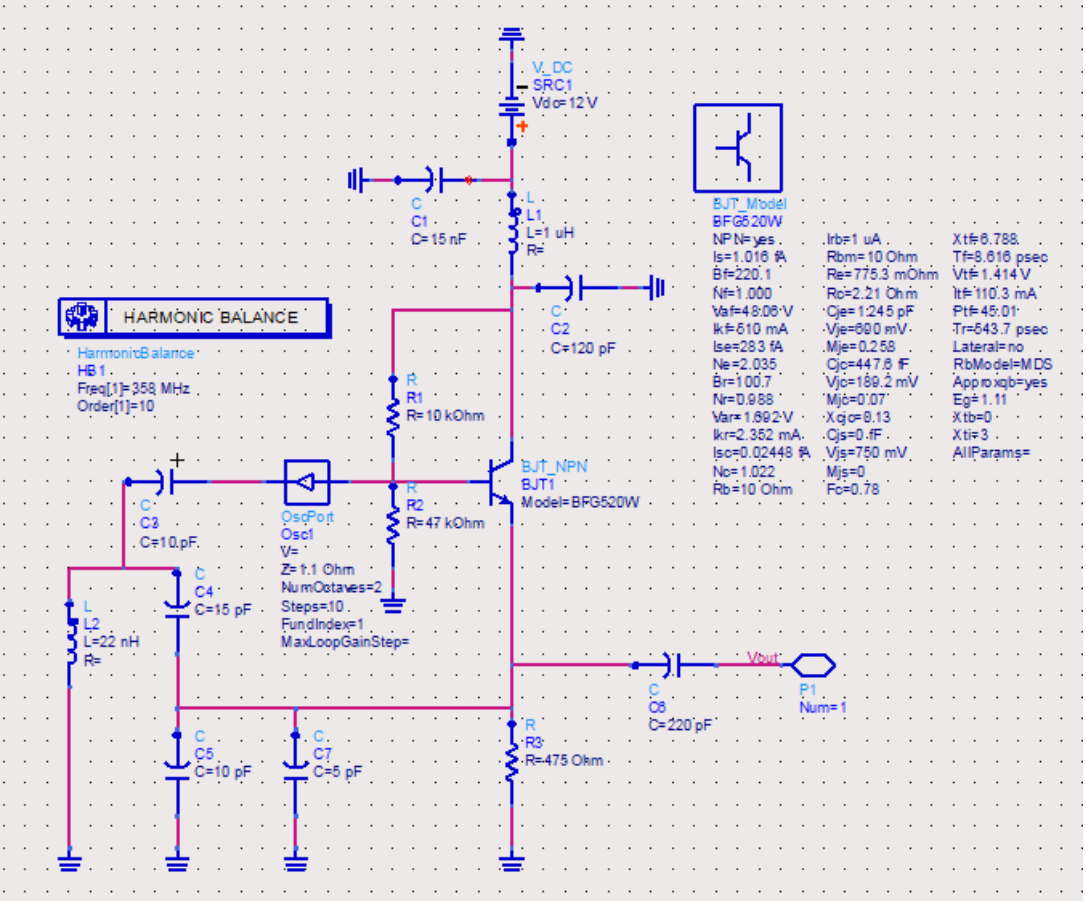

Figure 3.13: Circuit Schematic for Harmonic Balance Simulation

Phase noise of the Colpitts oscillator is also simulated. For this simulation "NoiseCon" simulation controller is added to the harmonic balance circuit schematic.

A final analysis is done to observe the frequency range of the oscillator. The trimmer capacitance range is chosen between 5-25 pF. This capacitor is connected to C_2 in Figure 3.2 in parallel configuration. Trimmer capacitance versus oscillation frequency graph is shown in Figure 3.16.

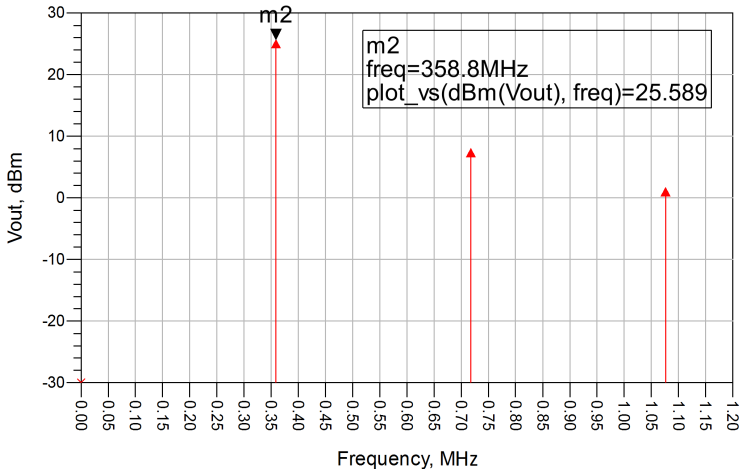

(a)

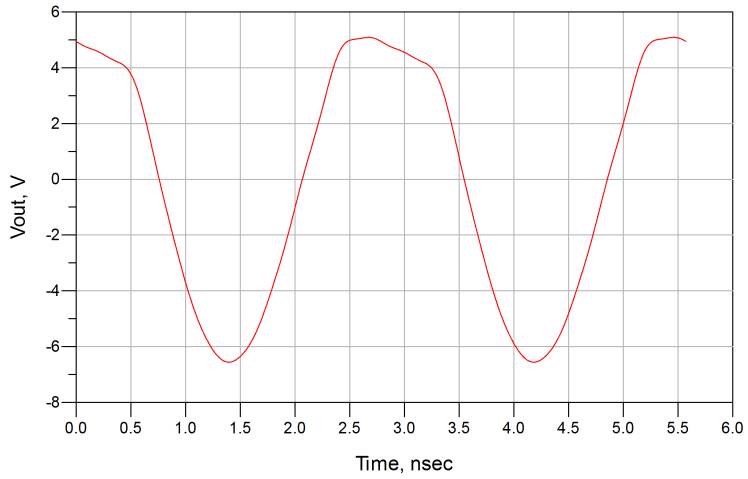

(b)

Figure 3.14: (a) Harmonic Balance Simulation Frequency Response (b) Harmonic Balance Simulation Time-Domain Response

3.4.2 Master-Slave System

Master-slave system simulations are done to observe the response of the Colpitts oscillator designed in above sections under injection by a signal generator. Since signal generator is more stable than the Colpitts oscillator, a change in its response is not expected through coupling. To examine the phase differences between master and slave, transient simulation is done. Frequency locking is observed from FFT of the time domain signal. Circuit schematic is given in Figure 3.17.

In this simulation, effects of the following parameters to the locking phenomena are

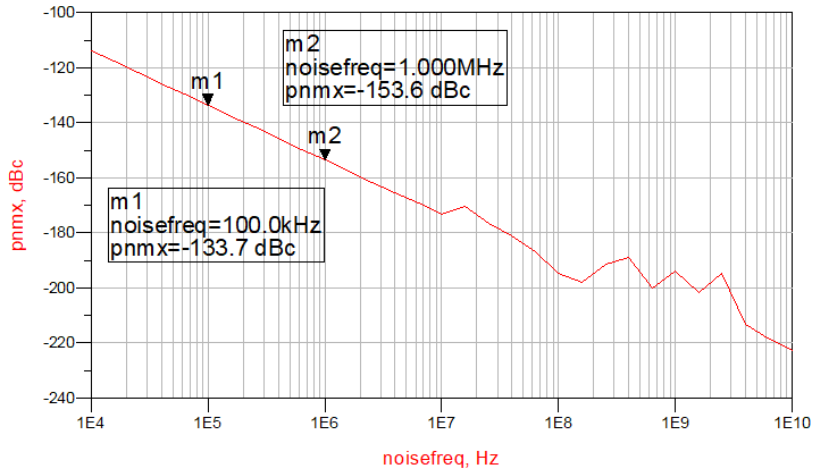

Figure 3.15: Phase Noise of Colpitts Oscillator

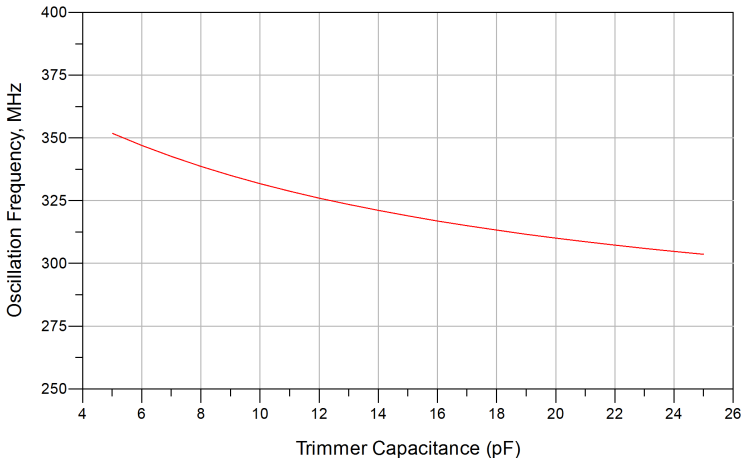

Figure 3.16: Trimmer Capacitance vs. Oscillation Frequency

observed.

1. Coupling resistor: R_c
2. Frequency of master oscillator: f_m
3. Amplitude of master oscillator: V_m

As the value of coupling resistor, R_c, is increased, injected signal amplitude, A_{inj} and therefore the amount of coupling are decreased. Coupling between signal generator and free-running oscillator is maintained until the value of R_c does not satisfy the locking bandwidth equation, (2.40), given in Chapter 2. The simulation results for

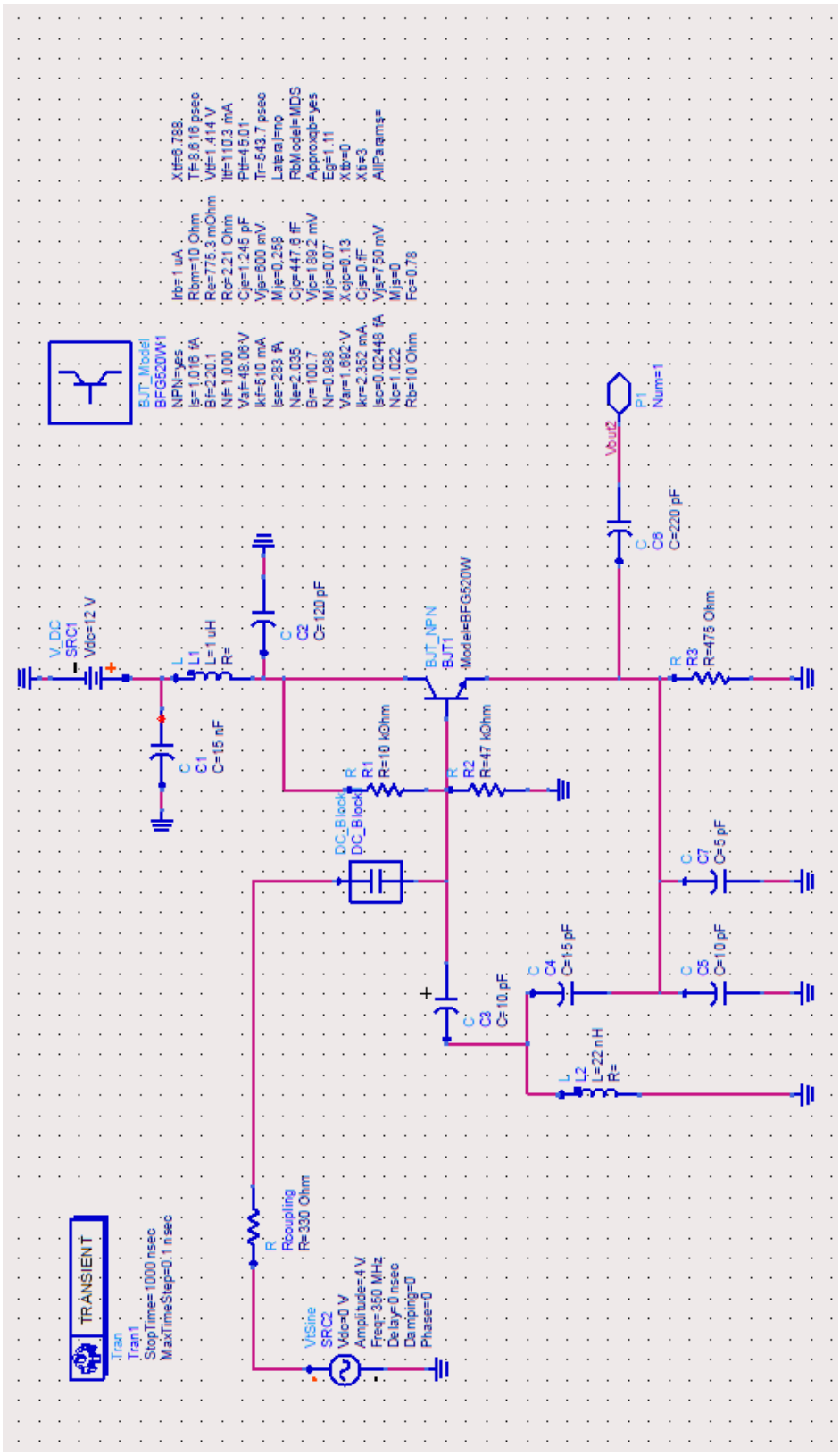

Figure 3.17: Circuit Schematic for Master-Slave Simulations

$R_c = 330\Omega, 1k\Omega, 4.7k\Omega, 10k\Omega$ are shown in Figures 3.18 and 3.19. In Figure 3.18d, the change in phase with respect to time can be seen. This means that phase locking does not occur for $R_c = 10k\Omega$.

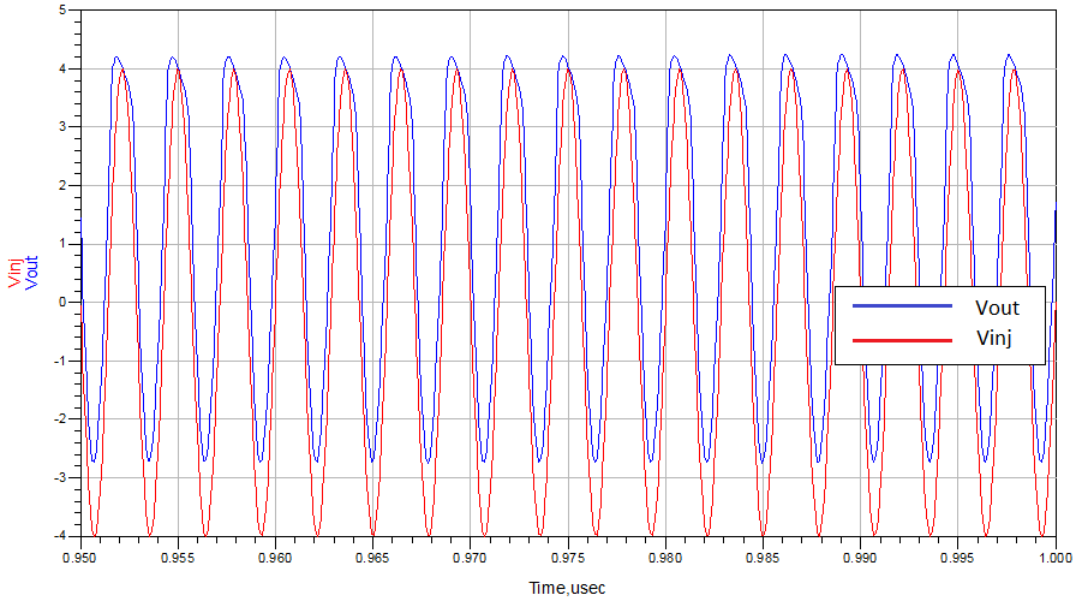

(a)

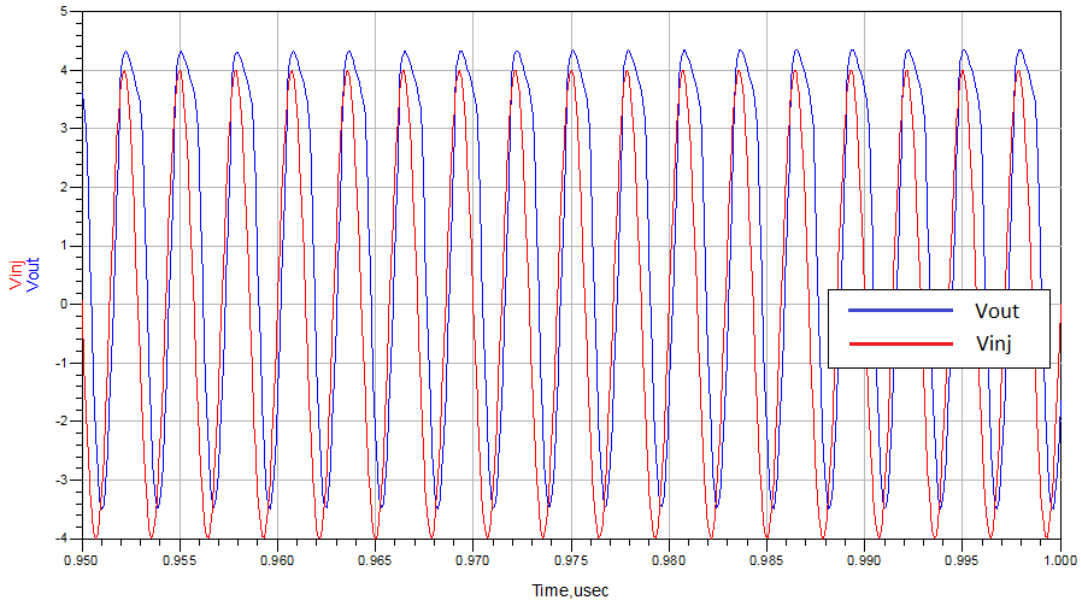

(b)

Figure 3.18: Time Domain Results for (a) $R_{coupling} = 330\Omega$, (b) $R_{coupling} = 1k\Omega$, (c) $R_{coupling} = 4.7k\Omega$ and (d) $R_{coupling} = 10k\Omega$

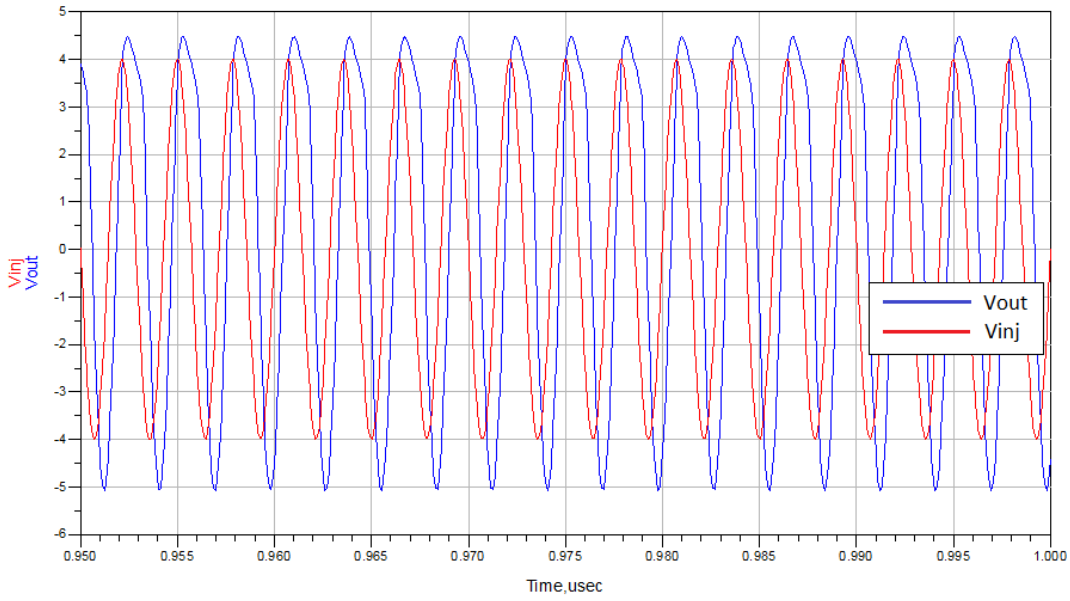

(c)

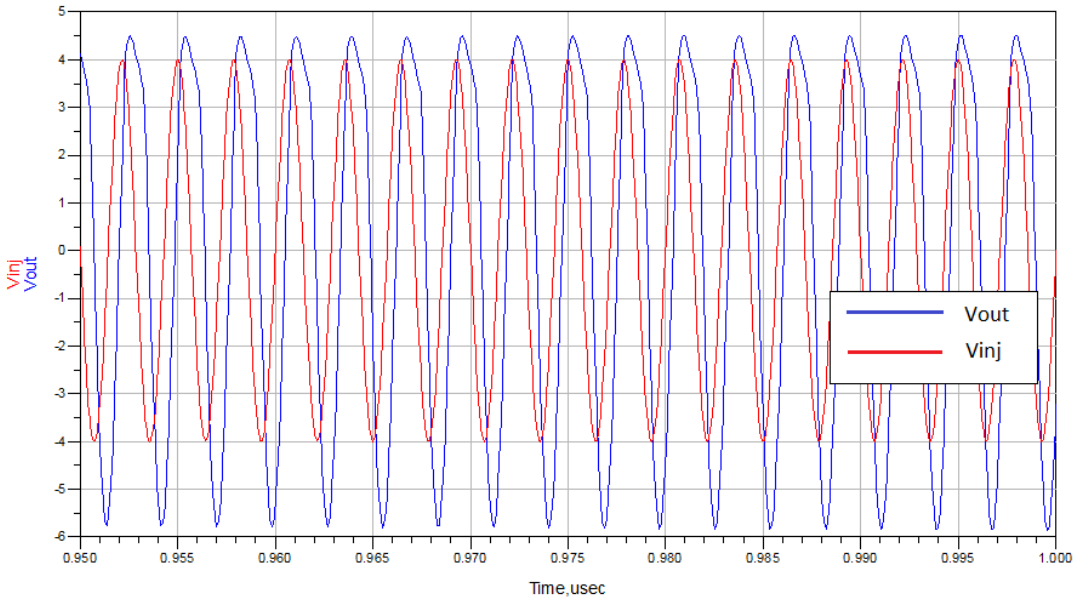

(d)

Figure 3.18: Time Domain Results for (a) $R_{coupling} = 330\Omega$, (b) $R_{coupling} = 1k\Omega$, (c) $R_{coupling} = 4.7k\Omega$ and (d) $R_{coupling} = 10k\Omega$

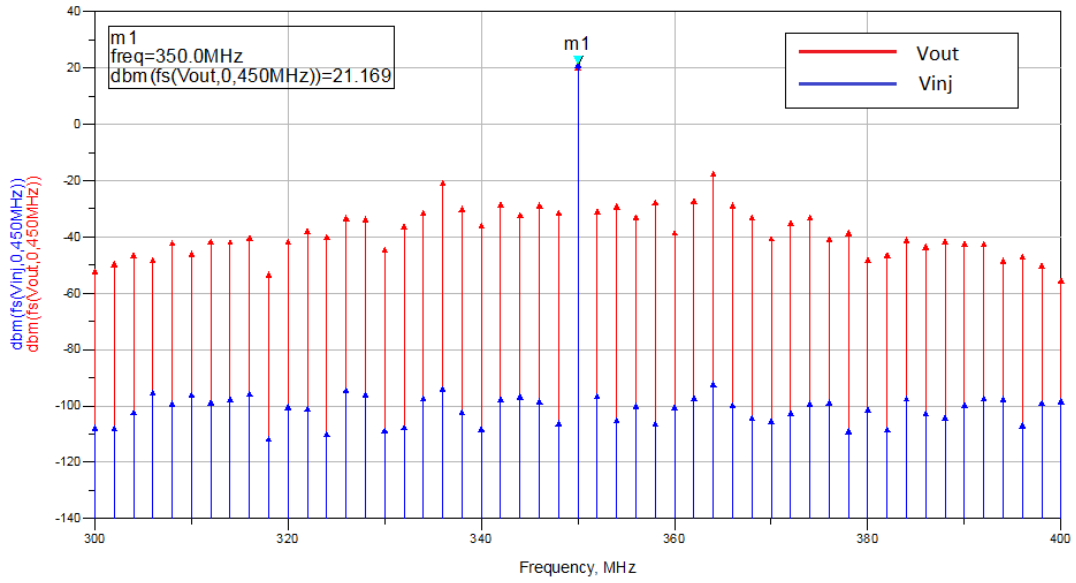

(a)

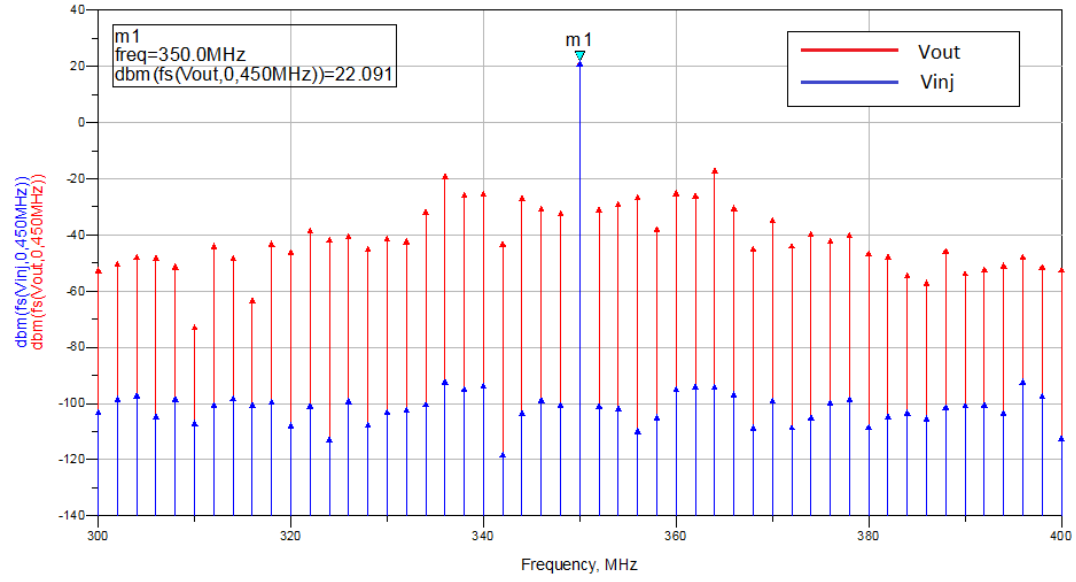

(b)

Figure 3.19: FFT Results for (a) $R_{coupling} = 330\Omega$, (b) $R_{coupling} = 1k\Omega$, (c) $R_{coupling} = 4.7k\Omega$ and (d) $R_{coupling} = 10k\Omega$

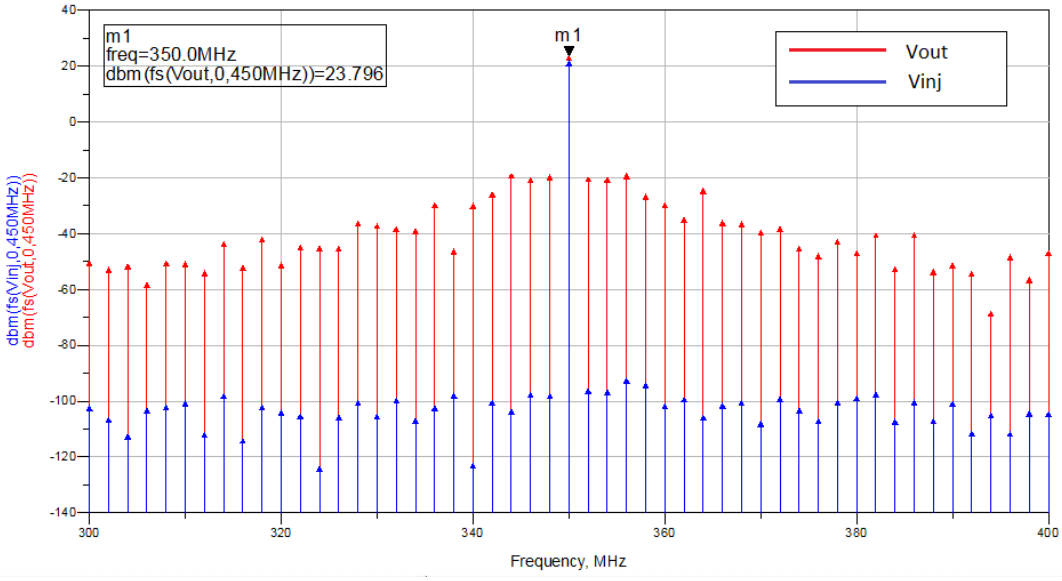

(c)

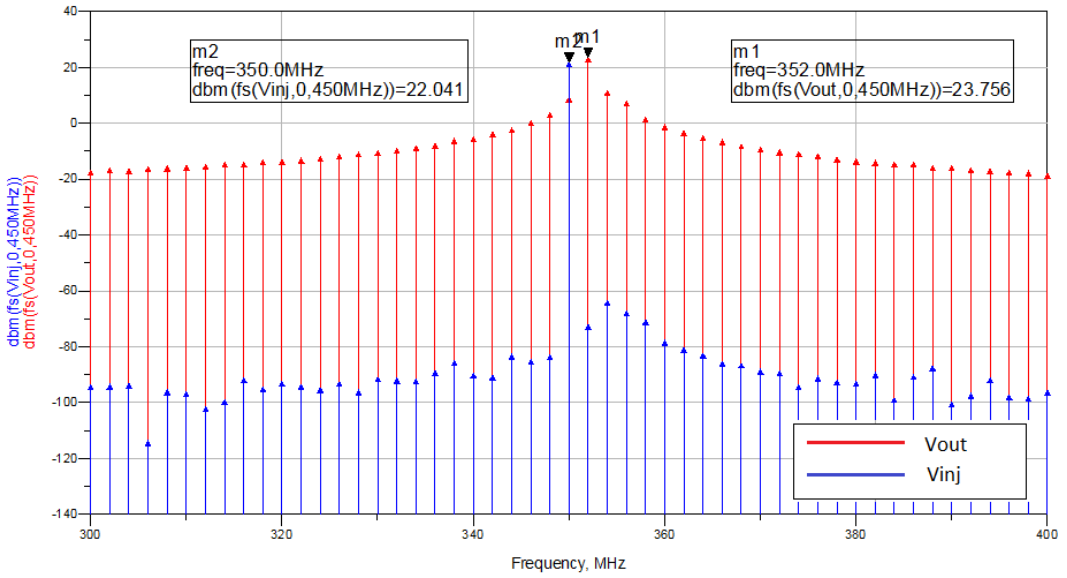

(d)

Figure 3.19: FFT Results for (a) $R_{coupling} = 330\Omega$, (b) $R_{coupling} = 1k\Omega$, (c) $R_{coupling} = 4.7k\Omega$ and (d) $R_{coupling} = 10k\Omega$

Frequency of the master oscillator should be in locking bandwidth defined by Equation (2.40). So, if f_m is above or below a certain frequency, locking cannot be achieved as shown in Figures 3.20d and 3.21d for $f_m = 372MHz$. For $f_m = 346, 354, 362MHz$, phase and frequency locking is achieved as shown in Figures, for time domain 3.20a, 3.20b and 3.20c and for frequency domain 3.21a, 3.21b and

3.21c respectively.

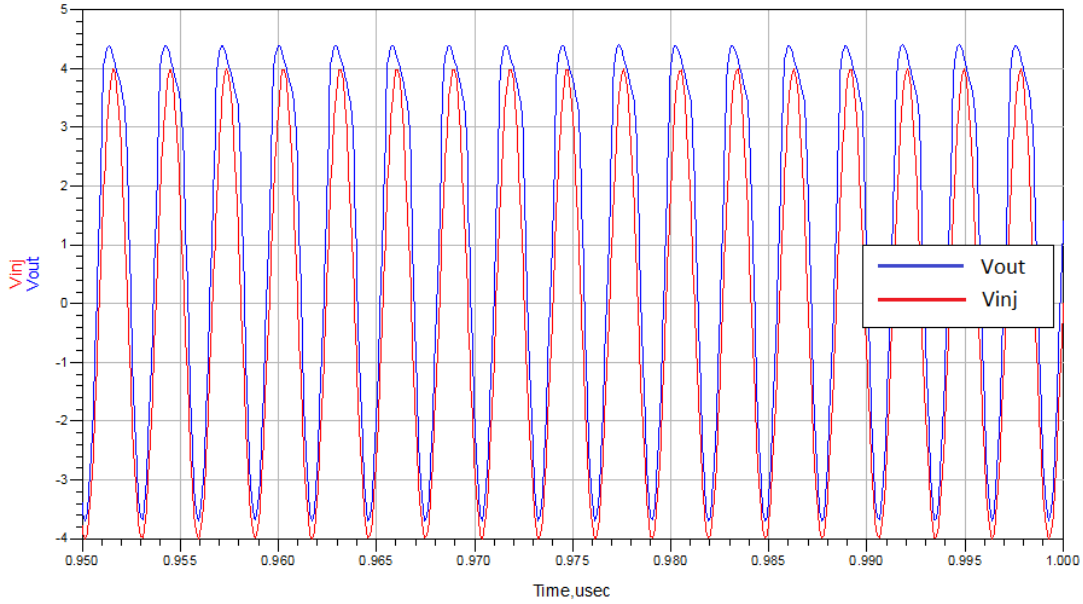

(a)

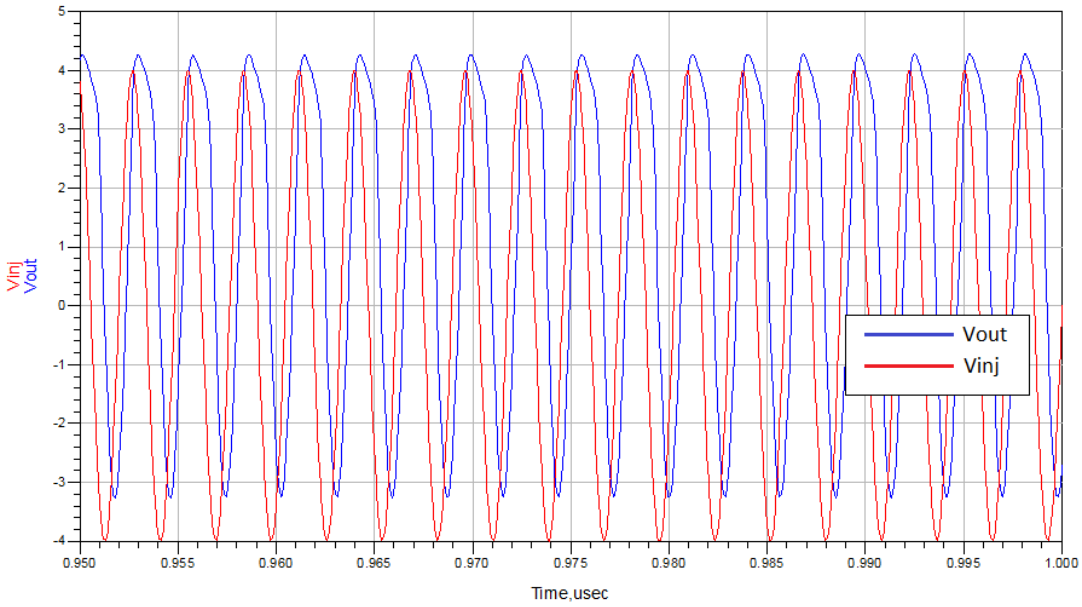

(b)

Figure 3.20: Time Domain Results for (a) $f_m = 346MHz$, (b) $f_m = 354MHz$, (c) $f_m = 362MHz$ and (d) $f_m = 372MHz$

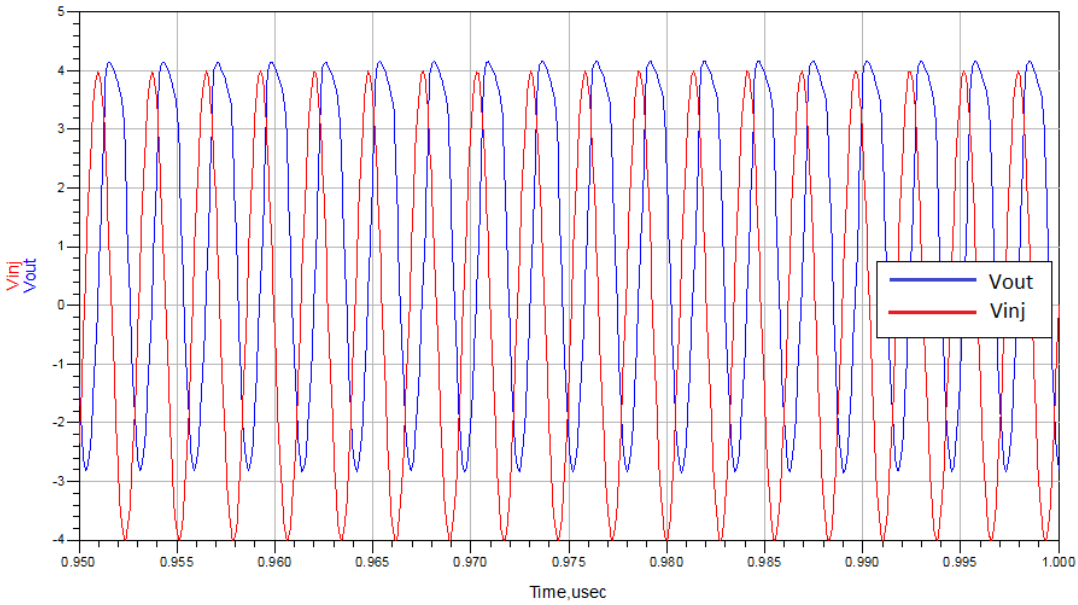

(c)

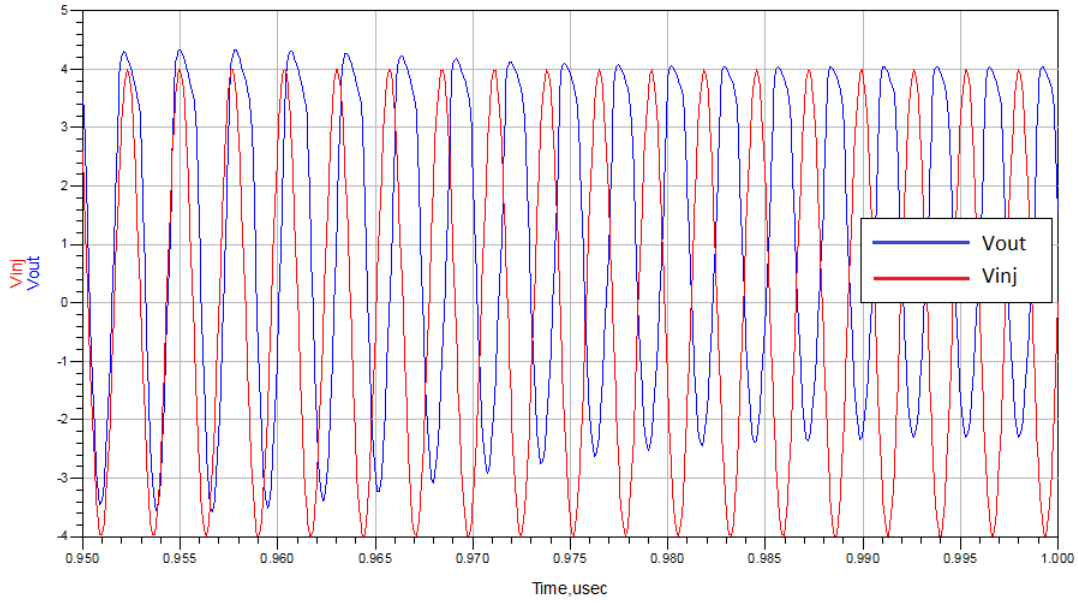

(d)

Figure 3.20: Time Domain Results for (a) $f_m = 346MHz$, (b) $f_m = 354MHz$, (c) $f_m = 362MHz$ and (d) $f_m = 372MHz$

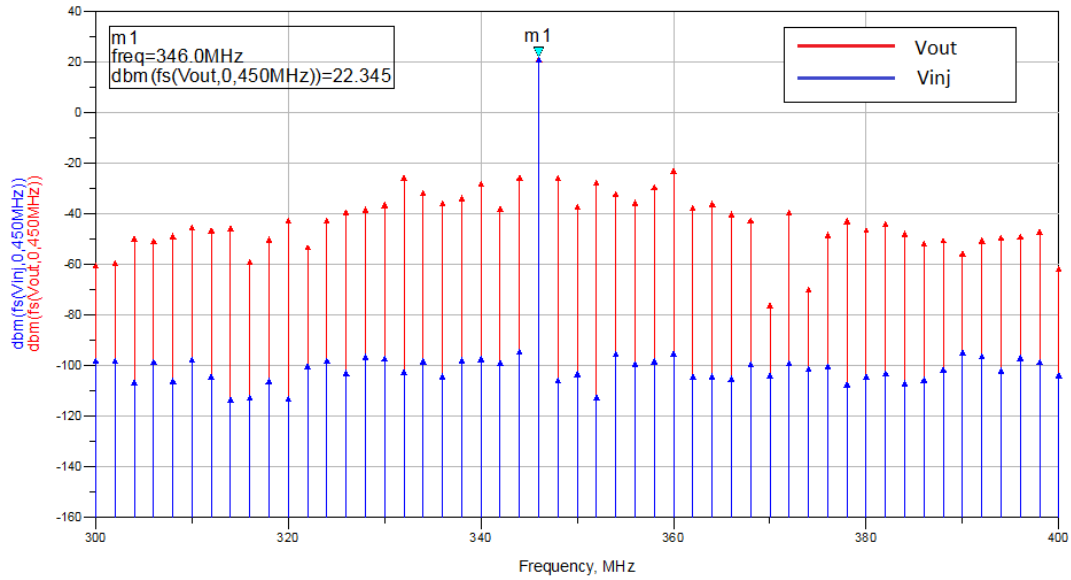

(a)

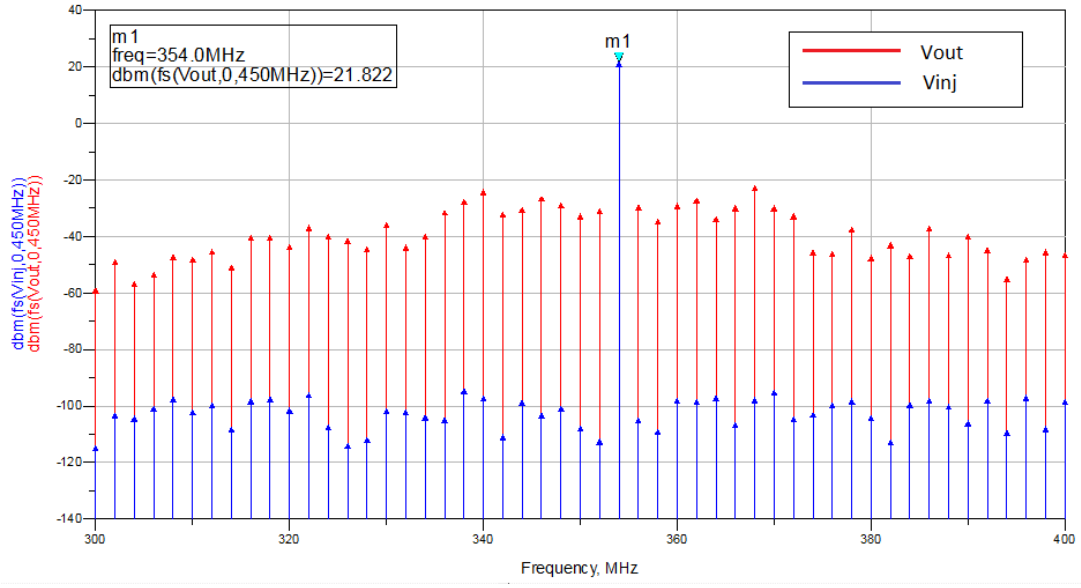

(b)

Figure 3.21: FFT Results for (a) $f_m = 346MHz$, (b) $f_m = 354MHz$, (c) $f_m = 362MHz$ and (d) $f_m = 372MHz$

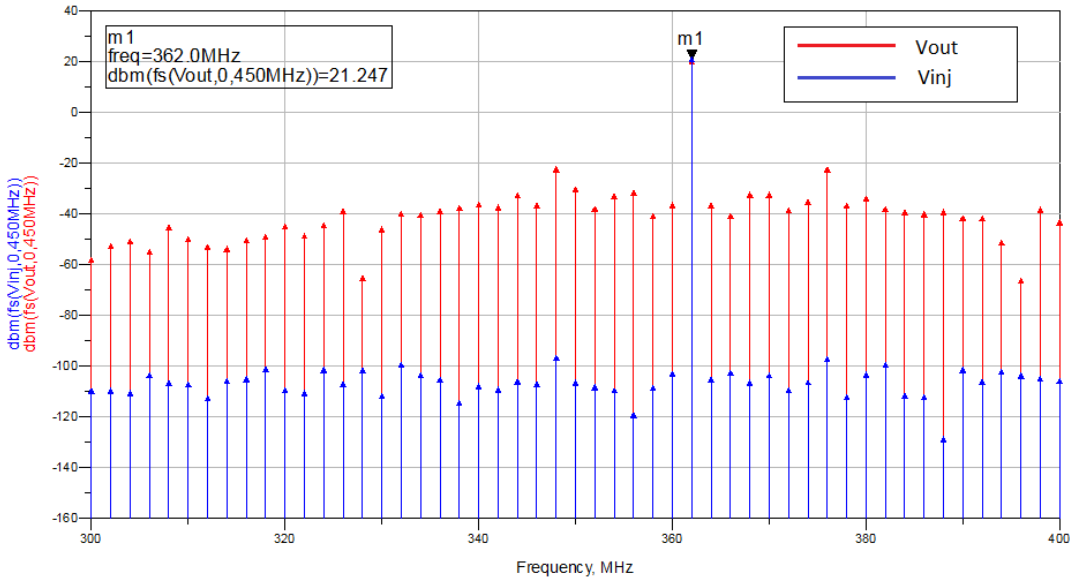

(c)

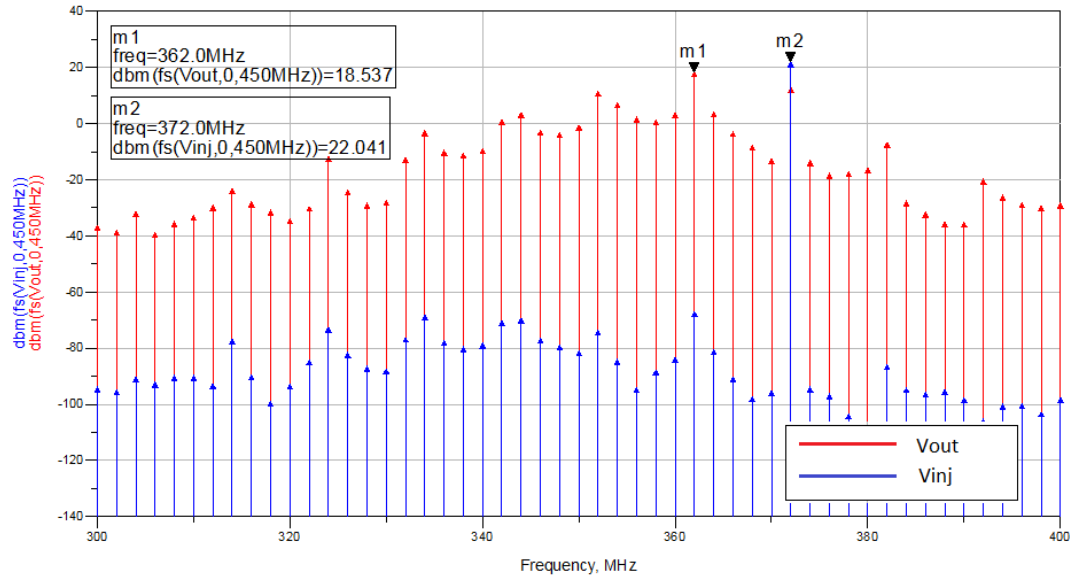

(d)

Figure 3.21: FFT Results for (a) $f_m = 346MHz$, (b) $f_m = 354MHz$, (c) $f_m = 362MHz$ and (d) $f_m = 372MHz$

The amplitude of the master oscillator has the same effect as the coupling resistor. As V_m changes A_{inj} changes and therefore locking bandwidth changes accordingly. For $V_m = 2.5V$ locking occurs as in Figure 3.22. However, while $V_m = 2V$ even if V_{inj} and V_{out} have same operating frequency, the change in phase versus time can be seen from Figure 3.23.

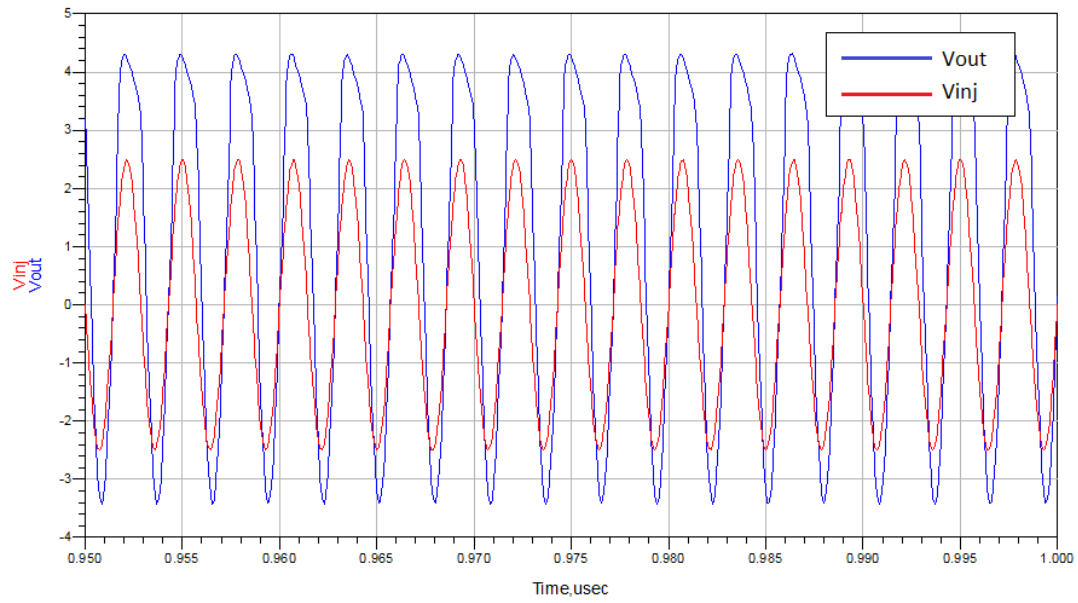

(a)

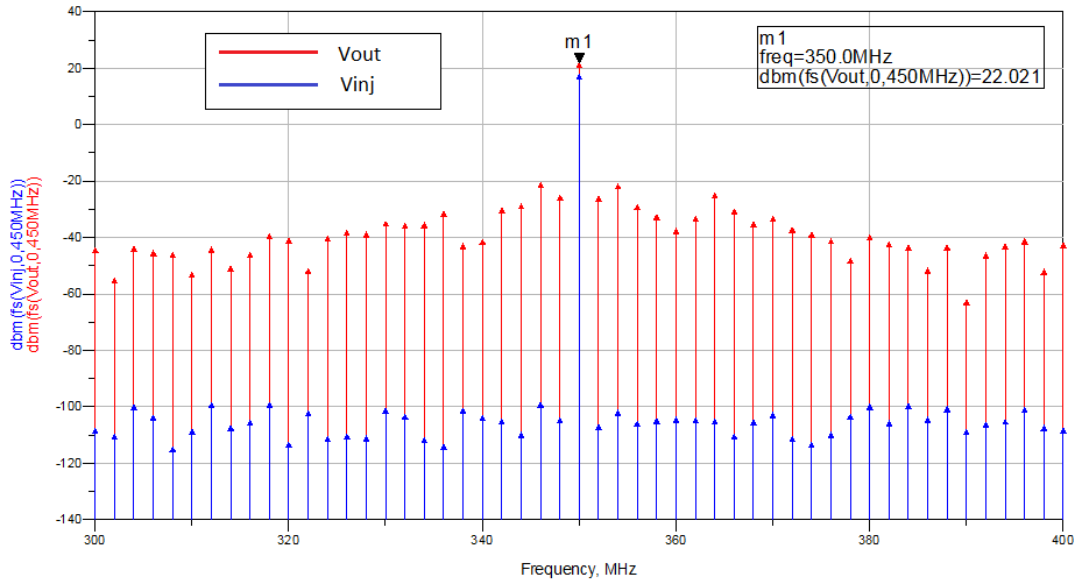

(b)

Figure 3.22: (a) Time Domain and (b) FFT Results $V_m = 2.5V$

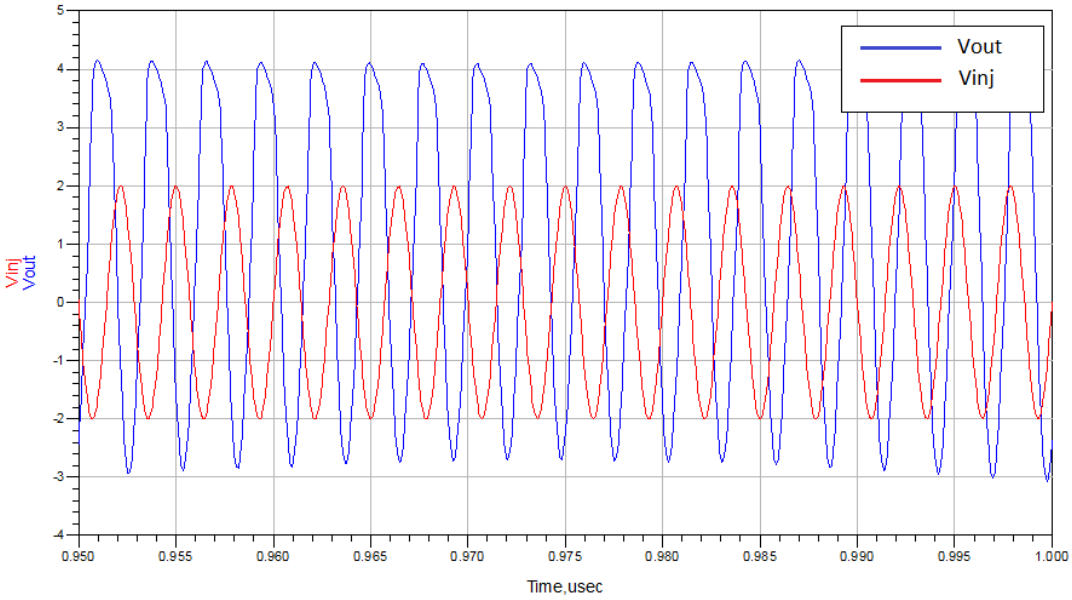

(a)

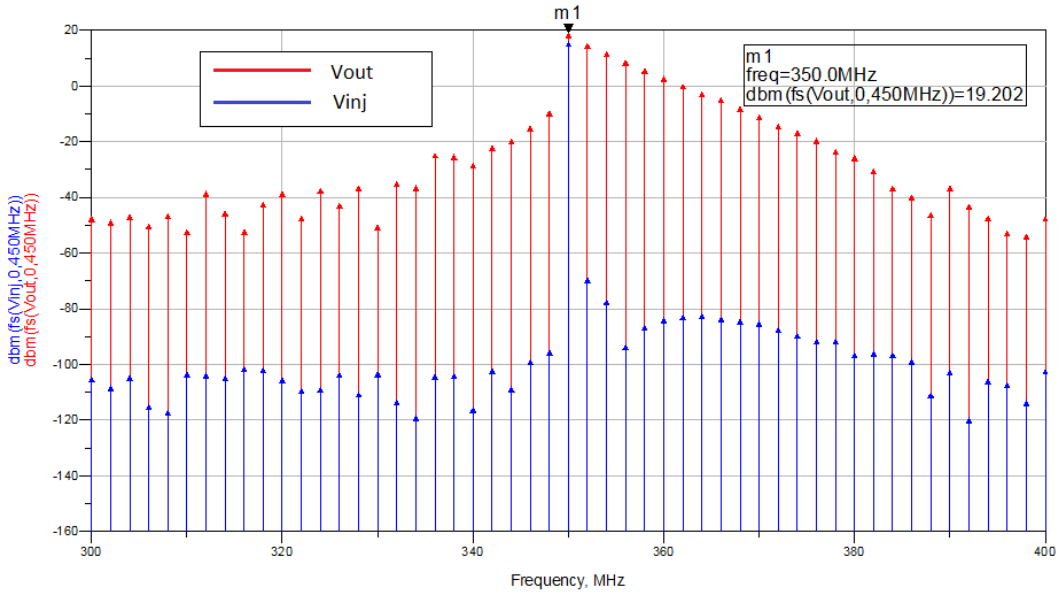

(b)

Figure 3.23: (a) Time Domain and (b) FFT Results $V_m = 2V$

3.4.3 Peer-Peer System

In this system, two Colpitts oscillators are connected through R_c between bases of the transistors. The two oscillators are identical in operation, but using trimmer capacitor frequency of oscillation can be adjusted. Time domain and FFT results are obtained

through transient simulation. The circuit schematic is shown in Figure 3.24.

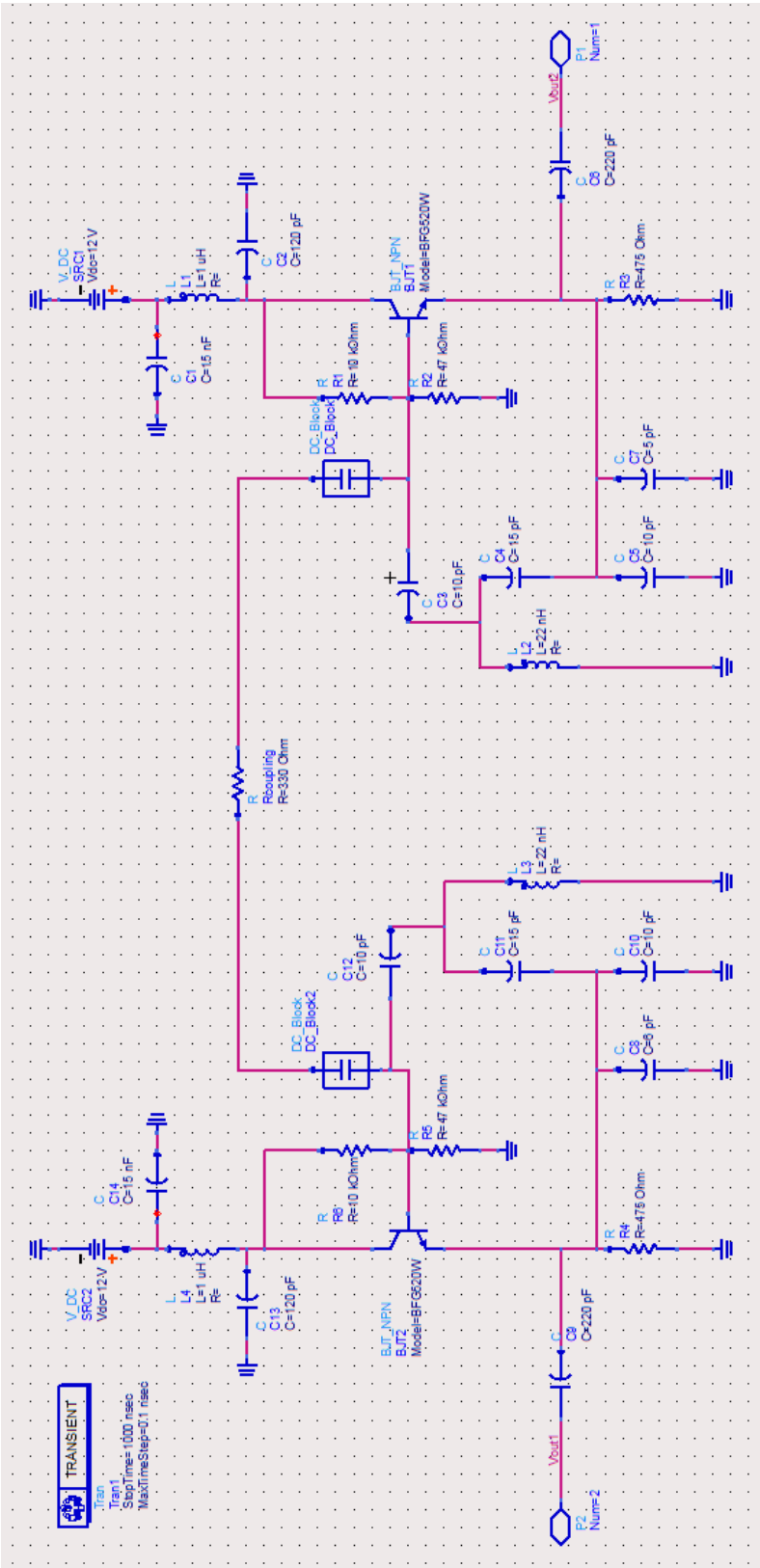

Figure 3.24: Circuit Schematic for Peer-Peer Simulations

In this simulation, the effect of the frequency difference between two oscillators is observed. The effects of R_c and amplitude of the injected signal is similar to master-slave system. In fact, each oscillator injects the other one. Since they are identical, amplitude effect cannot be observed for this case. Also, there is no need to simulate for different values of R_c. Figure 3.25 shows the case when there is no coupling between identical Colpitts oscillators. OSC1 oscillates at 352 MHz with $C_8 = 6pF$ and OSC2 oscillates at 358 MHz with $C_7 = 5pF$. Phase and frequency difference are seen in time-domain simulation result.

As the oscillation frequency of one oscillator changes the other is affected; since, their degree of stability is the same unlike master-slave case. In other words, OSC1 is affected from OSC2 and OSC2 is affected from OSC1 equivalently. Therefore, no oscillator is master and no oscillator determines the operating frequency, but two or more for N-OSC cases.

In order to determine the frequency of oscillation by calculation, the coupling coefficient between oscillators should be known. However, coupling coefficient cannot be calculated; since, oscillator circuit is a nonlinear circuit due to nature of the transistor. It is expected that two oscillators oscillate at the same frequency and this frequency could be different from free-running frequencies of oscillators or equal to at most one.

To observe the phenomena explained above, free-running frequency of OSC2 is held constant while free-running frequency of OSC1 is changed by variable capacitor. For each value of the capacitor, OSC1 oscillates at a different frequency and locking occurs at a different state. Once oscillators lock onto each other, they oscillate at the same frequency. For different capacitor values the locked frequency can be equal.

Tables 3.1 and 3.2 show the simulation results for $R_c = 330\Omega, 1k\Omega$. As expected for $R_c = 1k\Omega$, locking bandwidth is narrower. Since, coupling coefficient is smaller for $R_c = 1k\Omega$ than that of $R_c = 330\Omega$. Locking can only be achieved for four different capacitance values. Figures 3.26 and 3.27 show graphs for $R_c = 330\Omega$. Phase difference is different for $C_8 = 6pF$ and $C_8 = 12pF$. However, it is constant with respect to time for one capacitance value. This means that phase is locked. For $C_8 = 17pF$, locking bandwidth equation cannot be satisfied any more. So, oscillators are out of lock. In fact, one of the oscillators modulates the other as seen in time

Table 3.1: Locking Range for $R_c = 330\Omega$

$C_{trim1}(C_8)$	f_{out1}	f_{lock}
2 pF	376 MHz	372 MHz
3 pF	370 MHz	365 MHz
4 pF	364 MHz	360 MHz
6 pF	352 MHz	356 MHz
7 pF	348 MHz	354 MHz
8 pF	344 MHz	354 MHz
9 pF	340 MHz	354 MHz
10 pF	338 MHz	354 MHz
11 pF	334 MHz	354 MHz
12 pF	332 MHz	356 MHz
13 pF	330 MHz	356 MHz
14 pF	327 MHz	356 MHz
15 pF	324 MHz	366 MHz
16 pF	322 MHz	370 MHz
17 pF	320 MHz	No Locking

Table 3.2: Locking Range for $R_c = 1k\Omega$

$C_{trim1}(C_8)$	f_{out1}	f_{lock}
2 pF	376 MHz	No Locking
3 pF	370 MHz	370 MHz
4 pF	364 MHz	362 MHz
6 pF	352 MHz	356 MHz
7 pF	348 MHz	358 MHz
8 pF	344 MHz	No Locking

domain result.

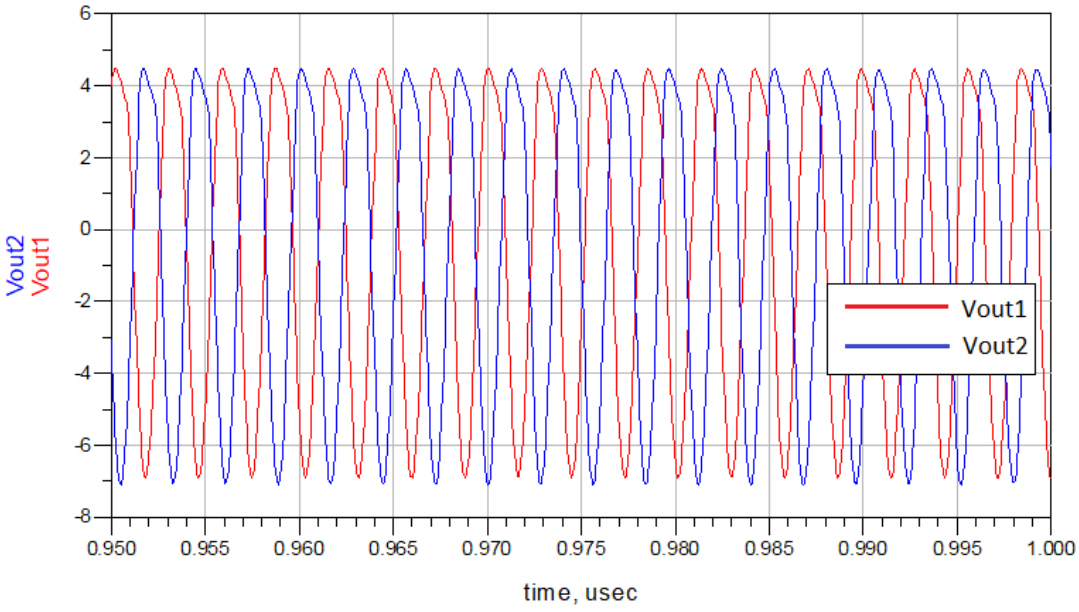

(a)

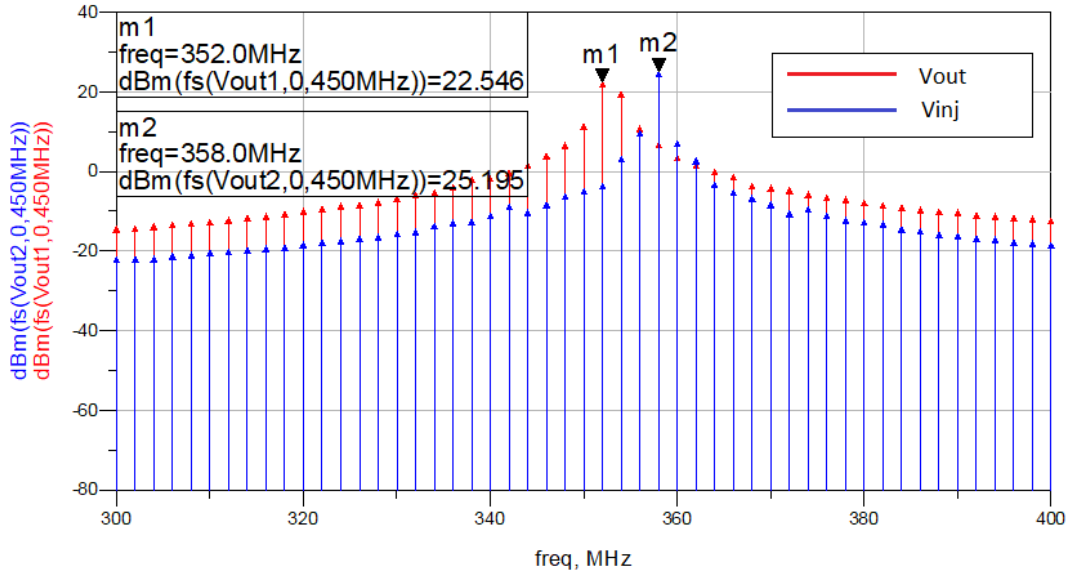

(b)

Figure 3.25: (a) Time Domain and (b) FFT Results for No Coupling Resistor

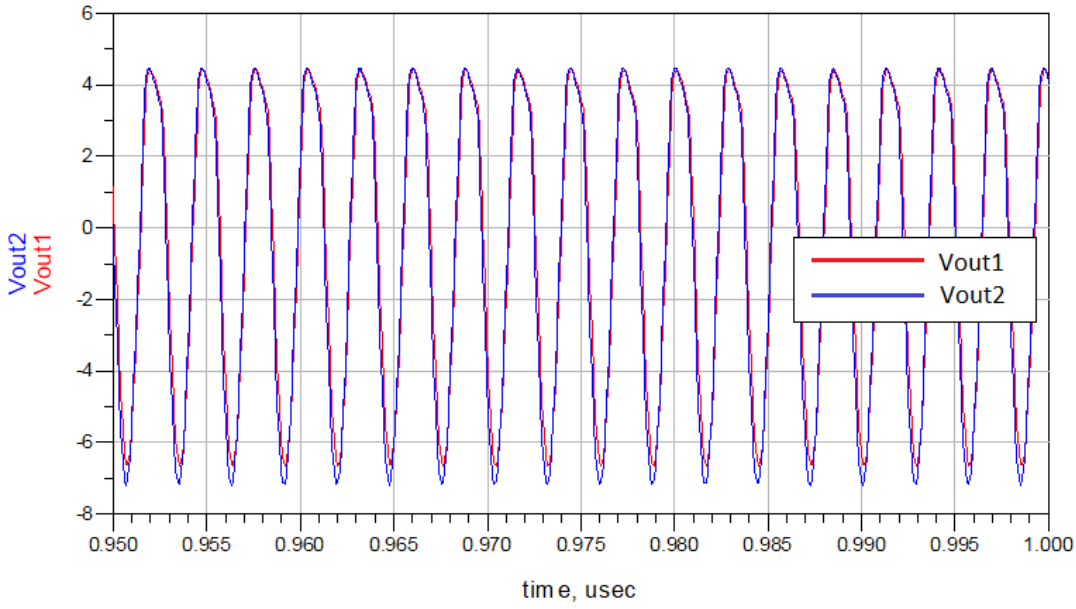

(a)

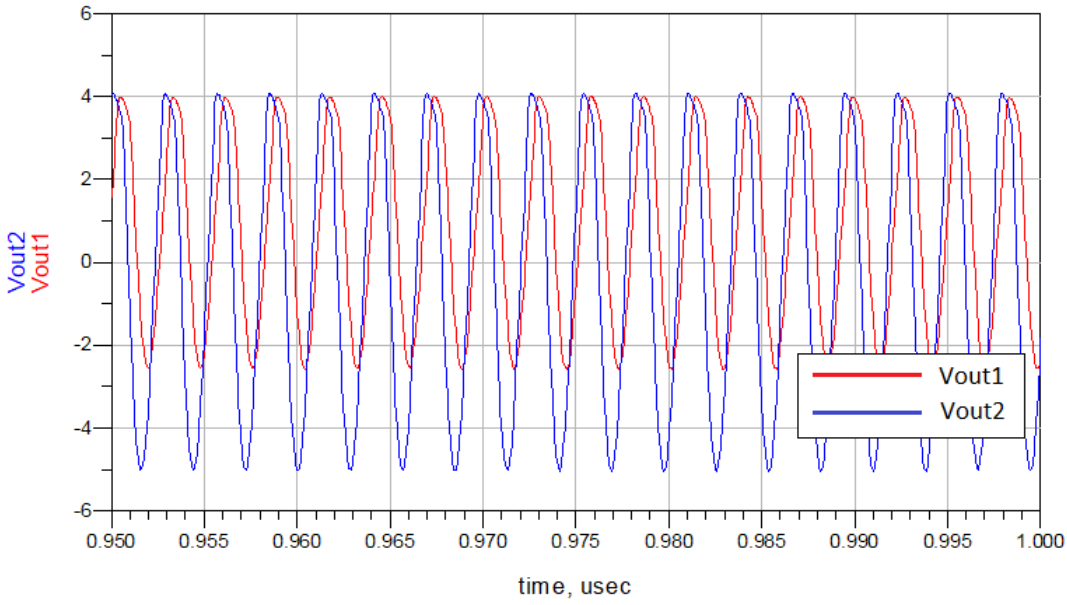

(b)

Figure 3.26: Time Domain Results for (a) $C_8 = 6pF$, (b) $C_8 = 12pF$ and (c) $C_8 = 17pF$

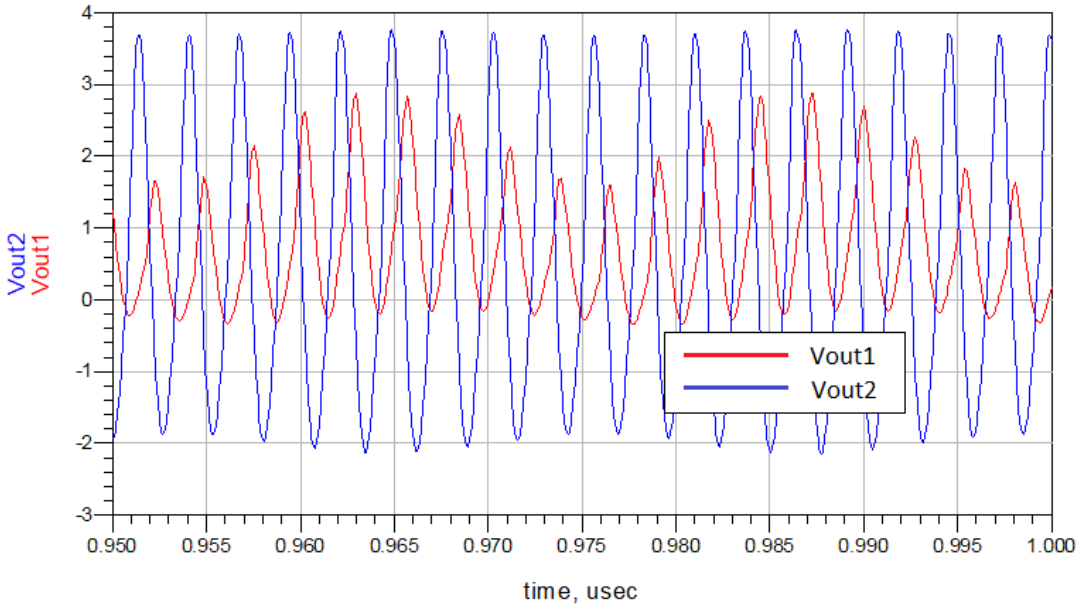

(c)

Figure 3.26: Time Domain Results for (a) $C_8 = 6pF$, (b) $C_8 = 12pF$ and (c) $C_8 = 17pF$

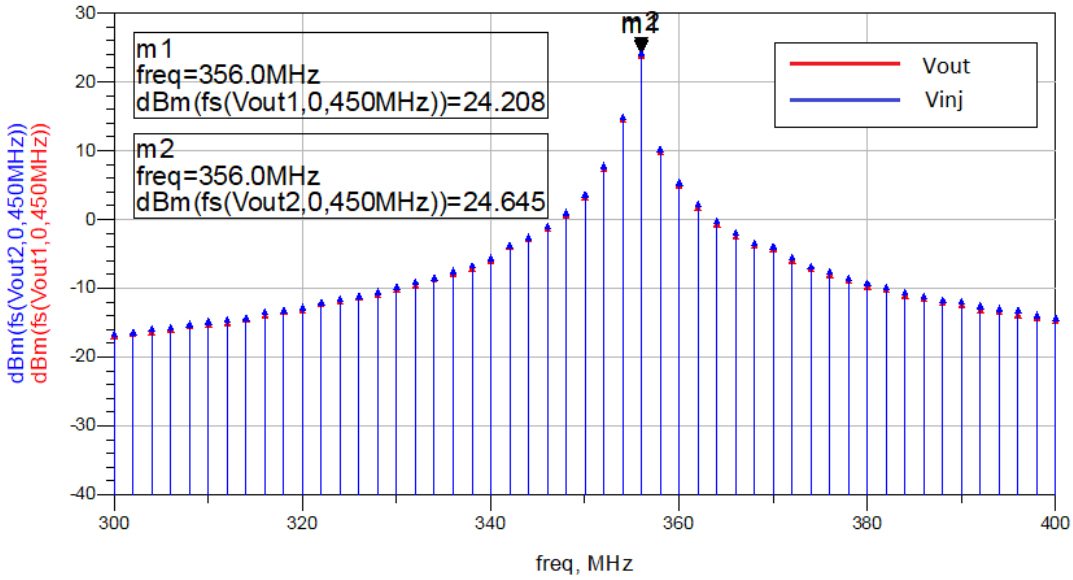

(a)

Figure 3.27: FFT Results for (a) $C_8 = 6pF$, (b) $C_8 = 12pF$ and (c) $C_8 = 17pF$

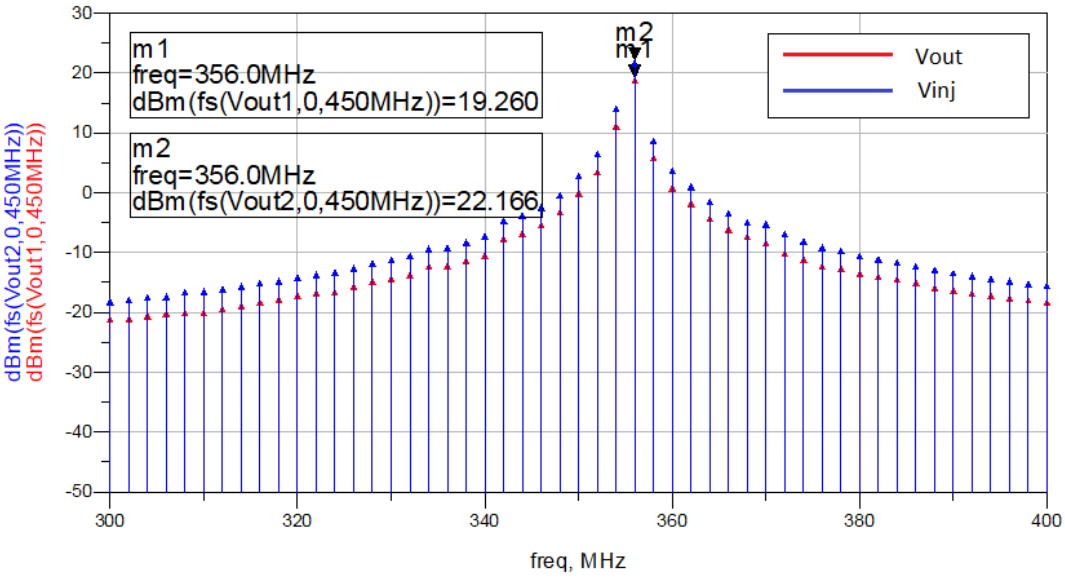

(b)

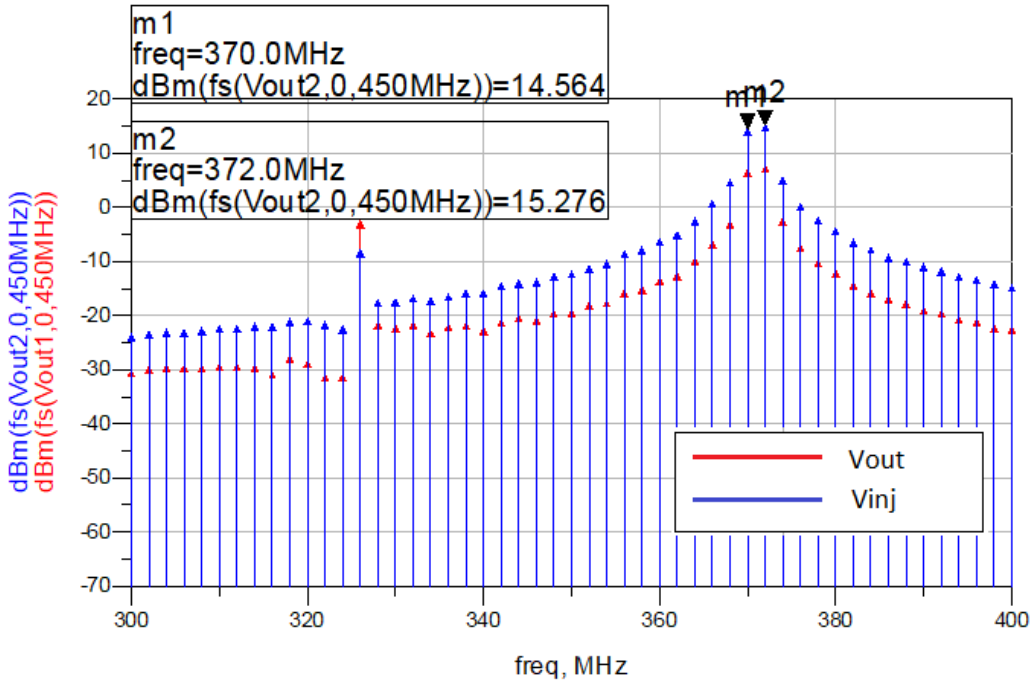

(c)

Figure 3.27: FFT Results for (a) $C_8 = 6pF$, (b) $C_8 = 12pF$ and (c) $C_8 = 17pF$

CHAPTER 4

EXPERIMENTS AND MEASUREMENT RESULTS OF FREE-RUNNING AND LOCKED COLPITTS OSCILLATORS

4.1 Introduction

In order to verify the simulation results of locking systems presented in Chapter 3, the circuit shown in Figure 4.1 is set up. The layout is prepared using Eagle layout program and it is printed on FR4 board Rapid Prototyping method of LPKF [31]. The transistor is BFG520W as explained in Chapter 3.

The circuit is composed of two equivalent oscillator circuits which are connected through an RF switch to establish peer-peer connection when needed. Two of the three connectors are used to observe the outputs of each oscillator while the other is an optional connector to observe combined output which is not needed during the experiments.

4.2 Measurement Results of Single Oscillator

For a free-running oscillator, start and steady-state of oscillation, its spectrum and phase noise performance are measured. Starting of oscillation is measured with Agilent Technologies MSO7054B oscilloscope as seen in Figure 4.2a. Steady-state time-domain measurement of free-running oscillator can be seen in Figure 4.2b. Spectrum and phase noise measurements are done using Keysight EXA Signal Analyzer N9010A as seen in Figures 4.3a and 4.3b.

Oscillation frequency is measured by changing capacitance in order to observe the

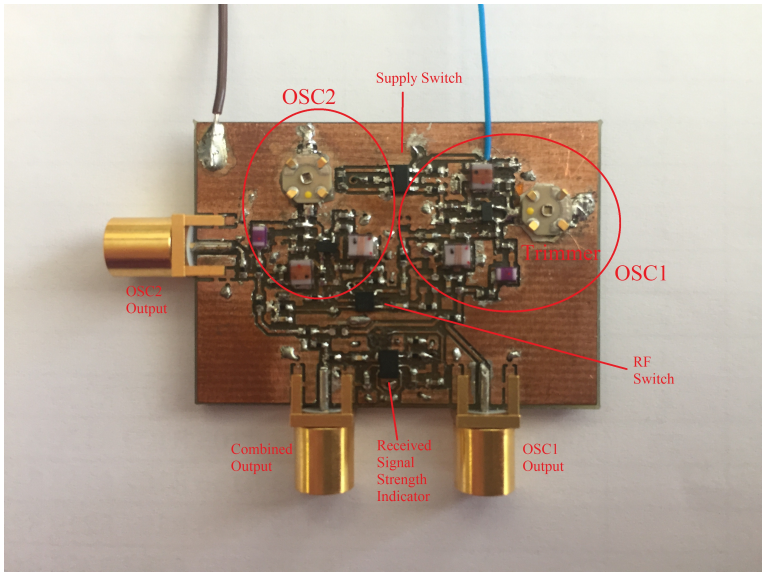

Figure 4.1: Manufactured Oscillator Circuit

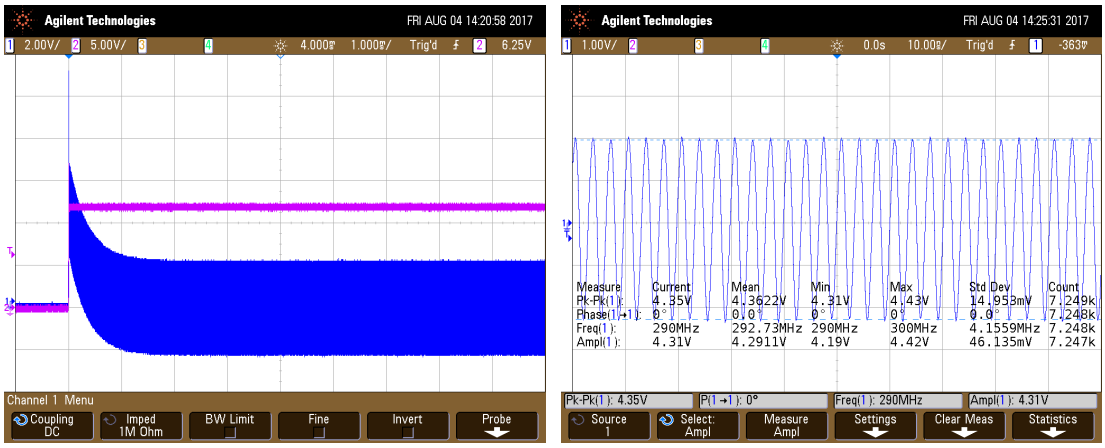

(a) (b)

Figure 4.2: (a) Start and (b) Steady-State of the Oscillation in Time-Domain

variable frequency characteristic of the oscillator circuit. Capacitance value is measured using Fluke PM6304 Programmable Automatic RLC meter. Free-running frequency of the oscillator with respect to trimmer capacitance value is presented in Table 4.1. The table also shows the output power with respect to capacitance value. It is normal to observe a variation of ± 2 dB over the tuning range.

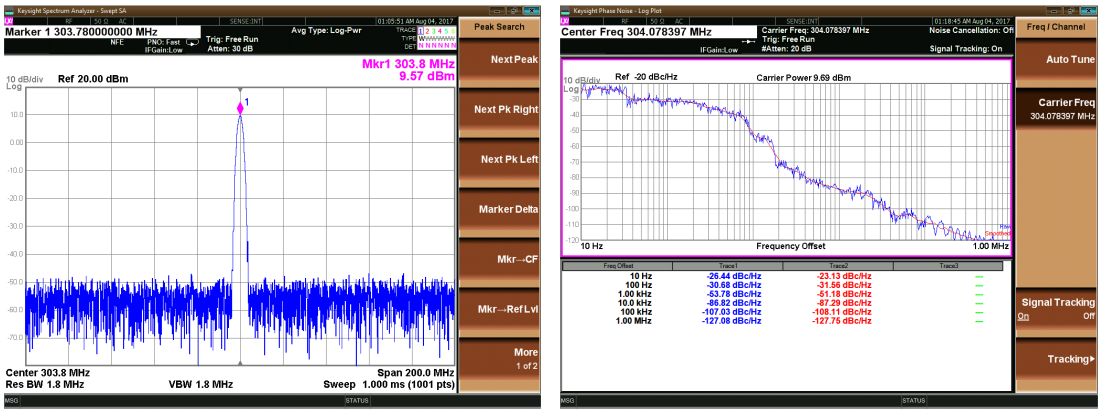

(a) (b)

Figure 4.3: (a) Output Signal of Single Colpitts Oscillator and (b) Phase Noise Measurement of Output Signal

Table 4.1: Trimmer Capacitance and Oscillation Frequency with Output Power

Capacitance Value (pF)	Frequency of Oscillation (MHz)	Output Power (dBm)
24.4	266.4	7
20.2	272.2	7.6
15.6	277.4	8.2
12.7	282	8.7
12	282.7	8.8
10.4	284.9	8.9
7.9	288.8	8.9
6.1	292.3	9
4	296.7	9
1.6	304.6	9.3
0.6	309.4	9.4

4.3 Measurement Results of Master-Slave System

For master-slave system, two measurement setups are prepared. Master oscillator is Rohde & Schwarz SMA100A signal generator and slave oscillator is the Colpitts oscillator. First, frequency domain output of the slave oscillator, which is locked to master, is observed using spectrum analyzer. Second, time-domain outputs of both

master and slave oscillators are observed using oscilloscope. Since signal generator is a very stable oscillator, a change in its output caused by slave oscillator is not expected.

In the first experiment, the effect of amplitude and frequency of the master oscillator to locking phenomena is observed. For this experiment free-running frequency and amplitude of the Colpitts oscillator are measured as 299.84 MHz and 9.52 dBm. Experimental setup shown in Figure 4.4 is prepared for $R_c = 4.7k\Omega$.

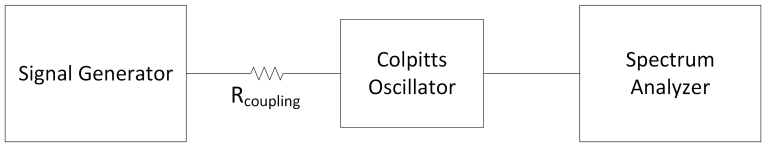

Figure 4.4: Experimental Setup for Spectrum Analyzer Measurements

First, the effect of change in master oscillator's frequency is examined. Since free-running frequency of the slave oscillator is $\approx$ 300 MHz, frequency of the master oscillator is increased and decreased around 300 MHz to find the locking bandwidth. Amplitude of the master signal is 9.52 dBm for all cases.

Table 4.2: Frequency of Signal Generator and Output of the Colpitts Oscillator

Frequency of the Master Signal	Output of Slave Oscillator
300 MHz $\pm$ 10 kHz	9.63 dBm @300.01 and 299.99 MHz
300 MHz $\pm$ 50 kHz	9.63 dBm @300.05 and 299.95 MHz
300 MHz $\pm$ 100 kHz	9.63 dBm @300.10 and 299.90 MHz
300 MHz $\pm$ 250 kHz	9.60 dBm @300.25 and 299.75 MHz
300 MHz $\pm$ 500 kHz	9.57 dBm @300.50 and 299.50 MHz
300 MHz $\pm$ 1 MHz	9.50 dBm @301.00 and 299.00 MHz
300 MHz $\pm$ 1.4 MHz	9.43 dBm @301.40 and 299.60 MHz
300 MHz $\pm$ 1.5 MHz	No Locking

Measurement results are presented in Table 4.2. For each locking case, frequency of the slave oscillator follows injected frequency of the master oscillator; however, its amplitude is constant. Locking is occurred for 14 cases but it is not for 2 cases. Locked output signal for f_m = 301.4 MHz is shown in Figure 4.5. For f_m = 301.5 MHz and f_m = 298.5 MHz, locking is not occurred. At output of the slave oscillator

mixing products of the master and slave signals are observed as seen in Figures 4.6a and 4.6b.

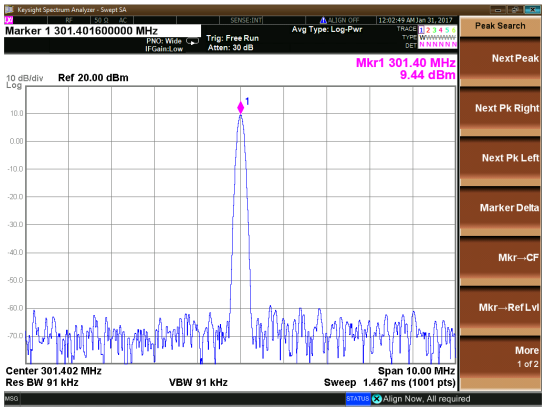

Figure 4.5: Output of the Slave Oscillator for $f_m = 301.4$ MHz

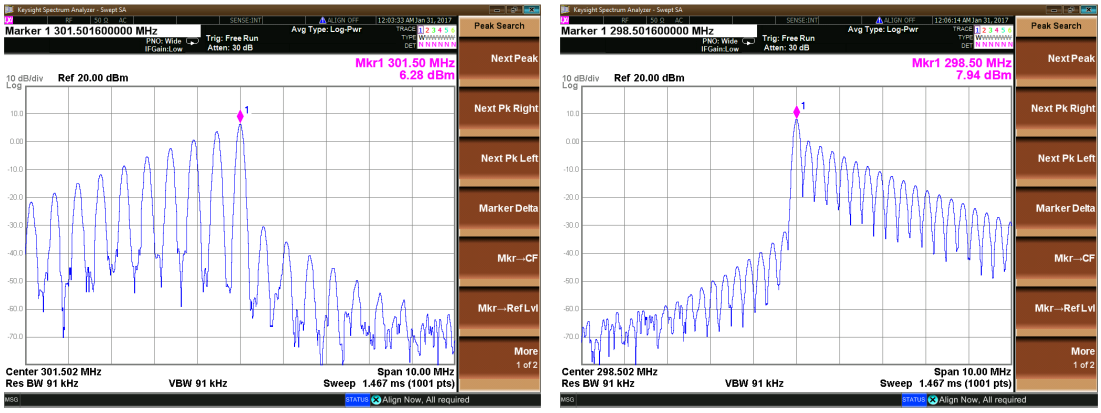

(a) (b)

Figure 4.6: Output of the Slave Oscillator for (a) $f_m = 301.5$ MHz and (b) $f_m = 298.5$ MHz

Second, the effect of change in master signal's amplitude is observed. Output frequency of the signal generator is 300.5 MHz for each case and amplitude is decreased by 1 dB starting from 9 dBm as seen in Table 4.3. For $A_m = 2$ dBm locking is not occurred and the mixing products of two oscillators are present at the output of slave oscillator as in Figure 4.7a.

Figure 4.7b shows the output for $A_m =$ -10 dBm. At the output, free-running output signal of the slave oscillator is clearly seen. Other signals are the survived mixing products. So, this shows that for $A_m =$ -10 dBm, the system is far from locking.

Table 4.3: Amplitude of the Signal Generator and Output of the Colpitts Oscillator

Amplitude of the Master Signal (@300.50 MHz)	Output of the Colpitts Oscillator
9 dBm	9.58 dBm @300.50 MHz
8 dBm	9.56 dBm @300.50 MHz
7 dBm	9.55 dBm @300.50 MHz
6 dBm	9.54 dBm @300.50 MHz
5 dBm	9.53 dBm @300.50 MHz
4 dBm	9.51 dBm @300.50 MHz
3 dBm	9.50 dBm @300.50 MHz
2 dBm	No Locking

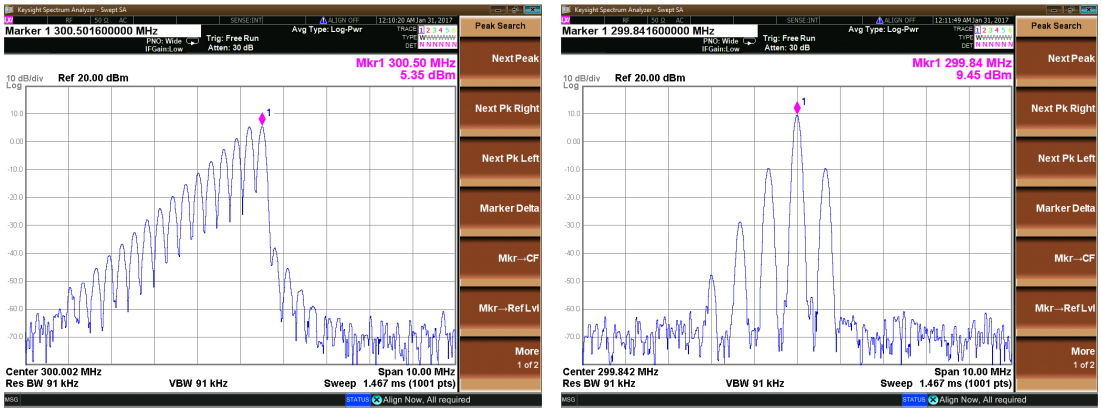

(a) (b)

Figure 4.7: Output of the Slave Oscillator for (a) $A_m = 2$ dBm and (b) $A_m = -10$ dBm

In the second experiment, time-domain output signals of both master and slave oscillators are examined. Measurement setup for this experiment is shown in Figure 4.8. These measurements are taken with the oscilloscope Agilent Technologies DSO9104A. To observe the output of the master signal, a power divider with insertion loss of 3.5 dB is used. Amplitude of the master signal is increased to compensate this loss during the experiment. Oscilloscope data is saved as a CSV file and FFT of the corresponding data is calculated using Matlab to observe the signals in frequency domain.

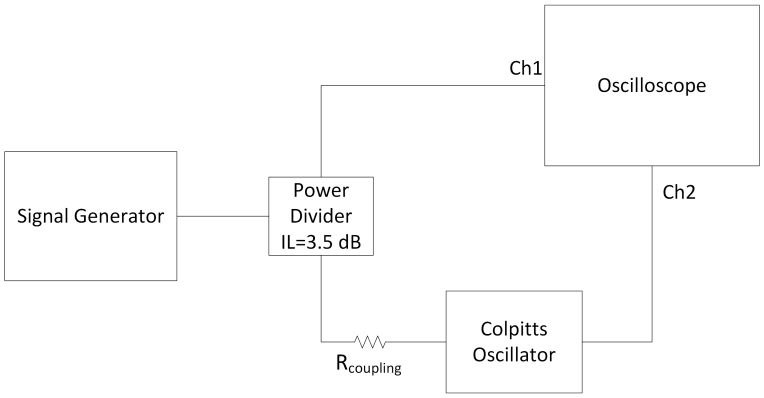

Figure 4.8: Experimental Setup for Oscilloscope Measurements

Free-running frequency of the slave oscillator is arranged using trimmer as $f_s = 309.3$ MHz and frequency of the master signal is chosen as $f_m = 310$ MHz to guarantee locking. First, time-domain signals are measured for uncoupled case by separating master and slave through the connector. Time-domain output signals is shown in Figure 4.9 and FFT of the corresponding signals are presented in Figures 4.10a and 4.10b.

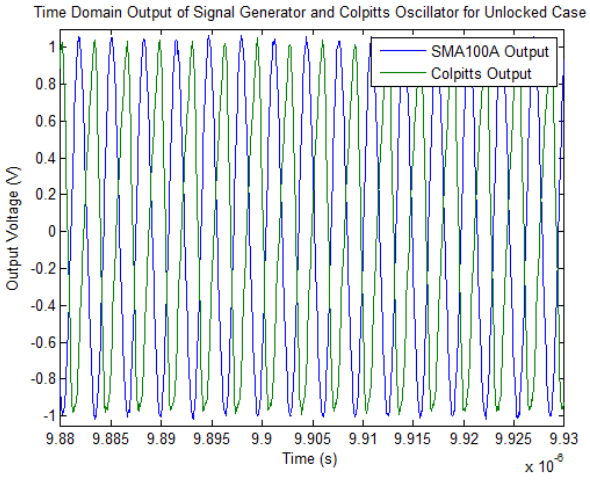

Figure 4.9: Time-Domain Output Signals of Master and Slave Oscillators for Unlocked Case

Connecting master and slave signals through power divider, locking is occurred. Locked signals in time-domain is shown in Figure 4.11. Slave signal is locked to master signal and it oscillates at signal generator's output frequency, 310 MHz as shown in Figures 4.12a and 4.12b.

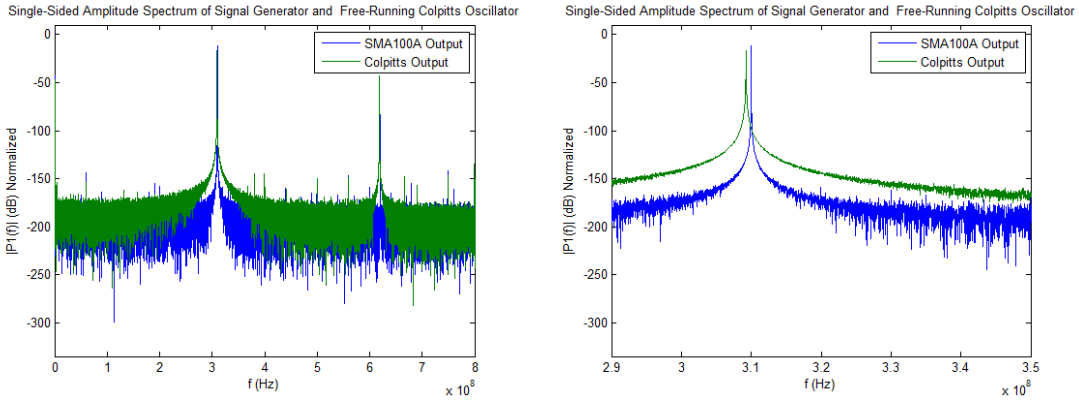

(a) (b)

Figure 4.10: (a) Output Signals of SMA100A and Free-Running Oscillator and (b) Narrower Spectrum of Same Signals

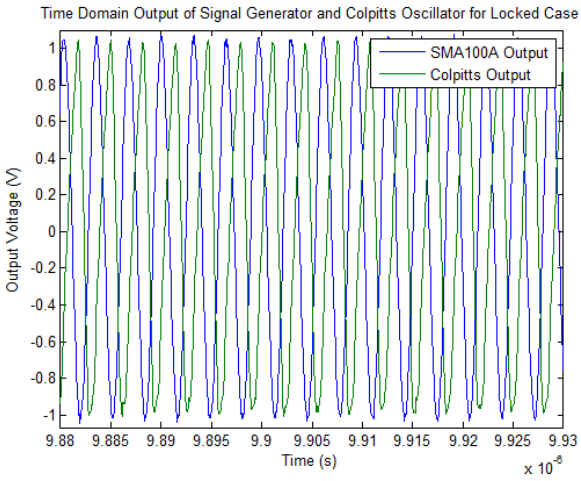

Figure 4.11: Time-Domain Output Signals of Master and Slave Oscillators for Locked Case

In order to say that phase locking is occurred, phase difference between each signal with respect to time should be constant. Also, phase difference value has to be the same each time locking is occurred. So, phase difference between each time-domain signal is calculated using a Matlab code for this experiment. The result is shown in Figure 4.13. Average of the phase difference is calculated as 133 degrees. Since oscilloscope data is a sampled data, phase difference is not the same for each period of oscillation. Oscilloscope data has 1 Mpts and captured signal duration is $50\mu s$. First, time resolution, which is the duration between each data point, should be calculated

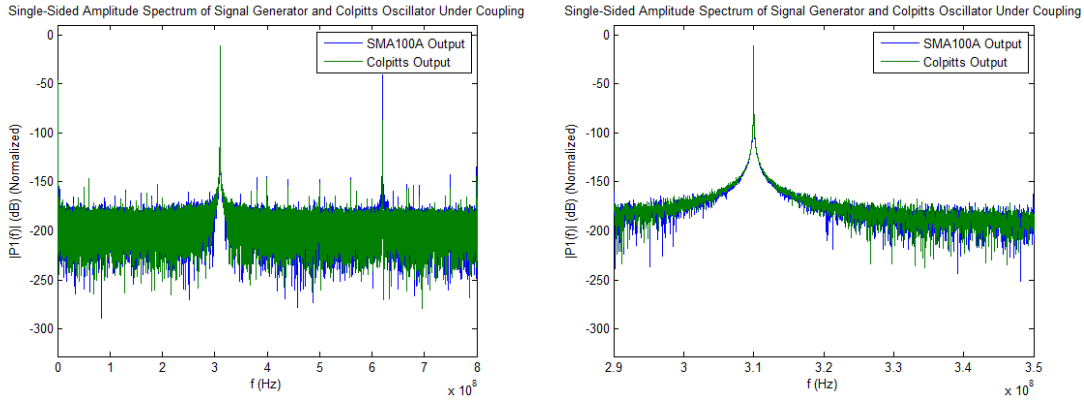

(a) (b)

Figure 4.12: (a) Output Signals of SMA100A and Free-Running Oscillator Under Locking and (b) Narrower Spectrum of Same Signals

as in Equation (4.1).

$$\text{time} = t = 50\mu s \tag{4.1a}$$

$$\text{points} = pts = 1Mpts \tag{4.1b}$$

$$\text{time resolution} = \frac{t}{pts} = 50 \times 10^{-12} s \tag{4.1c}$$

Period of the locked signal is calculated using Matlab as $3.2258 \times 10^{-9} s$. The phase angle resolution can be calculated using time resolution and period of the sinusoidal signal measured by oscilloscope as follows.

$$\text{angle resolution} = \left(\frac{\text{time resolution}}{\text{period}}\right) \times 360^o = \left(\frac{50 \times 10^{-12}}{3.2258 \times 10^{-9} s}\right) \times 360^o = 5.58^o \tag{4.2}$$

Another concern is the phase noise of locked oscillators. Phase noise is measured using spectrum analyzer's phase noise measurement option. Phase noise measurement of slave oscillator is presented in Section 4.2 in Figure 4.3b. Phase noise measurement of signal generator is shown in Figure 4.14a and phase noise measurement of locked signal at the output of slave oscillator is shown in Figure 4.14b. The blue graph shows the raw measurement data and red one shows smoothed result.

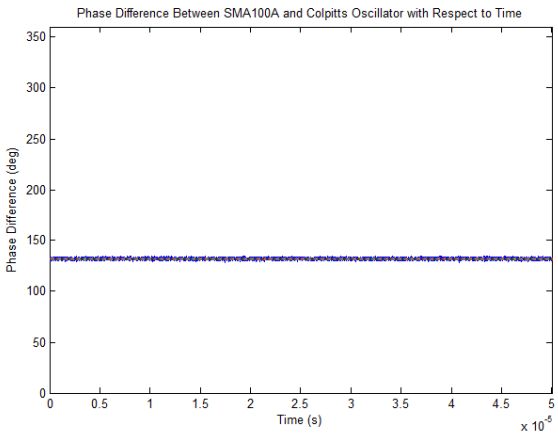

Figure 4.13: Phase Difference Between SMA100A and Free-Running Oscillator Over Time

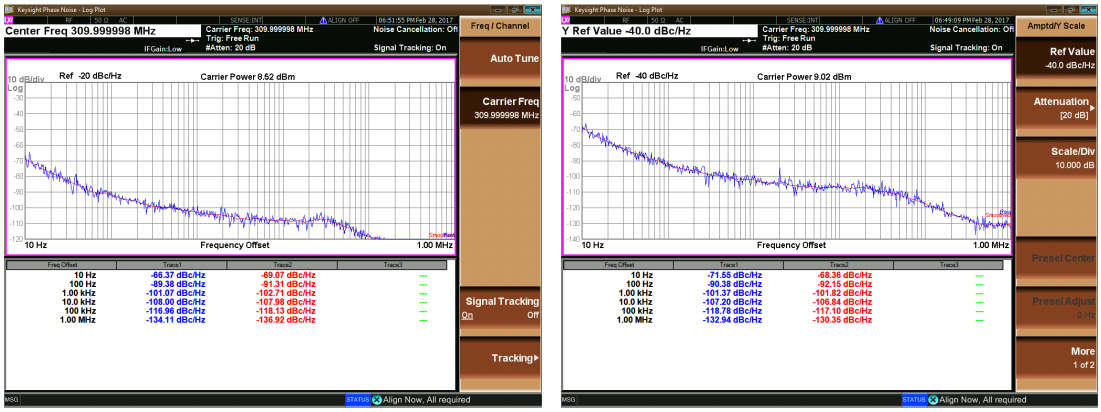

(a) (b)

Figure 4.14: Phase Noise Measurements of (a) SMA100A Signal Generator and (b) Locked Output Signal

CSV data of three measurements are plotted using Matlab in the same graph to compare the results. As seen in Figure 4.15, phase noise of the locked output signal is nearly the same as the phase noise of the SMA100A signal generator. From raw data measurements it can be seen that at 100 kHz offset, phase noise of the Colpitts oscillator is -107.03 dBc/Hz, while signal generator's and locked output signal's phase noise measurements are -116.96 dBc/Hz and -118.78 dBc/Hz respectively. So, not only phase and frequency of the slave signal are locked to master signal, but also phase noise is locked. This means that phase noise of a free-running signal can be improved using locking phenomena.

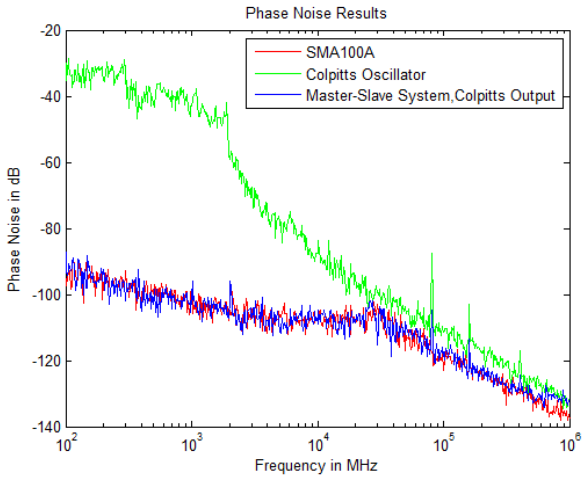

Figure 4.15: Phase Noise Measurements of SMA100A, Colpitts Oscillator and Locked Signal

4.4 Measurement Results of Peer-Peer System

Unlike master-slave system, in peer-peer system two identical oscillators will affect each other. Spectrum analyzer is not used for this experiment, since two output ports should be terminated by the same load. Therefore, locked output of two peer oscillators is monitored using oscilloscope with probe terminations of 50Ω. Experimental setup is shown in Figure 4.16.

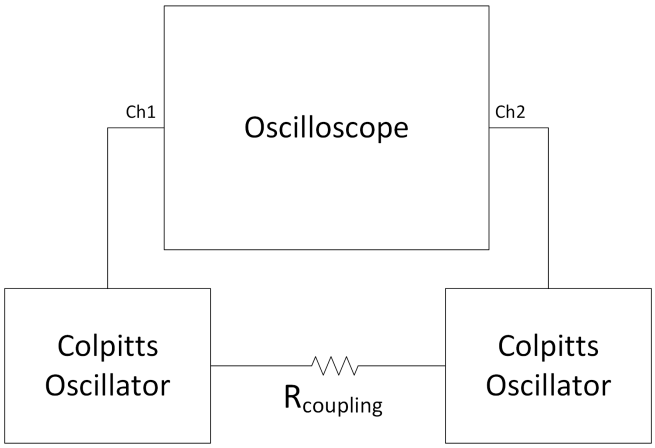

Figure 4.16: Experimental Setup for Oscilloscope Measurements

First, free-running outputs of two oscillators are measured to observe unlocked oscillations. In Figure 4.17, time-domain measurement results and in Figure 4.18, FFT of the corresponding measurement results can be seen. Free-running frequencies of

oscillators are calculated as 295.4 MHz and 301.5 MHz from Matlab.

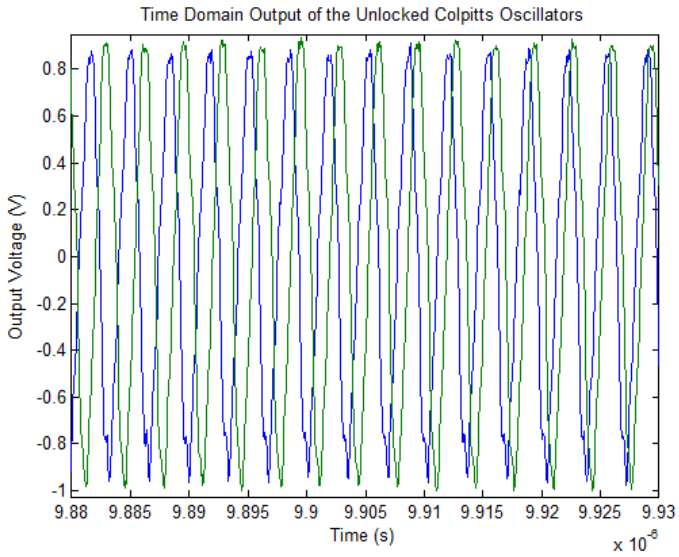

Figure 4.17: Time-Domain Output of Two Unlocked Colpitts Oscillators

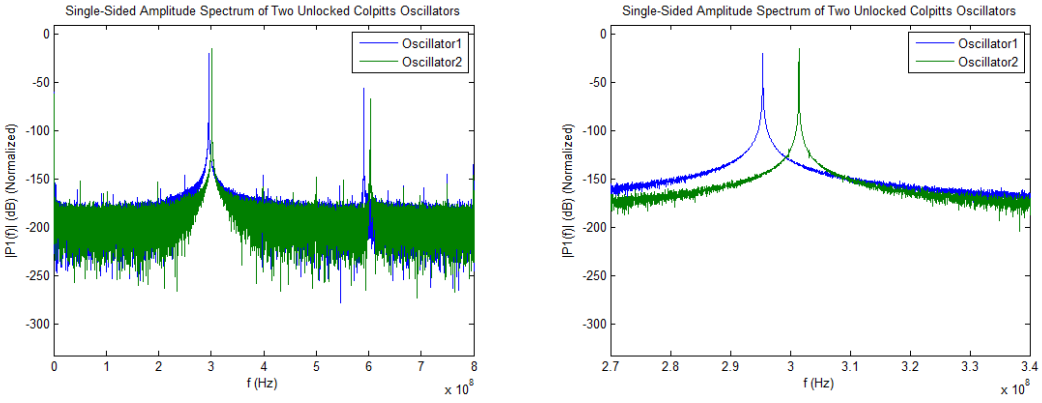

(a) (b)

Figure 4.18: (a) Output Signals of Two Unlocked Colpitts Oscillators and (b) Narrower Spectrum of Same Signals

Connecting two oscillators through $R_C = 4.7k\Omega$, locking is occurred. As shown in Figure 4.19, two signals are locked to each other. They follow each other in frequency and their phase difference through time is constant. Figures 4.20a and 4.20b show FFT of the corresponding time-domain results. Locked frequency is 296.4 MHz which is not equal to either of the free-running frequencies before locking.

Figure 4.21 shows phase difference between two time-domain locked oscillator out-

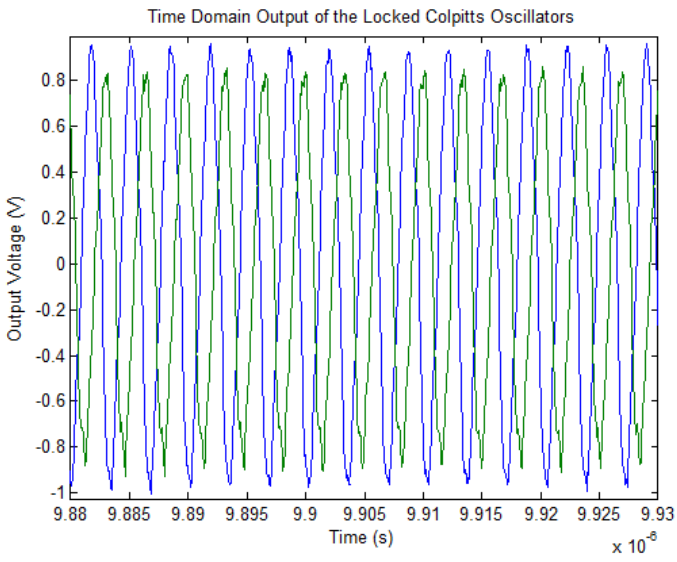

Figure 4.19: Time Domain Output of Two Locked Colpitts Oscillators

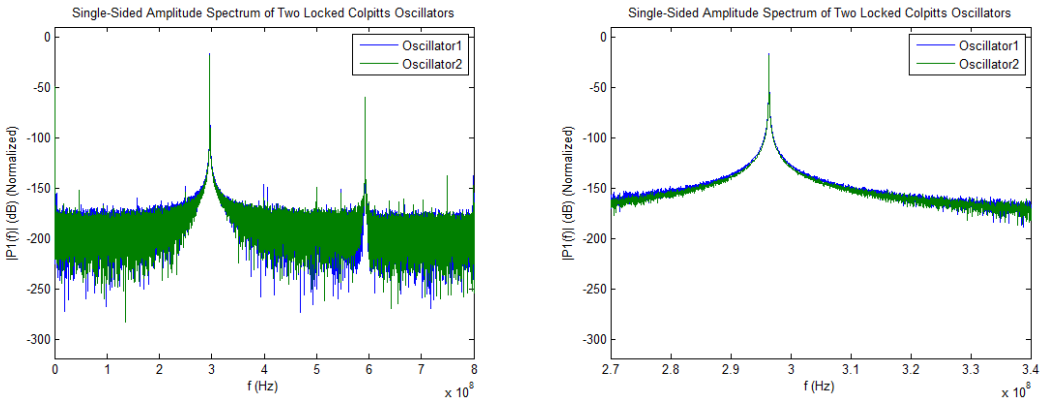

(a) (b)

Figure 4.20: (a) Output Signals of Two Locked Colpitts Oscillators and (b) Narrower Spectrum of Same Signals

put signals. Phase difference is constant through time. Time resolution is the same as calculated in equation (4.1). Period of the locked signals is calculated as $3.3739 \times 10^{-9}s$. Angle resolution is calculated as follows.

$$\text{angle resolution} = \left(\frac{50 \times 10^{-12}}{3.3739 \times 10^{-9}} \right) \times 360^o = 5.33^o \tag{4.3}$$

Phase noise of this oscillators is calculated from FFT data using Matlab. An improvement of 5 dBc/Hz @100 kHz offset frequency is observed. However, this is

impossible according to the given theory in Chapter 2 for phase noise. The improvement is expected as 3 dBc/Hz @100 kHz for 2 oscillator array according to equation (2.69).

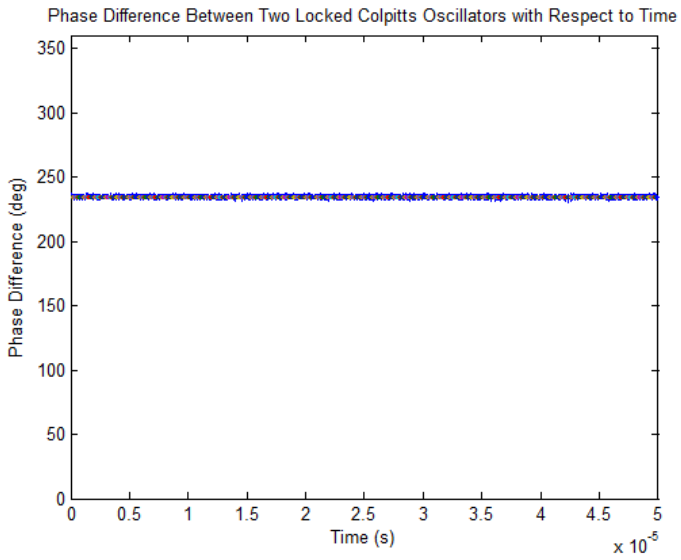

Figure 4.21: Phase Difference Between Two Locked Colpitts Oscillators

4.5 Measurement Results of Self-Locked Oscillator

In order to observe the self-locking phenomena, a feedback path using a coaxial cable is provided between input and output ports of the oscillator. In this case, injected signal is the output signal of the oscillator itself. A change in free-running frequency is expected since oscillator is disturbed by a cable which behaves as a resonator also. The experimental setup is shown in Figure 4.22.

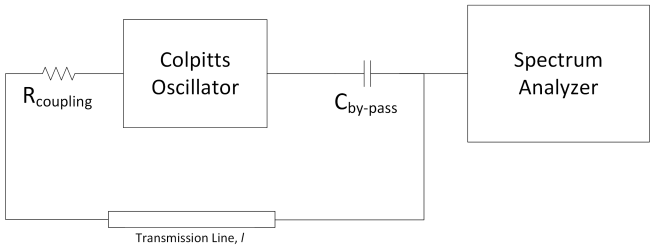

Figure 4.22: Experimental Setup for Self-Locking Experiments

Two different coaxial cables, RG178 and RG316 namely, are used to complete the feedback from output to input of the oscillator. Both cables have dielectric constant

of 2.1 but their dielectric and center connector diameters are different. Specification table for coaxial cables is given in Reference [32].

For each cable phase noise measurements of three different electrical lengths, $l = \lambda$, $l = 2\lambda$ and $l = \frac{\lambda}{2}$, are taken. Tables 4.4 and 4.5 show phase noise measurement results @100 kHz for cables RG178 and RG316. Figures 4.23, 4.24 and 4.25 show the spectrum analyzer screen shots for cable lengths $l = \lambda$, $l = 2\lambda$ and $l = \frac{\lambda}{2}$ respectively.

Table 4.4: Self-Locking Measurement Results for Cable RG178

State	Oscillation Frequency	Phase Noise @100 kHz
Free-Running	306.34 MHz	-102.5 dBc/Hz
$l = \frac{\lambda}{2}$	305.88 MHz	-106.84 dBc/Hz
$l = \lambda$	306.59 MHz	-109.29 dBc/Hz
$l = 2\lambda$	306.03 MHz	-112.33 dBc/Hz

Table 4.5: Self-Locking Measurement Results for Cable RG316

State	Oscillation Frequency	Phase Noise @100 kHz
Free-Running	306.34 MHz	-102.5 dBc/Hz
$l = \frac{\lambda}{2}$	302.62 MHz	-107.15 dBc/Hz
$l = \lambda$	306.65 MHz	-110.73 dBc/Hz
$l = 2\lambda$	305.31 MHz	-109.19 dBc/Hz

As seen in figures and tables, for each self-locking case phase noise is improved compared to free-running case. Best phase noise measurement for RG178 is taken for $l = 2\lambda$ and for RG316 it is taken for $l = \lambda$. In the measurement results for cable RG178, there is a jump around @1-2 kHz offset in the phase noise which is not present in cable RG316 measurement results. However, it is known that there is no change in measurement settings of the spectrum analyser. So, there is a possible inconsistency originating from the device for two sets of measurements. Improvements in phase noise are different in the spectrum with respect to cable length and cable radius. In Figures 4.23a and 4.25b @70 kHz, Figure 4.23b @1 kHz and @20 kHz, and Figure 4.24b @20 kHz, there are spikes in phase noise results. These spikes originate from switching circuits of the spectrum analyser.

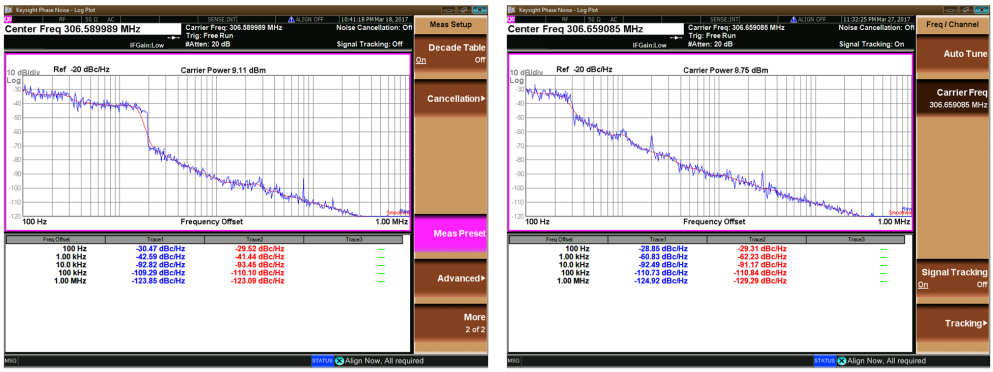

(a) (b)

Figure 4.23: Phase Noise Measurements of Self-Locked Oscillator for $l = \lambda$ with Cables (a) RG178 and (b) RG316

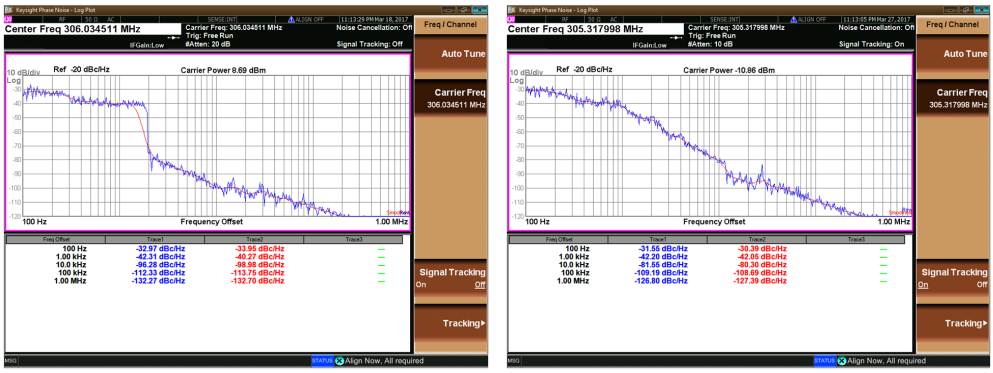

(a) (b)

Figure 4.24: Phase Noise Measurements of Self-Locked Oscillator for $l = 2\lambda$ with Cables (a) RG178 and (b) RG316

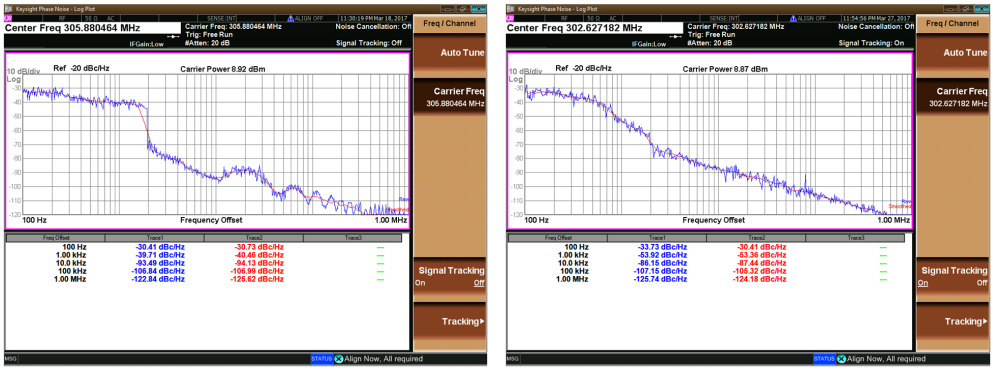

(a) (b)

Figure 4.25: Phase Noise Measurements of Self-Locked Oscillator for $l = \frac{\lambda}{2}$ with Cables (a) RG178 and (b) RG316

CHAPTER 5

MAGNETRONS AND INJECTION LOCKING OF MAGNETRONS

5.1 Introduction

In this chapter, magnetron theory of operation and measurement results of experiments conducted with industrial magnetrons will be given. Achieving locking with Colpitts oscillators, master-slave locking scheme will be applied to magnetrons.

5.2 Theory of Operation

A magnetron is a cylindrical diode with a magnetic field parallel to its axis in its simplest definition. A cylindrical anode, which houses resonant cavities, surrounds a centrally placed cathode. It is a self-excited oscillator whose purpose is to convert DC input power into RF output power [33].

5.2.1 Physical Structure

A magnetron consists of four main parts which are anode block, cathode, resonant system and interaction space as shown in Figure 5.1.

The functions of these components are explained below.

1. **Anode Block:** This cylindrical block is grounded and it is pierced by a number of resonant cavities in the axial direction. These cavities are open to the interaction space. The anode surface has some segments and gaps. The ends of the resonant cavities which is open to the interaction space are called end spaces.

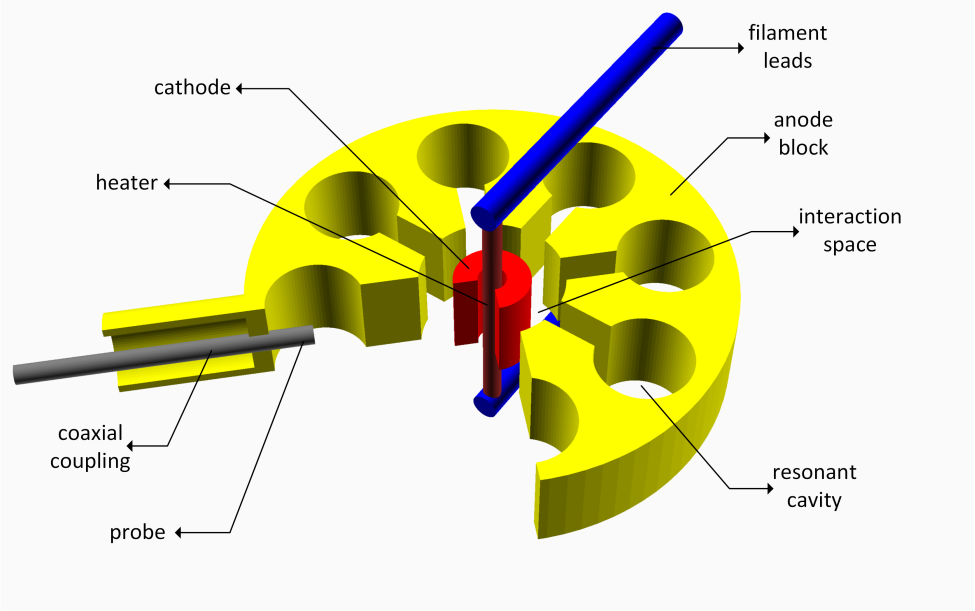

Figure 5.1: A Simple Magnetron Structure

2. **Cathode:** Cathode is kept at a negative voltage, $-V_o$, in order to produce the radial electric field in the interaction space. The heater surrounded by the cathode material, mostly Barium Oxide, is heated to provide source of electrons. In addition, it must prevent the axial escape of the electrons with end shields. RF currents are induced on the cathode's surface. Filament leads are used to keep cathode rigid and fixed. Cathode radius, r_c, is an important parameter. While too small radius may result in mode instabilities, too large radius may result in inefficient operation.

3. **Resonant System:** This system is composed of resonant cavities on the anode block. Physical dimension of the resonant cavity determines the frequency of oscillation. When a single cavity oscillates, it excites the next one to oscillate with a phase delay of 180 degrees. A good resonant system should provide a stable operation of magnetron. Each of resonant cavities is similar to a lumped oscillator tank circuit which consists of a parallel inductor and capacitor. The circular hole resembles the inductor and the parallel plane resembles the capacitance of the tank circuit as shown in Figure 5.2.

   The oscillation frequency can be calculated as

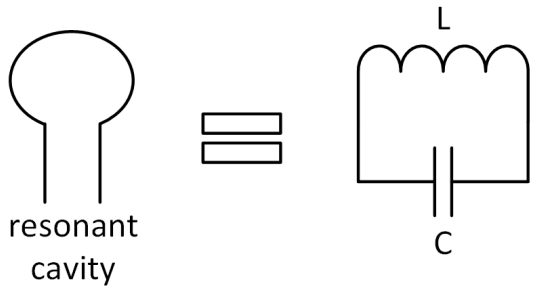

Figure 5.2: Resonant Cavitiy and Resembled Tank Circuit

$$f = \frac{1}{2\pi}\frac{1}{\sqrt{LC}} \tag{5.1}$$

Effective capacitance of magnetron is NC and effective inductance is L/N where N is the number of magnetrons.

The resonant system also transmits a portion of the generated RF power to an external load with probe and coaxial coupling parts as shown in Figure 5.1.

4. **Interaction Space:** This is the open space between anode block and cathode block. The conversion from DC input power to RF output power takes place in this space. A constant axial magnetic field is maintained here with an external magnet or by a solenoid.

5.2.2 Space Charge and DC Voltage - Magnetic Field Relationship

When there is no magnetic field in the interaction space, an electron, which is under the effect of electric force only, move towards anode block from the heated cathode. When axial magnetic field is present in the interaction space, the electron is acted on by both electric and magnetic force. These forces can be expressed as in equation (5.2), where *e* is the charge of electron, υ is the velocity of electron and *c* is velocity of light.

$$\overrightarrow{F_e} = -e\overrightarrow{E} \rightarrow \text{Electric Force} \tag{5.2a}$$

$$\overrightarrow{F_m} = \frac{e}{c}\left(\overrightarrow{\upsilon} \times \overrightarrow{B}\right) \rightarrow \text{Magnetic Force} \tag{5.2b}$$

The motion of an electron in a non-oscillating magnetron corresponds a slow rotation around the cathode with radius R_o, whose speed is $\frac{E}{B}$, and a fast rotation with a smaller radius r_o, which corresponds to the cyclotron frequency determined by B alone, $\omega_o = \frac{eB}{m}$. Therefore, the maximum distance, $R_o + r_o$, that an electron can proceed is limited by $\frac{E}{B}$, when there is no oscillations. The motion of the electron can be visualized as in Figure 5.3.

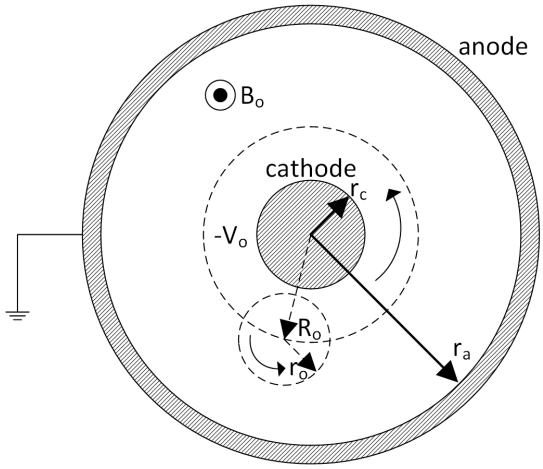

Figure 5.3: Path Followed by A Single Electron in A Non-Oscillating Magnetron

In an oscillating magnetron, a change in velocity of electrons results. While electrons, which speed up, return to the cathode with an increased curvature, electrons, which slow down, move toward to anode with a reduced curvature. The possible paths of an electron under E and B fields can be seen in Figure 5.4.

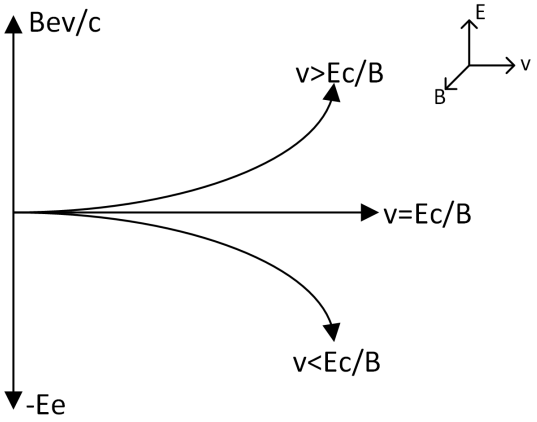

Figure 5.4: Possible Paths of An Electron Under E and B Fields

The force equation under these conditions is

$$\frac{Bev}{c} = eE + \frac{mv^2}{R} \tag{5.3}$$

where R is the orbit of an electron.

The condition $v = \frac{Ec}{B}$ is obtained, when letting $R = \infty$ for the straight line path of an electron.

For $v < \frac{Ec}{B}$, the electromagnetic force is reduced and the electron is deflected in the direction of electric force.

For $v < \frac{Ec}{B}$, the deflection will be in the direction of magnetic force.

Magnetron operating condition is $v \sim \frac{Ec}{B}$. Space charge for an oscillating magnetron can be seen in Figure 5.5. The blue area in this figure is named as space charge wheel. It rotates around the cathode at an angular velocity of 2 poles per cycle of the AC field, ω_n. This enables electrons to sustain RF oscillations.

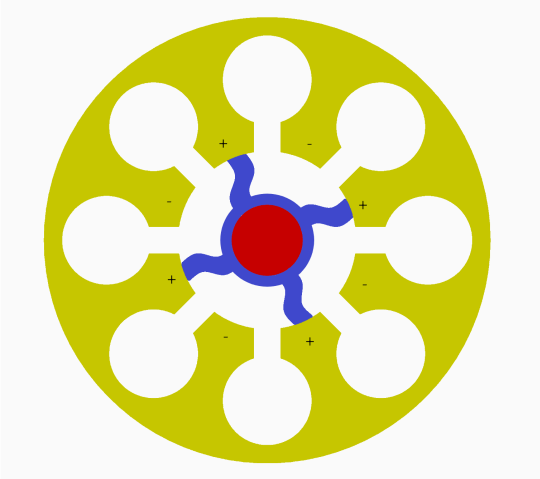

Figure 5.5: Space Charge in Oscillating Magnetron

The critical magnetic field to prevent the breakdown in the magnetron structure is Hull cut-off field, which is expressed as in equation (5.4) below [34].

$$B = \frac{mc}{ed_e}\sqrt{\gamma^2 - 1} \tag{5.4}$$

where d_e is the effective gap in the cylindrical geometry and

$$\gamma = 1 + \frac{eV_o}{mc^2} = 1 + \frac{V(\text{kV})}{0.511} \tag{5.5}$$

For a given anode-cathode voltage V_o, there is a maximum B_o above which electrons will be too slow to achieve resonance. This threshold DC voltage value is called as Buneman-Hartree voltage. The expression is given in equation (5.6) below. For a given V_o, if B_o is too weak, breakdown occurs. If B_o is too strong, there will be no oscillations.

$$\frac{eV_o}{mc^2} = \frac{eB_o\omega_n}{mc^2 n} r_a d_e - 1 + \sqrt{1 - \left(\frac{r_a\omega_n}{cn}\right)^2} \tag{5.6}$$

The operation regions for a magnetron is given in Figure 5.6 considering Hull cut-off equation and Buneman-Hartree threshold voltage.

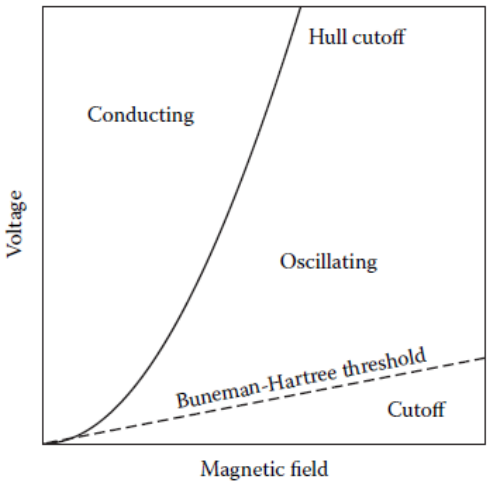

Figure 5.6: Magnetron Operation Regions According to $B_o - V_o$ Parameters

5.3 Proposal of Experimental Setups for Magnetron Measurements

For oscillations to begin in a magnetron, operation should be in the region between Buneman-Hartree threshold and Hull-cutoff curves as explained in the previous section. Unfortunately, oscillations do not start with a predictable phase. Hence, signals generated by the magnetron are not coherent. To overcome this problem, a magnetron

can be fed by an external oscillator with a continuous priming signal. In other words, phase locking theory, applied to the solid-state oscillator in previous chapters, can be used to stabilize frequency and phase of the magnetron.

In this section, two experimental setups for magnetron measurements are proposed. First setup is to measure output characteristics of a single magnetron ans second setup is proposed as a master-slave locking geometry with industrial magnetrons. These experimental setups are proposed for Muegge's MH1000B-250BH magnetron head.

5.3.1 Setup for an Industrial Magnetron Measurement

This experimental setup is proposed for measuring output characteristics of two separate MH1000B-250BH magnetrons. It is expected that their operating frequency is different from each other; since, their output phases are unpredictable as explained in previous sections.

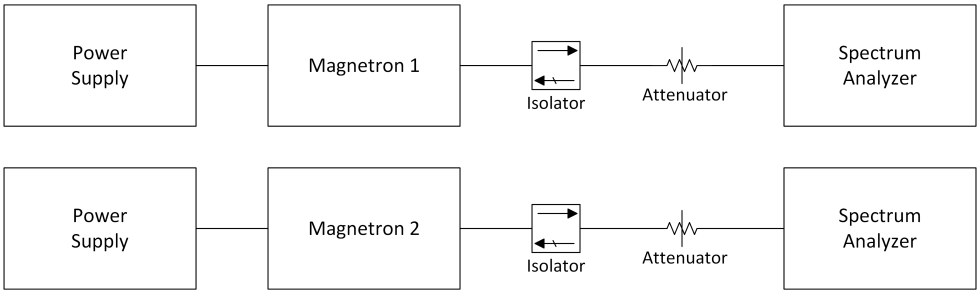

Figure 5.7: Experimental Setup for Measurements of Independent Magnetrons

5.3.2 Setup for Master-Slave Locked Magnetron Measurement

Experimental setup shown in Figure 5.8 is proposed for master-slave locking of Magnetron 1 and Magnetron 2, whose output characteristics can be measured by setups shown in Figure 5.7.

In this setup, Magnetron 1 is master oscillator and Magnetron 2 is slave oscillator. It is expected that phase locking will occur between magnetrons. Operating frequency of Magnetron 2 will follow operating frequency of Magnetron 1 and a stable phase difference between output signals will take place.

Isolator is used for making Magneron 1 master. Normally, isolator should be used at the output of a magnetron to protect it from reflected signals. But, for this experiment, in order to observe phase locking, reflected signals should reach Magnetron 2. Since, our industrial magnetron has only a waveguide output, there is no way to reach cavities, injection should be made through this waveguide by the reflected signals from Magnetron 1.

A 3-stub tuner is used to tune the coupling coefficient between magnetrons.

A T-junction is used to provide master-slave relationship and to observe the locked output signal from spectrum analyser.

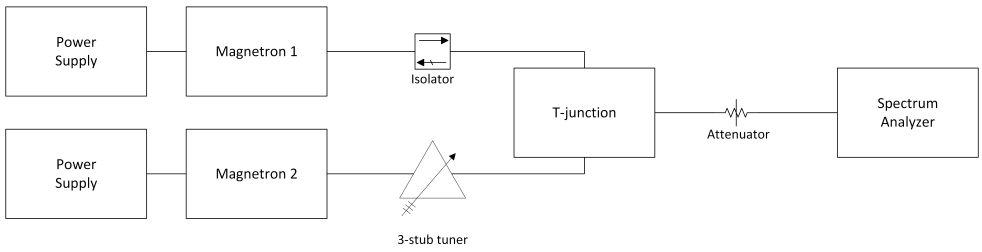

Figure 5.8: Experimental Setup for Master-Slave Locked Magnetrons

CHAPTER 6

CONCLUSION AND FUTURE WORK

6.1 Conclusion

This thesis focuses on frequency and phase locking of electrical oscillators. Frequency and phase of a free-running oscillator are unstable at the output, hence, combining output signals of two oscillators is a problem. Injection locking theory can be a solution for oscillators suffering from frequency and phase instabilities. While a pair of unlocked oscillators produces a fluctuating output power, a pair of locked oscillators produces an output power constant with respect to time.

The main purpose of this work is to propose an experimental setup for injection locking of magnetrons, which are HPM generators with poor frequency and phase stabilities. Magnetrons, when used in a phase coherent array, can supply a very high output power in the radiation field. Therefore, injection locking theory can be used to obtain a stable output power for magnetrons.

In this thesis, injection locking theory was examined in detail. In order to validate Adler's locking equation, a Colpitts oscillator was designed and manufactured. Design procedure for coupled oscillator systems was given. Simulations and experiments were applied on Colpitts oscillator and Adler's equation was verified. Applying the theory successfully, an experimental setup was proposed for magnetron injection locking.

In Chapter 2, equations for Adler's injection locking theory were derived for master-slave and peer-peer coupled oscillators. Phase noise for coupled oscillators were also explained briefly.

In Chapter 3, simulations for free-running oscillator, master-slave and peer-peer locked oscillator systems were conducted. For a single oscillator, output spectrum and phase noise simulations were run. For master-slave system, transient simulations were conducted and effects of coupling resistor, amplitude and frequency of injected signal were observed. For peer-peer system, effect of coupling resistor to locking range and frequency change of one of the peer oscillators to locking were observed. As a result, Adler's locking range equation is verified by these simulations.

In Chapter 4, experiments were conducted to verify simulation results on a manufactured Colpitts oscillator. For master-slave system, effects of amplitude and frequency of a signal generator, as master oscillator, were observed. Unlocked and locked output signals for both master-slave and peer-peer systems were captured using oscilloscope data. We achieved locking and observed phase noise improvement for both cases. In master-slave system, phase noise of the slave oscillator was locked to master signal's phase noise also. This important result can be used to improve phase noise of a low-Q oscillator array by selecting a stable master oscillator. For peer-peer system, 3 dB improvement was observed as theoretically expected. For self-locked oscillators, phase noise improvement of 5-10 dB @100 kHz offset was recorded. With a high-Q resonator as coupling network, phase noise improvement can be increased. This result can be used to improve stability of packaged oscillators.

In Chapter 5, operation of magnetrons was explained briefly and, a magnetron measurement setup and a setup with two magnetrons for master-slave locking were proposed. We expect that slave magnetron will follow master magnetron and injection coefficient can be arranged using a 3-stub tuner. This experiment can be repeated for different external signals as master. A much more stable master oscillator can improve output stabilities of the slave magnetron.

6.2 Future Work

Implementation of the proposed locking system is left as a future work. A more stable external signal as master can be used instead of magnetron. This method improves the stability of the slave magnetron. An array of magnetrons driven by such an oscillator

can be constructed to obtain higher output power with increased stability.

Peer-peer locking and self-locking systems of magnetrons can also be constructed. In self-locking system, a filter with high-Q resonator can be used to improve output stabilities of a single magnetron.

Magnetron driven vircator array can also be considered for future locking studies.

REFERENCES

[1] Encyclopædia Britannica, Magnetron. https://www.britannica.com/technology/magnetron. Accessed: 2017-07-31.

[2] R.Adler. A Study of Locking Phenomena in Oscillators. *Proceedings of the IRE*, 34(6):351–357, June 1946.

[3] Marconi in Newfoundland: The 1901 Transatlantic Radio Experiment. http://www.newscotland1398.net/nfld1901/marconi-nfld.html. Accessed: 2017-12-23.

[4] E.H.Armstrong. Wireless Receiving System. U.S.Patent, US1113149 A, October 1914.

[5] E.H.Colpitts. Oscillation Generator. U.S.Patent, US1624537 A, February 1918.

[6] U.L.Rohde. *Microwave and Wireless Synthesizers: Theory and Design*. New York: Wiley, 1997.

[7] U.L.Rohde and J.Whitaker. *Communications Receivers*. New York: McGraw-Hill, 3rd ed edition, 2000.

[8] U.L.Rohde, A.K.Poddar, and G.Böck. *The Design of Modern Microwave Oscillators for Wireless Applications, Theory and Optimization*. Wiley-Interscience, John Wiley & Sons, Inc, 2005.

[9] A.E.Siegman. *Lasers*. Mill Valley, CA: University Science Books, 1986.

[10] R.R.Ward. *The Living Clocks*. New York: Alfred Knopf, 1971.

[11] B.Razavi. A Study of Injection Locking and Pulling in Oscillators. *IEEE Journal of Solid-State Circuits*, 39(9):1415–1424, September 2004.

[12] S. Humphries Jr. *Charged Particle Beams*. Department of Electrical and Computer Engineering, University of New Mexico, 2002.

[13] B.Van der Pol. The Nonlinear Theory of Electric Oscillations. *Proceedings of the IRE*, 22(9):1051–1086, September 1934.

[14] L.J.Paciorek. Injection Locking of Oscillators. *Proceedings of the IEEE*, 53(11):1723–1727, November 1965.

[15] G. Şener. Phase Control by Injection Locking. Master's thesis, METU, 2004.

[16] K.Kurokawa. Noise in Synchronized Oscillators. *IEEE Transactions on Microwave Theory and Techniques*, MTT-16(4):234–240, April 1968.

[17] K.F.Schünemann. Nonlinear Noise Theory for Synchronized Oscillators. *IEEE Transactions on Microwave Theory and Techniques*, MTT-27(5):452–458, May 1979.

[18] H.C.Chang, X.Cao, U.K.Mishra, and R.A.York. Phase Noise in Coupled Oscillators: Theory and Experiment. *IEEE Transactions on Microwave Theory and Techniques*, 45(5):604–615, May 1997.

[19] H.C.Chang, X.Cao, M.J.Vaughan, U.K.Mishra, and R.A.York. Phase Noise in Externally Injection-Locked Oscillator Arrays. *IEEE Transactions on Microwave Theory and Techniques*, 45(11):2035–2042, November 1997.

[20] H.C.Chang. Phase Noise in Self-Injection-Locked Oscillators-Theory and Experiment. *IEEE Transactions on Microwave Theory and Techniques*, 51(9):1994–1999, September 2003.

[21] J.C.Slater. The Phasing of Magnetrons. Technical Report 35, Research Laboratory of Electronics, MIT, April 1947.

[22] W.Woo, J.Benford, D.Fittinghoff, B.Harteneck, D.Price, R.Smith, and H.Sze. Phase Locking of High-Power Microwave Oscillators. *Journal of Applied Physics*, 65(2):861–866, January 1989.

[23] D.Price, H.Sze, and D.Fittinghoff. Phase and Frequency Locking of a Cavity Vircator Driven by a Relativistic Magnetron. *Journal of Applied Physics*, 65(12):5185–5189, June 1989.

[24] H.Sze, D.Price, and B.Harteneck. Phase Locking of Two Strongly Coupled Vircators. *Journal of Applied Physics*, 67(5):2278–2282, March 1990.

[25] H.Sze, D.Price, B.Harteneck, and N.Cooksey. A Master-Oscillator-Driven Phase-Locked Vircator Array. *Journal of Applied Physics*, 68(7):3073–3079, October 1990.

[26] J.S.Levine, N.Aiello, J.Benford, and B.Harteneck. Design and Operation of a Module of Phase-Locked Relativistic Magnetrons. *Journal of Applied Physics*, 70(5):2838–2848, September 1991.

[27] H.Sze, R.R.Simth, J.Benford, and B.Harteneck. Phase locking of strongly coupled relativistic magnetrons. *IEEE Transactions on Electromagnetic Compatibility*, 34(3):235–241, August 1992.

[28] C.Liu, H.Huang, Z.Liu, F.Huo, and K. Huang. Experimental Study on Microwave Power Combining Based on Injection-Locked 15-kW S-Band Continuous-Wave Magnetrons. *IEEE Transactions on Plasma Science*, 44(8):1291–1297, August 2016.

[29] J.J.Choi and G.W.Choi. Experimental Observation of Frequency Locking and Noise Reduction in a Self-Injection-Locked Magnetron. *IEEE Transactions on Electron Devices*, 54(12):3430–3432, December 2007.

[30] U.L.Rohde and A.M.Apte. Everything You Always Wanted to Know About Colpitts Oscillators. *IEEE Microwave Magazine*, 17(8):59–76, August 2016.

[31] Lpkf Rapid PCB Prototyping. `http://www.lpkf.com/products/rapid-pcb-prototyping/`. Accessed: 2017-09-13.

[32] Rf Cable Specifications. `http://suddendocs.samtec.com/productcharts/rf_cable_chart.pdf`. Accessed: 2017-08-31.

[33] G. B. Collins. *Microwave Magnetrons*. McGraw-Hill Book Company Inc., 1948.

[34] J.Benford, J.A.Swegle, and E.Schamiloglu. *High Power Microwaves*. Taylor and Francis Group, 2nd edition, 2007.

APPENDIX A

INTEGRAL CALCULATION OF OSCILLATOR OUTPUT VOLTAGE

In order to obtain the phase and amplitude dynamics equations for injection locked system, $\int V_{out}(t)\,dt$ should be calculated and inserted in equation 2.8.

$$V_{out}(t) = A(t)\,e^{j\theta(t)} = e^{j(\omega_0 t+\phi(t))} \tag{A.1}$$

$$\int V_{out}(t)\,dt = \int A(t)\,e^{j(\omega_0 t+\phi(t))}dt \tag{A.2}$$

This integral could be calculated by using integration by parts theorem.

$$\int V_{out}(t) = uv - \int v du \tag{A.3}$$

Let u, v, du and dv be

$$u = A(t) \Longrightarrow du = A^{'}(t)\,dt \tag{A.4}$$

$$dv = e^{j(\omega_0 t+\phi_0)} \Longrightarrow v = \frac{1}{j\omega_0}e^{j(\omega_0 t+\phi_0)} \tag{A.5}$$

Inserting the variables into the equation A.3

$$\int V_{out}(t) = \frac{A(t)\,e^{j(\omega_0 t+\phi_0)}}{j\omega_0} - \frac{1}{j\omega_0}\int A^{'}(t)\,e^{j(\omega_0 t+\phi_0)}dt \tag{A.6}$$

$$\int V_{out}(t) = \frac{V_{out}(t)}{j\omega_0} - \frac{1}{j\omega_0}\int A^{'}(t)\,e^{j(\omega_0 t+\phi_0)}dt \tag{A.7}$$

Applying integraton by parts one more time for $\int A^{'}(t)\,e^{j(\omega_0 t+\phi_0)}dt$

$$u = A^{'}(t) \Longrightarrow du = A^{''}(t) \tag{A.8}$$

$$dv = e^{j(\omega_0 t+\phi_0)} \Longrightarrow v = \frac{1}{j\omega_0} e^{j(\omega_0 t+\phi_0)} \tag{A.9}$$

$$\int A^{'}(t)\, e^{j(\omega_0 t+\phi_0)} dt = uv - \int v du = \frac{A^{'}(t)}{j\omega_0} e^{j(\omega_0 t+\phi_0)} - \frac{1}{j\omega_0} \int A^{''}(t)\, e^{j(\omega_0 t+\phi_0)} dt \tag{A.10}$$

Inserting A.10 into A.7 the integral expression is obtained.

$$\int V_{out}(t)\, dt = \frac{V_{out}(t)}{j\omega_0} - \frac{1}{j\omega_0} \left[\frac{A^{'}(t)}{j\omega_0} e^{j(\omega_0 t+\phi_0)} - \frac{1}{j\omega_0} \int A^{''}(t)\, e^{j(\omega_0 t+\phi_0)} dt \right] \tag{A.11}$$

$$\int V_{out}(t)\, dt = \frac{V_{out}(t)}{j\omega_0} + \frac{A^{'}(t)}{\omega_0^2} e^{j(\omega_0 t+\phi_0)} - \frac{1}{\omega_0^2} \int A^{''}(t)\, e^{j(\omega_0 t+\phi_0)} dt \tag{A.12}$$

In order to replace the term $A^{'}(t)$ with terms containing $V_{out}(t)$, the derivative of equation A.1 should be taken.

$$\frac{dV_{out}(t)}{dt} = \frac{d\left[A(t)\, e^{j(\omega_0 t+\phi_0)}\right]}{dt} = A^{'}(t)\, e^{j(\omega_0 t+\phi_0)} + j\omega_0 A(t)\, e^{j(\omega_0 t+\phi_0)} \tag{A.13}$$

$$A^{'}(t)\, e^{j(\omega_0 t+\phi_0)} = \frac{dV_{out}(t)}{dt} - j\omega_0 V(t) \tag{A.14}$$

Inserting A.14 into A.12 and rearranging the equation

$$\int V_{out}(t)\, dt = \frac{V_{out}(t)}{j\omega_0} + \frac{1}{\omega_0^2} \left[\frac{dV_{out}(t)}{dt} - j\omega_0 V_{out}(t) \right] - \frac{1}{\omega_0^2} \int A^{''}(t)\, e^{j(\omega_0 t+\phi_0)} dt \tag{A.15}$$

$$\int V_{out}(t)\, dt = -\frac{jV_{out}(t)}{\omega_0} + \frac{1}{\omega_0^2} \frac{dV_{out}(t)}{dt} - \frac{jV_{out}(t)}{\omega_0} - \frac{1}{\omega_0^2} \int A^{''}(t)\, e^{j(\omega_0 t+\phi_0)} dt \tag{A.16}$$

The remaining integral in equation A.16 can also be calculated using integration by parts one more time. However, since the amplitude terms are slowly varying in comparison to the oscillation frequency, this higher order terms can be neglected for calculating the amplitude and phase dynamics equations of the injection locked oscillator system.

$$\int V(t)\,dt = -\frac{j2V(t)}{\omega_0} + \frac{1}{\omega_0^2}\frac{dV(t)}{dt} + H.O.T. \tag{A.17}$$

APPENDIX B

DESIGN OF A COLPITTS OSCILLATOR

Oscillators are essential circuits for modern communication systems. Colpitts oscillator design is one of the most used oscillator designs for high-performance microwave applications. Figure B.1 shows the conventional circuit diagram based on the design developed by Edwin H. Colpitts [5] in 1918. This circuit employs a capacitive voltage divider and an inductor as resonator circuit.

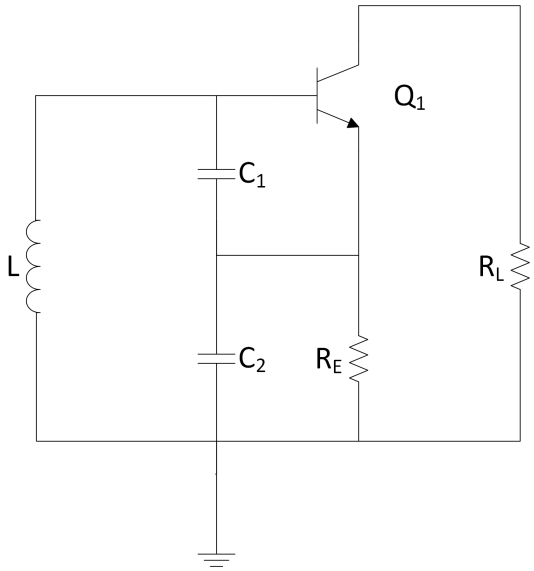

Figure B.1: Conventional Colpitts Oscillator Configuration

Selecting the Right Transistor

The basic design of a Colpitts oscillator is the same, whether FET or BJT used as transistor. The advantage of using BJT is the lower flicker noise corner frequency.

For the purpose of this thesis work, BFG520W transistor, which is a highly linear transistor, is used. The key parameters are $V_{CEO} = 15$ V, $I_C = 70$ mA and $P_{tot} = 300$

mW. The noise figure F_{min} at 350 MHz is lower than 1 dB and at 5 mA the associated gain is more than 17 dB.

1. Step 1: Initial Specification

   Based on the requirements for output power and harmonics for a specific load of the oscillator, a drive level from the table given in Reference [30] and [8] should be chosen. This normalized drive level is chosen for enough drive level to sustain oscillation and not to produce excessive harmonic products. Emitter current is calculated at this step.

2. Step 2: Biasing

   This step for the oscillator used in this work is given in Chapter 3 in the thesis script. Important point here is to reduce flicker noise and distortion using appropriate bias resistor ratio. Detailed calculations can be found in [30].

3. Step 3: Determining the Large-Signal Transconductance

   The purpose of this step is to determine the feedback factor *n*.

   From the drive level table mentioned above, the DC transconductance equals at the fundamental frequency

$$Y21 = \frac{I_1}{V_1} \tag{B.1}$$

   Based on KVL, the following set of equations are used to determine *n*:

$$Y_1 = G_1 + jB_1 = G_1 + j\omega C_1 \tag{B.2}$$

$$Y_2 = G_2 + jB_2 \tag{B.3}$$

$$Y_3 = G_3 + jB_3 = G_3 + j\omega C_2 \tag{B.4}$$

   The ratios for the capacitors in the resonator can be written as follows in terms of feedback ratio

$$\frac{V_{eb}}{V_{cb}} = \frac{C_2}{C_1 + C_2} = \frac{1}{n} \tag{B.5}$$

$$\frac{V_{ce}}{V_{cb}} = \frac{C_1}{C_1 + C_2} = \frac{n-1}{n} \tag{B.6}$$

Following Reference [30], *n* is calculated using transconductance values and, C_1 C_2 are determined. L is chosen using the following equation according to the wanted frequency of oscillation.

$$\omega = \sqrt{\frac{1}{L}\left(\frac{1}{C_1} + \frac{1}{C_2}\right)} \tag{B.7}$$

Colpitts oscillators can be optimised for noise reduction and maximum oscillation power.

The detailed design procedure of a Colpitts oscillator can be found in References [30] and [8].